Valorization of Silica Enriched Industrial Byproduct for Partial Replacement of Cement Clinker and Synthesizing of Zeolite Based Catalyst for Polyethylene Cracking

Fana Teklemariam Gebregiorgis

Thesis Paper Submitted to Chemical Engineering

School of Mechanical, Chemical and Material Engineering

Presented in Partial Fulfillment of the Requirement for the Degree of Master's in Chemical Engineering (Specialization in Process Engineering)

Office of Graduate Studies

Adama Science and Technology University

June, 2022

Adama, Ethiopia

Valorization of Silica Enriched Industrial Byproduct for Partial Replacement of Cement Clinker and Synthesizing of Zeolite Based Catalyst for Polyethylene Cracking

Fana Teklemariam Gebregiorgis

Advisors: Maleku Tesfaye (Ph.D.)

Zelalem Tumsa (Ph.D.)

Thesis Paper Submitted to Chemical Engineering

School of Mechanical, Chemical and Material Engineering

Presented in Partial Fulfillment of the Requirement for the Degree of Master's in Chemical Engineering (Specialization in Process Engineering)

Office of Graduate Studies

Adama Science and Technology University

June, 2022

Adama, Ethiopia

Declaration

I hereby declare that this Master Thesis entitled "Valorization of Silica Enriched Industrial Byproduct for Partial Replacement of Cement Clinker and Synthesizing of Zeolite Based Catalyst for Polyethylene Cracking" is my original work. That is, it has not been submitted for the award of any academic degree, diploma or certificate in any other university. All sources of materials that are used for this thesis have been duly acknowledged through citation.

Fana Teklemariam _____ _____

Name of the student Signature Date

Recommendation

We, the advisor(s) of this thesis, hereby certify that we have read the revised version of the thesis entitled “Valorization of Silica Enriched Industrial Byproduct for Partial Replacement of Cement Clinker and Synthesizing of Zeolite Based Catalyst for Polyethylene Cracking” prepared under my/our guidance by Fana Teklemariam submitted in partial fulfillment of the requirements for the degree of Mater’s of Science in Chemical Engineering (Specialization Process Engineering). Therefore, I/we recommend the submission of revised version of the thesis to the department following the applicable procedures.

_____	_____	_____
Major Advisor	Signature	Date
_____	_____	_____
Co-advisor	Signature	Date

Approval Page

We, the advisors of the thesis entitled “Valorization of Silica Enriched Industrial Byproduct for Partial Replacement of Cement Clinker and Synthesizing of Zeolite Based Catalyst for Polyethylene Cracking” and developed by Fana Teklemariam hereby certify that the recommendation and suggestions made by the board of examiners are appropriately incorporated into the final version of the thesis.

_____	_____	_____
Major Advisor	Signature	Date
_____	_____	_____
Co-advisor	Signature	Date

We, the undersigned, members of the Board of Examiners of the thesis by Fana Teklemariam have read and evaluated the thesis entitled “Valorization of Silica Enriched Industrial Byproduct for Partial Replacement of Cement Clinker and Synthesizing of Zeolite Based Catalyst for Polyethylene Cracking” and examined the candidate during open defense. This is, therefore, to certify that the thesis is accepted for partial fulfillment of the requirement of the degree of Master of Science in Chemical Engineering (Specialization in process engineering).

_____	_____	_____
Chairperson	Signature	Date
_____	_____	_____
Internal Examiner	Signature	Date
_____	_____	_____
External Examiner	Signature	Date

Finally, approval and acceptance of the thesis is contingent upon submission of its final copy to the Office of Postgraduate Studies (OPGS) through the Department Graduate Council (DGC) and School Graduate Committee (SGC).

_____	_____	_____
Department Head	Signature	Date
_____	_____	_____
School Dean	Signature	Date
_____	_____	_____
Office of Postgraduate Studies, Dean	Signature	Date

ACKNOWLEDGEMENT

First of all, I would like to gratitude and praise my GOD for the successful completion of my thesis research work.

I would like to express my gratitude to my advisors Dr. Melaku Tesfaye Aleme and Dr. Zelalem Tumsa for their support, guidance and valuable criticisms. This thesis would not have been accomplished without their outstanding supervision, scientific knowledge and experience.

I would like to thank, Hungnawe Bayu head of the department of Chemical Engineering, for his valuable comment and support.

With respect, honor and appreciation I dually acknowledge all lab technicians at Chemical Engineering laboratory and Mr Welaye Girmay, control laboratory head at Dira Dawa National cement for his generous aid on this thesis.

I wish to extend my warm thanks to all the good people of Geological Survey of Ethiopia for their complete silica analysis results.

ABSTRACT

*With increasing urbanization industries waste, CO_2 emission and energy audit are some of huge challenge to the world. Awash Melkassa is chemical factories in Ethiopia that discharge silica enriched byproducts during aluminum sulfate manufacturing. This waste is dumped inside industry compound in huge landfill. These have been a challenge for the factory. Therefore this byproduct was valorized for application of cement sector as partial replacement of cement clinker and catalysts sector for synthesis of zeolite based catalysts for PE degradation. This silica enriched Industrial byproduct was valorized by first altering crystalline nature to amorphous phase by calcination with immediate quenching with various temperatures. Highly amorphous phase had been achieved by 600 ^oC calcination with immediate quenching. With the successful achievement of amorphous chemical factory waste (CFW), cement clinker had been partially replaced by amorphous CFW with (5, 10 and 15%) by weight, proportions. The blaine air permittivity test, chemical analysis, compressive strength test, flexural strength test, setting time and soundness test result were in total agreement with standard of ordinary portland cement. Initial setting time increased with replacement compare with benchmark. This was due to the increasing content of Al_2O_3. 10% CFWB replacement had showed maximum compressive strength with 120% strength index. Fineness of clinker blend had showed significant effect on 2days curing of cement rather than 28 days curing. With 15% replacement 5.65*104 KJ/Qtl energy is saved that reduced production cost by $71,568. In addition to saving energy and cost it has reduced CO_2 emission by 105 Qtl. It was concluded that the partial cement clinker replacement using activated CFW have a great influence on Strength of cement mortar, the reduction of CO_2 emission and energy saving in cement manufacturing. On the other hand Nano Zeolite Y had been synthesized successfully from activated CFW by gel formation, aging, hydrothermal treatment and drying with gel composition of 13.2 Na_2O. Al_2O_3. 11SiO_2.263H_2O. The XRD, SEM, FTIR, PSA and BET results was obtained from the analysis totally agreed with the standards. Aging temperatures, duration of aging and Na2O/SiO2 ratio were chosen as room temperature, 12 hr and 0.8, respectively. The performance of synthesized Zeolite Y also was evaluated by degradation temperature shifted from 398 ^oC to 334 ^oC at 95% weight loss (T_5), with HDPE-30Z which implies that breakdown temperature reduced by 64 ^oC compared to pure HDPE.*

Keyword: Cement Clinker, Silica, CO_2 Emission, Activated CFW, HDPE, Nano Zeolite

Table of Contents

LIST OF TABLES

TABLES PAGE

LIST OF FIGURES

FIGURES PAGE

LIST OF ACRONYMS AND ABBREVIATION

AIC - Advanced Iso Conversional

AQCFW - Air Quenched Chemical Factory Waste

BFA - Bagasse Fly Ash

C&D - Construction and Demolition

CCP - Coal Combustion Products

CCW - civil construction waste

CFA - Coal Fly Ash

CFW- Chemical Factory Waste

CSH - Calcium Silicate Hydrate

DLS - Dynamic light scattering

HDPE - High Density Polyethylene

IZA - International Zeolite Association

JCPDS - Powder Diffraction Standards

LSF - Lime Saturation Factor

AR - Alumina Ratio

MSW - Municipal Solid Waste

OPC - Ordinary Portland Cement

PBU - Primary Building Unit

PCS - Photon Correlation Spectroscopy

PDI - Poly Dispersity Index

PE - Polyethylene

PET - Polyethylene Terephthalate

PFa - Pulverized Fly Ashes

POMFA - Palm Oil Mill Fly Ash

PP - Polypropylene

PPC - Portland Pozzolanic Cement

QELS - Quasi Elastic Light Scattering

RMC - Recycled Monolithic Columns

RDC - Recycled Drainage Channel

RRS - Recycled Railway Sleeper

SBU - Secondary Building Unit

SF - Silica Fume

SM - Silica Modulus

SRISW - Silica Rich Industrial Solid Waste

SSC - Steel Slag Clinker

STP - Standard Temperature and Pressure

CHAPTER 1

1. INTRODUCTION

1.1. Background

Rapid industrialization, urbanization, technical advancements, population increase, and economic activity place a significant strain on the earth's finite natural resources. People have had a problem figuring out what to do with leftover materials known as waste that may be of no use to them since ancient times, and so the term pollution was coined. Waste is produced as a result of processes such as the extraction of raw materials, the processing of intermediate or final products, the intake of final products, and other human activities; it can include all organic and inorganic fractions of domestic waste, as well as kitchen waste, package waste, grass clippings, cloth, bottles, paper, containers, and used batteries (Ramachandra et al., 2007). Manufacturing trash from a wide range of operations, such as sludges, product residues, kiln dust, slags, and ashes, is referred to as industrial waste. The three types of industries that generate the most industrial waste are metallurgy, nonmetallurgy, and food processing. The waste generated by industries varies according to the raw materials utilized, production processes, and product outlets; however, waste may be classified into three categories: solids, liquids, and gases. There are inorganic fractions, organic fractions, biodegradable fractions, nonbiodegradable compounds, recyclable materials, and so on.(JeyaSundar et al., 2020).

One of major industrial waste is silica enriched industrial byproducts such as silica fume, paper mill sludge ash, rice husk ash, blast furnace slag, fly ash, coal gangue, iron ore tailing, waste glass and so on. Those industrial wastes mainly contain silicon dioxide in large amount. With few transformations it can be used to synthesize valuable material from this potential wastes. Different researches indicates silica enriched industrial by products have been applicable for synthesis of zeolite, fertilizer, adsorbents, waste water treatment, cement replacement materials, mesoporous silica, glass–ceramics and geopolymer foams (Chinnam et al., 2013; J. A. S. Costa et al., 2020; Dikshit et al., 2001; Hartmann et al., 2014; Miao et al., 2022).

The Awash Melkassa Chemical Factory is located 105 kilometers south east of Addis Ababa, Ethiopia, on the main road to Assella in the Oromia Regional State. Council of Minister

Regulations No.235/1995 established the factory as a Public Enterprise. The firm's major goal is to manufacture and sell chemicals like aluminum sulphate and sulfuric acid, and recently the corporation has built a hydrogen peroxide facility and is producing the chemical hydrogen peroxide. Aluminum sulfate and sulfuric acid production are separated into two industrial segments: aluminum sulfate manufacturing and sulfuric acid manufacturing. The aluminum sulfate and sulfuric acid plants were developed in this fashion to have a manufacturing capacity of 13,600 and 17,000 tons per year, respectively. Awash Melkassa Chemical Factory is one of the industries in Ethiopia which discharge silica enriched byproduct from the industry during Aluminum Sulphate production. This indicated there is a huge potential waste that can be used to produce valuable products like catalysts as well as cement replacement material.

In the light of the increasing economic system and commercial improvement, society's growing desires result in a large consumption of natural resources and an era of even more waste. As a result, commercial waste and product control is a growing topic of research, requiring the definition of sustainable production and waste generation optimization. Another possible application for this waste is in the building industry, particularly in cement manufacture. Cement is a hydraulic binder, which is a finely powdered inorganic material that, when mixed with water, forms a paste that sets and hardens through hydration reactions and processes and retains its strength and stability even when submerged.

Cement clinker is the most important component of cement. Cement clinker is a hydraulic material that must contain at least two-thirds calcium silicates by mass (3CaO. SiO_2 and 2CaO. SiO_2). The remaining is made up of aluminum and iron clinker phases, as well as other compounds. The mass ratio (CaO)/(SiO_2) must not be less than 2. The amount of magnesium oxide (MgO) in the product must not exceed 5% by mass. The use of numerous wastes rich in CaO, SiO_2, and Fe_2O_3 to produce environmentally friendly cement is in high demand. As a result, a silica-rich byproduct has been used to partially replace cement clinker. These silica enriched industrial byproduct have also used for synthesis of catalyst which are applicable for various sectors.

Zeolite is one of the catalysts, which have huge application on petroleum cracking. This catalyst can also used for plastic degradation. Plastic usage has increased as society has progressed.

Because most of plastic is not biodegradable, it accumulates on landfills and floats in bodies of water. Various investigations on catalytic decomposition of plastic trash for the manufacture of valuable fuel products have been conducted. (Onwudili et al., 2019) worked with a variety of plastics using catalytic pyrolysis and catalysts such as FCC, ZSM-5, and zeolites Y. (Santos et al., 2018)investigated the catalytic pyrolysis of polyethylene (PE) and polypropylene (PP) plastic waste with catalysts including HZSM-five, USY, NH_4ZSM5. This work investigates the opportunity of partial replacement of cement clinker as well as syntheses of zeolite based catalyst via valorization of silica enrich byproduct from Awash Melkassa chemical factory.

1.2. Statement of the Problem

Awash Melkassa chemical factory produces sulfuric acid and aluminum sulfate. The company releases solid byproducts at the end of the production of aluminum sulfate. There is a huge buildup of this chemical factory waste (CFW) inside the factory compound as shown in figure 1.1. This causes possible health problem on the community around that area such as silicosis and needs to be dealt with properly, which need to be overcome this defies

FIGURE 1.1 Huge Build up Waste in Awash Melkassa Chemical Factory

Production of cement clinker shares energy cost compared to the total production cost in the cement industries is in the range of 20 to 60% of operational costs, which requires great attention for improving the energy efficiency in the industry (J. Wang et al., 2009). In average cement industry is estimated to produce 2000 tons/day with specific energy consumption of $3.735*10^6$

KJ/ton. This energy intensive section of cement production needs improvement to overcome those issues. In addition, 5-7% of CO_2 emissions in the world are caused by cement plants with the specific emission being around 900 kg CO_2 per ton of cement produced (Ali et al., 2011; Benhelal et al., 2013). It is estimated from an average cement industry $1.08*10^9$ Kg of CO_2 per year is emitted to the environment therefore the cement industries have caused unbalance in the green world. To overcome these issues, new approach is needed. In addition to the increasing price of raw materials and many several reasons, the purchasing price of cement is getting very expensive. This study will also try to partially replace the raw material for clinker in cement with cheaper raw material as well as property enhancer for cement.

On the other hand several researches have investigated the potential of Ethiopian kaolin for zeolite synthesis; however, no such attempt has been carried out yet to synthesize zeolite-based catalysts from industrial byproducts (CFW). Thus to fill this gap silica enrich CFW was utilized as raw material to synthesize zeolite based catalyst. This work targeted to eliminate the byproduct build up and produce valuable zeolite-based catalysts simultaneously with the potential to acquire and produce foreign currency.

In addition, environmental crises of plastic waste accumulation got huge attention in developing countries, Therefore, there is the need to find a way of at least managing plastic wastes efficiently, to eliminate this problem by reprocessing the waste plastic to usefull forms such as fuels are essential and also the crude oil refining process this can be related catalytic cracking of PE plastic waste and change to useful hydrocarbon products.

1.3. Objective of Study

1.3.1. General Objective

The general objective of this study is to partially replace cement clinker and synthesize zeolite based catalyst for PE cracking from valorized silica enriched industrial byproduct.

1.3.2. Specific Objective

The specific objectives of this study are:

- ✓ To prepare amorphous silica from silica enriched industrial byproduct.

- ✓ To study the effect of amorphous condition and mixing ratio of pretreated silica enriched industrial byproduct on strength (Compressive and flexural strength), setting time and expansion of cement.
- ✓ To study the effect of fineness of clinker blend on strength of cement.
- ✓ To study the effect of gel formation and hydrothermal treatment condition on synthesis zeolite based catalyst.
- ✓ To evaluate the performance of zeolite based catalyst, related to catalyst dosage and cracking temperature in PE catalytic cracking using thermalgravirometic analysis (TGA).

1.4. Scope of the Study

The focus of this thesis works covers preparation and characterization of valorized silica enriched industrial byproduct for partial replacement of cement clinker. The reference and partially replaced cement has been characterized by flexural strength, compressive strength, blaine air permittivity test, Vicat needle test and Le Chatelier test. Zeolite Y catalyst from silica enriched industrial byproduct has been synthesized by physical treatment, hydrothermal synthesizing and crystallization steps. Solid catalysts zeolites has been characterized by using FT-IR, TGA, PSA, XRD, SEM and BET. The catalytic performance of synthesized zeolite based catalyst has been showed using TGA analysis by thermal degradation of HDPE using catalyst.

1.5. Significance of study

This work can predict alternative resource for the production of cement clinker by partial replacement using valorized silica enriched industrial byproduct. The production of cement clinker is the most energy intensive production unit of all production units. Therefore by decreasing the energy usage of cement industry by alternative resource it can increase revenue of the cement company and also reduced CO_2 emission.

Another significance of this work is to protect environmental pollution by developing safe and green catalyst from industrial waste (Awash Melkassa chemical factory). The catalyst has its own unique properties: it can be easily synthesized, efficient, safe, environmentally friendly and economically feasible more than commercial solid catalyst.

Additionally, it is beneficial for petroleum industry sector to improve liquid fuel quality and intermediate products during cracking, using zeolite based catalysts. It can be help to minimize the cost of energy during plastic degradation by using zeolite based catalyst.

CHAPTER 2

2. LITERATURE REVIEW

2.1. Silica Enriched Industrial Byproducts

Silica, or SiO_2, is a colorless or white crystalline component found in quartz, sand, flint, and a variety of other minerals. Silica is a significant component in the production of a wide range of products. Silicon dioxide is used in the construction industry to make concrete, in its crystalline form in hydraulic fracturing, in the manufacture of glass, in the manufacture of elemental silicon, as an anti-caking agent in powdered foods like spices, as a fining agent in juice, beer, and wine, and in the manufacture of pharmaceutical tablets and toothpaste to remove plaque. (Nisrinah, 2022) The construction sector uses silicon dioxide (sand) for around 95% of its commercial use, such as in the making of concrete (Portland cement concrete plaque). (Tang et al., 2003) Certain deposits of silica sand, with desirable particle size and shape and desirable clay and other mineral content, were important for sand casting of metallic products.(Kanyo et al., 2020; Looms, 1988) Because of its high melting point, silica can be utilized in applications like iron casting; modern sand casting occasionally incorporates different minerals for other purposes. The silicon atom is tetrahedral coordinated in the bulk of silicates, with four oxygen atoms around a core Si atom. The quartz polymorphs are the most common example. It's a three-dimensional network solid in which each silicon atom is covalently connected to four oxygen atoms in a tetrahedral pattern. silica is transparent to gray, odorless, crystalline or amorphous solid, melting point is 1600 ºC, boiling point is 2230 ºC, density is 2.65 g ml^{-1}, thermal diffusivity is 0.009 cm^2/sec, thermal conductivity is 0.01 w/cm k, and dielectric constant is 3.9 (Nishi et al., 2000; Y. Zhu et al., 2005) Non-metallic oxides, metal oxides, carbonates, and other components make up the majority of general industrial solid wastes, which are potentially complex mixed resources. (Tan et al., 2020; Wen et al., 2014). The main chemical components include SiO_2, Al_2O_3, Fe_2O_3, CaO, MgO, Na_2O, K_2O and organic matter. The chemical composition, crystal structure, breakdown characteristics, particle size distribution, and production techniques of the minerals themselves all influence the physicochemical features of the wastes. Industrial solid wastes with high SiO_2 content are referred to as silica rich industrial solid waste (SRISW). Silica is present in almost 80% of industrial solid wastes. To realize the efficient and reasonable conversion of SRISW to

porous materials, it is required to accurately characterize the physicochemical attributes and hazardous degree of different forms of SRISW. Preparing useful products from silicon-rich industrial solid waste (SRISW) is a cost-effective and ecologically responsible technique to use industrial solid waste. Iron ore tailing is a high-value industrial byproduct. Iron ore tailing is one of industries waste with high SiO_2 content. This waste is generated by Iron mining sector. Approximately 1.4 billion tons per year of iron ore tailing wastes are generated, mainly in Australia, Brazil, and China (Carmignano et al., 2021). Coal gangue is a solid waste produced in coal production with high SiO_2 content. Coal gangue production accounts for about 10–15% of raw coal production (Dong et al., 2020). Coal combustion in the energy sector produces around 150 million tons of waste every year across Europe. (Łach et al., 2019). Red mud is a byproduct of the Bayer process during the production of alumina which have significant amount of SiO_2. About 120 million tons of red mud is produced worldwide each year (Silveira et al., 2021). Fly ash is the finest of coal ash particles produced from the combustion of coal-based thermal power plants. Over 600 million tons of fly ash is produced worldwide annually (Pandey, 2020). It is recognized as a silica-enriched industrial byproduct (Gajić et al., 2019).

Blast furnace slag is a byproduct of blast furnace iron production that results from the smelting of iron ore, coke, and fluxes during the operations of extracting iron from iron ore. (G. C. Wang, 2016). Every year, approximately 600 million tons of slag from the steel industry is produced worldwide, with blast furnace slag accounting for 58% of this total. Another waste material produced in glass industries with a high SiO_2 content is waste glass. Bagasse ash is a byproduct of the sugar industry's combustion process. Bagasse ash is a silica-rich alternative source (SiO_2). Silica fume is produced as a byproduct of the silicon and ferrosilicon alloy industries. It is micro silica with a silicon content of 75% or higher and non-crystalline silica. (Panesar, 2019). Total annual silica fume production in the world is around 1 million tons (Türköz et al., 2021). Rice husk ash is a by-product obtained from the rice mill process whose generation accounts up to 200 kg per ton of rice (Tayeh et al., 2021). It is the highest silica enriched waste. Awash Melkassa factory also releases solid byproduct at the end of the production of aluminum sulfate which is enriched in silica content. The factory is expected to have the capacity to produce 13,600 metric tons of aluminum sulfate when it fully functions. Around 40% of produced aluminum sulfate is expected to generate waste. These filter cake have high silica content.

Table 2.1 Silica Content in Silica Enriched Industrial Byproducts

Materials	SiO_2	Reference
Iron Ore Tailings	24–75	(J. Zhao et al., 2021)
Coal Gangue	39–61	(Y. Zhang et al., 2020)
Red Mud	17–25	(M. Wang et al., 2021)
Fly Ash	46–56	(Majchrzak-Kucęba et al., 2011)
Blast Furnace Slag	30–40	(Özbay et al., 2016)
Waste Glass	60–77	(Zimmer et al., 2019)
Rice Husk Ash	90-98	(Tayeh, et al., 2021)
Bagasse Ash	50-55	(Chindaprasirt et al., 2020)
Silica Fume	85-95	(Siddique et al., 2020)
Awash Melkassa Aluminum Sulfate Filter Cake	50-70	(Tadesse et al., 2018)

Many industrial solid wastes are rich in silica (SiO_2) which can be used as supplementary cementitious material (SCM) (Zheng, Cui, et al., 2021), synthesis of zeolite (Hartmann, et al., 2014), fertilizer (Dikshit, et al., 2001), Mesoporous Silica (Amin et al., 2021), Adsorbent (Rovani et al., 2018) and many more application of silica enrich industrial waste have been conducted by researchers. In this study Awash Melkassa chemical factory silica enrich byproduct has been used for both application of partial replacement of cement clinker and synthesis of zeolite.

2.2. Valorization of Silica Enriched Industrial Byproduct Raw Materials on Replacement Material for Cement Clinker

2.2.1 Cement

Cement is the most commonly used material in infrastructure development projects. It is regarded as a long-lasting building material. However, the environmental impact of cement is becoming a growing concern, as cement industries account for approximately 2.5% of total global waste emissions from industrial sources. Portland cement is the most common type of cement. It is produced using the drying method. The first step is to crush and mix raw materials (limestone, clay, and other materials) using continuous millers. The material is then heated to around 1450 ^{o}C in cylindrical steel rotary kilns, where chemical transformation occurs to form a new compound known as clinker. After cooling and grinding, the clinker is mixed with gypsum and limestone. Finally, fine cement is produced. The cement clinker production process generates large quantities of CO_2. Therefore, since cement clinker is the key source of CO_2, a good approach to reducing CO_2 emissions during cement manufacturing may be to use less cement clinker.

Cement clinker is made by sintering a precisely specified mixture of raw materials (raw meal, paste or slurry) containing elements, usually expressed as oxides, CaO, SiO_2, Al_2O_3, Fe_2O_3 and small quantities of other materials. The raw meal, paste or slurry is finely divided, intimately mixed and therefore homogeneous.

Generally cement is classified as ordinary portland and portland pozzolanic cement. Ordinary Portland cement (OPC) is the most widely used type of cement, which is suitable for all general concrete construction. It is the most commonly produced and used type of cement around the world, with annual global production of around 3.8 million cubic meters per year. This cement is suitable for all kinds of concrete construction. It has good resistance to cracking and dry shrinkage but less resistance to chemical attack. OPC is not suitable for the construction work which is exposed to sulphate in the soil (B. Guo et al., 2022; Sha et al., 1999; Y.-S. Wang et al., 2018; J. Zhang et al., 2018; J. Zhu et al., 2021). Portland pozzolanic cement is prepared by grinding pozzolanic clinker with Portland cement. It is also produced by adding pozzolanic with the addition of gypsum or calcium sulfate or by intimately and uniformly blending Portland

cement and fine pozzolanic aggregate (Taher et al., 2019). Pozzolanic cement is manufactured by mixing 30% of pozzolanic to Ordinary Portland cement clinkers(El-Diadamony et al., 2018). Ordinary Portland Type I cement is typically considered general-purpose cement and is most often used for general construction purposes. This research study select OPC cement type due to its wide application which can be used for dams, road construction, high load construction, high load construction, despite PPC which can only be applicable to house hold construction with less application than OPC.

2.2.2. Silica Enrich Industrial Byproduct for Cement Clinker Replacement

Various types of industrial byproducts are produced. With increased environmental awareness and the potential dangers of industrial byproducts, utilization has become an appealing alternative to disposal. Silica fume (SF), a byproduct of the smelting process in the silicon and ferrosilicon industries, is one such by-product. Amorphous silicon dioxide SiO_2 is a component of silica fume that ranges from 85 to 98%. Carbon, silicon carbide, and alkaline (earth) metal oxides are the most common impurities. In the design and development of high strength, high performance concrete, silica fume is extremely effective (Smirnov et al., 2022). (Karein et al., 2017) studied the effect of silica fume as a partial replacement for cement in concrete, which increases the durability of reinforced concrete and reduces cement usage. The highest compressive strength was achieved by silica fumes-containing samples with w/b = 0.35 and 350 kg/m^3 cementitious material samples at all ages; the strength was 54.7 MPa at 7 days and increased to 81 MPa at 90 days. When compared to the control sample, the obtained results showed an increase in strength and surface electrical resistivity, as well as a decrease in permeability for both slurry silica fume and granule. (Tripathi et al., 2020) studied effect of nitric acid on concrete made with SF was investigated and the optimum replacement level of OPC with SF in terms of compressive strength. The OPC was replaced in part with SF (5, 10, 15, 20, and 25%) to obtain the optimum replacement level in terms of compressive strength. The best replacement levels were found to be 20% after 7 and 28 days curing. (S. Zhao et al., 2019) studied impact of SF on the mechanical properties and dynamic behaviors of concrete under impact loading was investigated. The physical structure and chemical composition of concrete have changed as a result of the use of SF instead of cement. Cement, fine aggregates, coarse aggregates, water, and SF were among the components used. The SiO_2 content of the SF used in

this experiment is 93.67%. On 18% SF replacement, higher compressive strength was observed. For high-performance concrete with improved mechanical qualities, SF is especially recommended as a substitute for moderate amounts of cement.

Fly ash is a waste product from coal-fired power plants. Pulverized coal is blown into combustion chambers for immediate combustion. The smaller ash particles (Fly Ash) fly out with the exhaust flow, while the heavier ash particles (bottom ash or slag) settle to the bottom of the burning chamber. Electrostatic precipitators, bag houses, and other technologies are used to catch Fly Ash particles before they leave the stack. Fly ash is a pozzolanic, which means it's a siliceous and aluminous mineral that combines with the lime freed during the hydration of cement to generate cementitious materials when exposed to moisture (Giergiczny, 2019).

(Darweesh, 2020) studied effect of pulverized waste of fly ash as a raw meal component for partial replacement of OPC Clinker at a lower temperature. Clay, limestone and pulverized fly ashes (PFa) are burned in a rotating kiln to temperatures of 1410-1280 °C for the creation of clinker. OPC was made by mixing each of the prepared clinkers with a variable quantity of raw gypsum (4 wt%) OPC. The cement was then cured for 1, 3, 7, 28, and 90 days to compare and determine the optimum PFa concentration using compressive strength testing. The inclusion of PFa resulted in a decrease in free lime concentration at the expense of other primary raw materials. All mix composites can be precisely matched to ASTM requirements. With the addition of PFa, temperature was reduced significantly, and compressive strength was nearly identical to that of the blank. In terms of compressive strength, 25-35 wt. percent PFa would be ideal. The author determined that the optimal PFa content should not exceed 35 wt%. Further increases had a negative impact on both cement phases and cement clinker compressive strength.

Many researchers have recommended using meta kaolin to replace Portland cement in order to improve quality and minimize the cement industry's CO_2 emissions. Meta kaolin is made by calcining and heating kaolin, and it typically comprises 40–45% Al_2O_3 and 50–55% SiO_2 (Kalpokaitė-Dičkuvienė et al., 2019). In a study, residual ash from incinerators was combined with meta kaolin as a cement substitute in concrete. It was discovered that replacing 10% of the cement with Meta kaolin increased cement hydration and, as a result, concrete characteristics.

(Tawfik et al., 2019) concluded that the flexural strength of concrete was satisfactory with 10% meta kaolin content. (Mohd Nasir et al., 2021) reported 10% meta kaolin treated crumb rubber replacement respect to its permeation durability behavior is discovered. The results showed that reduction in permeation properties.

Construction and demolition (C&D) wastes are considered the primary wastes produced by the construction and demolition industries. C&D wastes are considered the major wastes produced by the construction and demolition industries. Packaging materials and land-clearing waste are examples of construction and demolition waste. Some research looked into making Portland cement clinker using civil construction waste as an alternative raw source, such as recycled concrete waste. (Ai et al., 2015; Papastamoulis et al., 2021; Yuanyuan et al., 2021; Zahiri et al., 2019).

(F. Costa et al., 2021) studied civil construction waste (CCW) from water treatment center for replacement of clinker in portland cement. The CCW contains a higher concentration of Ca, Si, Al and Fe, which are important for the formation of the crystalline phases of the Portland clinker. 3 granulometric fractions CCW0-10: concrete (1%), mortar (47%), rock (2%), ceramic (13%), and soil (37%). • CCW10-20: concrete (41%), mortar (39%), rock (13%), and ceramic (7%). • CCW20-40: concrete (57%), mortar (34%), rock (7%), and ceramic (2%). CCW was beneficiated, separated, mixed and calcined at 1450 ^{0}C. It was observed that the potential waste can substitute clay up to 14.3% and high C_3S content was observed. Some experimental cement with CCW showed compressive strength performances at 28 days higher than those seen in the cements used as reference.

(Zhutovsky et al., 2021) investigated use of recycled concrete waste in to new clinker. The hydrated cement paste is a product of a Portland cement reaction with water. It mainly consists of calcium silicate hydrate (C-S-H) and Portlandite (H. F. W. Taylor). The phase transformations in hydrated cement paste upon heating in the temperature range from 600 to 1450 ^{o}C were investigated. Ferrite phase ferrite is higher in the recycled clinker, and aluminate phase content is lower than the normal clinker content.

(Prošek et al., 2020) studied different type of recycled concrete for clinker replacement. Four recycled concrete from recycled railway sleeper (RRS), recycled drainage channel (RDC) and monolithic columns (RC1 and RC2) were prepared. Replacing Portland cement with the recycled

material in pastes led to a significant increase of tensile strength, while deterioration of compressive strength was negligible when the concrete fines contained higher amounts of residual clinker and when the amount of fines did not exceed 30% of Portland cement weight. RRS 9.5 wt. %, RDC 7.9 wt. %, RC1 12.5 wt. %, RC2 7.9 wt. % of C_2S amount was recorded. The author concluded that replacement by recycled concrete materials in paste have significant enhancement on tensile strength with 50% of the recycled concrete from monolithic columns showed twice fold increment in tensile strength. Although compressive strength seems to be affected negatively, but replacements up to 30% did not lead to significant deterioration.

(Cao et al., 2019) studied utilization of crushed steel slag in cement industry directly using multi-phased clinker sintering technology. Steel slag used in this study was basic oxygen furnace steel slag supplied from Wuhan Iron and Steel. The multi-phased cement clinker prepared at 1400 ℃ with substitution contains 16.86% steel slag had comparable grind ability and soundness to the normal Portland cement clinker. The compressive strength reduced with different content of steel slag while increasing curing time. 12.42% and 16.86% of steel slag content showed comparable compressive strength with OPC with 42.5 grades.

(Gao et al., 2021) investigated use of steel slug in cement clinker. The steel slag, limestone, sand stone, clay, and iron ore used in the preparation of raw meal were provided by Shanxi SS Cement. The steel slag used in this work, sourced from the steel making process in a basic oxygen furnace, was collected from Taiyuan Steel and Iron Group. 3 raw meal have been prepared steel slag clinker(SSC) A (80.46 wt% limestone, 5.52 wt% sandstone, 6.64 wt% clay, and 7.39 wt% steel slag), B(81.57 wt% limestone, 8.15 wt% sandstone, 3.41 wt% clay, and 6.87 wt% steel slag) and iron ore clinker(84.34 wt% limestone, 5.53 wt% sandstone, 5.68 wt% clay, and 4.44 wt% iron ore). The authors concluded that SSC A showed slight decrement in distribution of major phases compared with iron ore clinker. The main phases of SSC B showed a relatively higher C_3S and a lower C_2S than those of iron ore clinker.

(Abdul-Wahab et al., 2019) investigated application of zeolite/kaolin combination for replacement of partial cement clinker in Oman. Kaolin and zeolite was also collected from mountains in Oman and spent hydro-processing catalyst generated in Oman by the petroleum refining industry respectively. Cement clinker, gypsum, and additives (zeolite and kaolin) are mixed together in the required proportions to produce the final cement product. Effect of only

zeolite and zeolite combined with kaolin on compressive strength in replacement for cement clinker was studied. Best compressive strength values were obtained with 88% cement clinker, 5% gypsum, and 7% zeolite for the zeolite-containing cement. Quantities of 70% cement clinker, 5% gypsum, 10% zeolite, and 15% kaolin gave the best results for zeolite-kaolin-based cement, resulting in a substitution of than 25% cement clinker.

It have been seen that various research attempt to decrease CO_2 emissions from cement production through making use of industrial waste as opportunity fuels and growing secondary concrete product. In concrete cement may be partly changed through exceptional supplementary cementitious materials. In the latest years pozzolonic materials, glass powder and silica fume are utilized in concrete as a partial cement substitute to enhance the strength of concrete.

The utilization of silica enriched byproduct in the cement industry makes good economic sense in managing waste and reducing the cement industry's demand for raw materials. They are suitable materials that can partially replace the clinker in the cement production because they have some similar physical and chemical characteristics to that of cement. More than 80% of silica enriched byproducts contents are silicate and aluminate, which are basic constituents that are required in the cement industry. This indicates it can be used as partial replacement of cement.

2.2.3. Mineral Composition of Portland Cement Clinker

CaO, SiO_2, Al_2O_3 and Fe_2O_3 are the major component of cement clinker, it accounts for more than 95% and MgO, TiO_2, P_2O_5 and alkalis are the minor components in initial less than 3%. The major components are not present in individual oxide, but exist as compound formed by two or more oxides C_3S, C_2S, C_3A and C_4AF are the composition minerals of the clinker and these minerals are the result of the pyro processing or reaction of oxides in the kiln.

Alite (C_3S) has a nesosilicate structure with isolated ($0SiO_4$) tetrahedra which are connected by Ca–O polyhedral (Ludwig et al., 2015). Because of the importance of alite, many research works has been done on the crystal structure of C_3S in the past 80 years. C_3S exhibits a complex polymorphism depending on temperature or impurities. Due to the complicated structure and the difficulty in preparing single crystal of C_3S, it is difficult to obtain crystal structure information

of individual polymorphs. Studies have shown that amorphous silica would affect the hydration of C_3S (Oertel et al., 2014; X. Wang et al., 2020; Zheng, Monasterio, et al., 2021). This component is responsible to Generates more heat rapidly, Hydrates more rapidly, Possess less resistant to chemical attack and Develops early strength. Belite (C_2S) is known to exist in six crystalline polymorphs. The polymorph present at very high temperatures is α-belite that transforms into the αH′-polymorph at 1425 °C which is stable down to 1160 °C being transformed to αL′-belite. The latter is replaced by the β-form at approximately 650 °C. Polymorphs from the α-family and the β-form have an almost identical crystal structure. When further cooled, β transforms into γ that is stable at room temperature and the only polymorph with a clearly distinct structure (H. F. Taylor, 1989). It imparts ultimate strength to the cement, offers more resistant to chemical attack, hardens more slowly and hydrates slowly. Tricalcium aluminate (C_3A) is the most reactive component of the portland cement; C_3A contributes to the strength of the cement paste at one to three days. SiO_2 exhibited pozzolanic reaction activity to form additional C-S-H gels, thereby promoting the hydration process of C_3S and improving the compactness of hardened cement paste. C_3A shows weak against sulphur attack, reacts fast, generating large amount of heat, does not contribute to develop strength, causes initial setting of cement and first to react with water. C_4AF is poor cementing value which reacts slowly and generating small amount of heat and comparatively inactive. Gypsum is calcium sulphate with two molecules of water. Gypsum reacts with C_3A and turns it into Calcium Sulpho Alumintate. Since Gypsum reacts with C_3A and C_3A reduces. Thus C_3A is not available for reaction with water and hence setting action is reduced. Reduction in setting action means elongation of setting of cement i.e. setting time increases.

Table 2.2 Approximate Mineral Composition of the Portland Cement Clinker

Compound	Formula	Notation	Wt.%	Reference
Celite	$Ca_3Al_2O_6$ $[3CaO{\cdot}Al_2O_3]$	C_3A	8-10	(Elmrabet et al., 2021; Kleib et al., 2021; Rmaidh et al., 2021; Sorrentino et al., 2021)
Ferrite	$Ca_4Al_2Fe_2O_{10}$ $[4CaO{\cdot}Al_2O_3{\cdot}Fe_2O_3]$	C_4AF	8	(Z. Guo et al., 2021; Kleib, et al., 2021; Mrak et al., 2021)
Belite	Ca_2SiO_4 $[2CaO{\cdot}SiO_2]$	C_2S	18-20	(Kleib, et al., 2021; Mrak, et al., 2021; Stutzman et al., 2014)
Alite	Ca_3SiO_5 $[3CaO{\cdot}SiO_2]$	C_3S	55-65	(Kleib, et al., 2021; Rajiman et al., 2021; Schraut, 2021)
Gypsum	Ca_3SiO_5 $[3CaO{\cdot}SiO_2]$	CSH_2	3-5	(Awadh et al.; Barbosa; Kleib, et al., 2021)

Silica has significant influence on major component of cement, although few minor components in cement can affect cement property. Alkaline like Na_2O, K_2O, SO_3, MgO and Fluorine, Chloride are minor constituent of cement clinker. Alkalis in the cement react with CO_2 (in the atmosphere) to form alkali carbonates, which they react with $Ca(OH)_2$ liberated by the hydrolysis of C_3S to form $CaCO_3$. This precipitates and induces a rigidity of the paste. Therefore alkaline in cement should be maintained on allowable range. The allowable amount of minor constituent in cement clinker is summarized (Table 2.3).

Table 2.3 Influence of Commonly Minor Constituents on Manufacturing Process

Minor constituent	**Typical range of levels in clinkers**	**Effect on Cement Clinker**
Na_2O	0.07 - 0.22	favors the formation of β-C_2S decrease the viscosity
K_2O	0.52 - 1.00	Decreases sulphatisation
SO_3	0.50 - 1.50	A lower strength development
Fluorine	0.01 - 0.20	Accelerate and enhance the reactivity of the cement raw mix.
Chloride	0.005 - 0.05	Increased solubility of cement solids
MgO	0.80 - 2.50	Low mobility / solubility in alkaline solutions

2.2.4. Cement Clinker Composition Calculation

A technique of calculation proposed by Bogue in 1929 can be used to estimate the levels of the four clinker minerals(Bogue, 1955). The method involves the following assumptions:

- All the Fe_2O_3 is combined as C_4AF
- The remaining Al_2O_3 (i.e. after deducting that combined in C_4AF) is combined as C_3A

The CaO combined in the calculated levels of C_3A and C_4AF and any free lime are deducted from the total CaO and the level of SiO_2 determines the proportions of C_3S and C_2S. The procedure can be expressed mathematically (in mass %) as follows:

$$C_3S = 4.071(\text{Total CaO} - \text{Free Lime}) - 7.6 * SiO_2 - 6.718 * Al_2O_3 - 1.43 * Fe_2O_3 \ldots\ldots 2.1$$

$$C_2S = 2.867 * SiO_2 - 0.7544\, C_3S \ldots\ldots 2.2$$

$$C_3A = 2.65 * Al_2O_3 - 1.692\, Fe_2O_3 \ldots\ldots 2.3$$

$$C_4AF = 3.043\, Fe_2O_3 \ldots\ldots 2.4$$

The calculated figures may differ slightly from the clinker mineral proportions measured by quantitative X-ray diffraction or microscopic point counting. However, in terms of strength development, heat of hydration, and sulfate resistance, it provides a solid indication to cement

qualities. When determining the compound composition of cements (rather than clinkers), the standard assumption is that all SO_3 is mixed with Ca (i.e. present as calcium sulfate). The total CaO is thus lowered by 0.7 * SO_3 and the free lime level.

The Bogue equations were formulated with a small data set of samples, which meant that the quantification was limited only to four clinker phases and the estimation of the phases was not accurate for all cases. It was apparent when (H. F. Taylor, 1989)found that the Bogue method consistently under predicted the alite and over predicted the aluminate contents in cement. The Modified Bogue method, proposed by Taylor (H. F. Taylor, 1989). It took into account the measurement of sulfate and other minor phases in cement from a finish mill. Modified Bogue's equations were formulated in a similar style to the Bogue approach, implying that there was still insufficient data to be regarded statistically reliable.

2.3. Valorization of Silica Enriched Industrial Byproduct Raw Materials in to Zeolite based catalyst

2.3.1. Zeolite

The term “zeolite” is primarily based totally at the Greek phrases for “to boil” and “stone” and it's been recognized for the reason that 250 years ago. At that time, the Swedish mineralogist, A.F. Cronstedt (1722–1765), located the formation of a massive quantity of steam whilst heating the cloth Stibnite which indicated porous and adsorption capacity. At present, over two hundred extraordinary zeolite frameworks were identified. In general, zeolites are crystalline aluminosilicates with a described micro pore structure. Within zeolites, an excellent variety of factors may be isomorphously included and lots extra factors or their oxides may be hosted via means of zeolites.

Zeolites occur naturally as well as could be prepared in the laboratory. Zeolites are generally divided into 2 fundamental categories: natural (e.g., clinoptilolite, mordenite and garronite), and the synthetic zeolite (e.g., zeolite A, P, X and Y)(Oruji et al., 2018). It is observed that natural zeolites have higher resistivity and thermal stability in the distinctive environments. Thermal stability and chemical resistance increase with the increase of silica-alumina ratio as well as in the presence of alkali cations in the zeolite framework.

The interest in zeolites and their application has not stopped increasing for decades. This can be explained by the exceptional versatility of those particular structures and the almost infinite variety of use they allow. On top of the 34 different species of zeolite minerals (natural), hundreds of structures can be artificially tailor made; this widens the scope of use of those materials.

Synthetic zeolites are highly pure with uniform crystal size and beneficial for specific industrial applications. In contrast, natural zeolites include specific foreign substances that have a no uniform crystal size. Natural zeolite takes several days to decades to create, whilst synthetic zeolites can be produced in the laboratory from a few hours to a few days with controllable pore size, surface characteristics of the adsorbent and excellent thermal stability. However, at a slightly higher cost, this makes a much greater uniform product than naturally occurring zeolites. Synthetic zeolite may be synthesized from numerous sources with distinctive chemical compositions and physic-chemical properties. The crystal length of artificial zeolites is normally observed withinside the variety of 1.0– 10.0 μm whilst the density varies in among 2.0 to 23.0 g/cm^3. Synthetic zeolites bulk precise gravity lies in among 0.80 and 0.90 gm/cm^3. Optically, the refractive indices of synthetic zeolite are ranging between 1.47 and 1.52. Zeolite has a water absorption potential of 45.0 to 75.0 ml/100 gm.

Zeolites are crystalline, hydrated aluminosillicates. The general formula representing their structure could be written as follows:

$$M_{x/n}[(AlO_2)_X(SiO_2)_Y] \bullet wH_2O \quad \text{..... 2.5}$$

In this general formula we can note that M is the positive counter ion of valence $+n$ which balances the positive charge due to the x (AlO_2^-) groups. The ratio y/x represents the Silicon-to-Aluminum ratio and is a parameter of paramount importance to describe the zeolite's properties. Eventually, the sum ($x + y$) represents the total number of tetrahedral in a unit cell of the particular zeolite.

The microscopic structure of each zeolite is based on the tetrahedral formed between small silicon (Si^{4+}) or Aluminum (Al^{3+}) Cation and four oxygen atoms. Figure 2.1 shows the tetrahedral of oxygen coordinated with silicon and aluminum.(Lemoine, 2013)

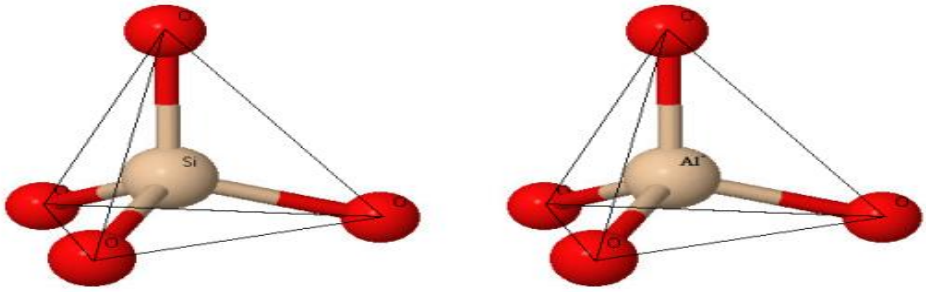

FIGURE 2.1 Tetrahedral of Oxygen Coordinated with Silicon (Left) and Aluminum (Right)

Nowadays, zeolites have plenty capacity ranges of applications such as technical, environmental, industrial, commercial, agricultural, cracking and alkylation processes, and biomedical because of their porous character and their ion-exchange properties(Yilmaz et al., 2009). Naturally occurring zeolites are used as materials for the construction and paper industry. It also used in agriculture and other applications. Laboratory synthesized zeolites with defined pore sizes have a wide variety of applications in adsorbents, catalysts or molecular sieves and catalysts of oil refineries (Minachev et al., 1973) removing radioactive contaminants (Malekpour et al., 2008) and laundry (Fruijtier-Pölloth, 2009).

2.3.2. Silica Enrich Industrial Byproduct for Zeolite Synthesis

The studies of zeolite synthesis from coal fly ashes have been published since 1990. Coal ash is the major solid residue produced by coal combustion in thermoelectric power plants. As it contain available Si and Al in their composition, are suitable to zeolite synthesis (Bukhari et al., 2015). Coal fly ash as Al and Si sources for zeolite synthesis was studied by (Höller et al., 1985).

Coal combustion products (CCPs) are produced in coal-fired power plants, and coal fly ash (CFA) is the abundant component. Due to the high and increasing energy need, the 7000 coal-fired power plants produce MT600 of CCPs annually and CFA is the 80% (Belviso, 2018; Lee et al., 2017; Pedrolo et al., 2017). Most of the CFA is not emitted because power plants clean the flue gases by particle removal, but it requires large areas to storage so is mixed with water to deposit in controlled dumps. The main problems of CFA management are the large area required for disposal, its toxicity and the expensive costs of transportation. With an expected 0.6 ha per MW, the area required in 2020 was 82,200 ha. CFA disposal costs are function of the type of

ash, distance from the plant to the landfill, transportation, weather, legal requirements and potential for future uses. Alkaline-fusion and alkali-digestion activation have been studied to synthesize high pure zeolites from CFA. Zeolites A and X are synthesized by alkali-fusion activation while zeolite P by alkali-digestion.

According to (Belviso, 2018; Koshy et al., 2016; Lee, et al., 2017; Ozdemir et al., 2019; Z. Zhang et al., 2017) zeolites Na-X (FAU), Na-Y (FAU), Na-A (LTA), Na-P (GIS), ZSM-5 (MFI) and phillipsite (PHI) have been synthesized by hydrothermal treatment in alkaline medium. Alkali activation is suitable to extract the Si and Al from the CFA waste. The characterization of the waste zeolites synthesized by alkali activation and hydrothermal method shows that the amount of Si and Al dissolved from glass, quartz and mullite are 50%, 2% and 2%, respectively. Studies also reveal that quartz and mullite dissolve completely applying fusion and hydrothermal activation (Belviso, 2018; Koshy, et al., 2016; Lee, et al., 2017; Ozdemir, et al., 2019; Z. Zhang, et al., 2017).

Zeolite X and Y are synthesized from CFA by fusion and hydrothermal processes. The SiO_2/Al_2O_3 ratio in the CFA is from 3.3 to 3.5, what is better for zeolite Y than for zeolite X, but not selective. So, it must be increased adding Na_2SiO_3 or decreased with $NaAlO_2$ to have a specific synthesis of zeolite Y or X. Crystallinity also depends on the amount of Na^+ because it balances the Al^{3+} that went into the zeolite. As zeolite Y transforms to hydroxysodalite at high pH, NaOH is not adequate neither as alkaline medium either to increase Na^+. Na_2SiO_3 and $NaAlO_2$ are proper reagents to adjust Si/Al ratio and add Na^+ without increasing the pH (Lee, et al., 2017).

(Z. Zhang, et al., 2017) reported an interesting procedure to synthetize zeolite 13X by hydrothermal treatment using CFA as the only sources for Si and Al. The zeolite 13X obtained has highly crystalline structure and uniform octahedral particles.

Palm Oil Mill Fly Ash (POMFA) is used as source for concrete or solid additives but it can also be used as Si source to synthesize zeolites. As it has been commented, zeolites have good CO_2 adsorption and desorption properties and zeolite X, especially zeolite 13X, has higher absorption capacity and better selectivity for CO_2 than other types of zeolite(Kongnoo et al., 2017) studied an interesting and low-cost method to synthesize zeolite 13X from POMFA by alkaline fusion

and hydrothermal treatment. They studied the effects of mass ratio of NaOH/ (SiO_2 and Al_2O_3 precursors), fusion temperature and fusion time, and the acid activation to increase the CO_2 adsorption capacity. The higher efficiency, zeolite 13X 85%, was obtained with NaOH/(SiO_2 and Al_2O_3 precursors) ratio of 1.6, 600 ºC, 1h. Inactivated POMFA zeolite 13X has a BET surface area of 643 m^2 /g and a CO_2 adsorption capacity of 223 mg/g. Acid-activated POMFA zeolite 13X has 22% higher CO_2 adsorption capacity than inactivated and 11% higher commercial zeolite 13X. However, the crystallinity of the zeolite 13X decreases 17% in acid activation although FAU structure is stable (Kongnoo, et al., 2017).

Bagasse fly ash (BFA) is a solid residue from bagasse combustion system in sugar industries and contains various types of particles with different size, morphology and chemical composition. Fine particles contain Si and are a suitable source for zeolite synthesis. (Purnomo et al., 2012) studied the synthesis of high pure and regular zeolites using BFA as Si and Al sources with low residual waste. Extraction is performed with NaOH fusion and residual waste is separated to remove impurities that reduce zeolite formation. The Si/Al ratio of the alkaline aqueous solution is adjusted according to the zeolite pursues and synthesis is made by hydrothermal method. Adjusting the pH is also important because zeolites dissolve in high alkaline medium. Low temperature leads to synthesize zeolite with higher purity and smaller particle size.

(Gil et al., 2016) commented in their review article about the studies of aluminum dross valorization, interesting results have been published about the synthesis of zeolite X from aluminum and silicon wastes. Synthesized zeolite X was based on silicon sludge and aluminum black dross. Silicon sludge was hydrolyzed with aqueous NaOH to obtain Na_2SiO_3, H_2 was also generated. The available Al of the aluminum black dross was precipitated as $Al(OH)_3$ with aqueous NaOH and hydrolyzed to $NaAlO_2$, generating H_2 but not CO_2. Si and Al sources were mixed in the proper Si/Al ratio to synthesize zeolite X and the residual liquid is saved to other synthesis. The waste zeolites X prepared were characterized by XRD, Si/Al molar ratio and BET surface area. It has Si/Al ratio from 1.0 to 1.5. The selective synthesis of zeolites A and X from crushed stone powder and aluminum ash was reported by (Kusakabe et al., 1997). The procedures used by the authors include a step of extraction of Si and Al components by HCl treatment, followed by a hydrothermal treatment with NaOH at 80 – 120 ºC. (L. Ma et al., 2019)

reported the synthesis of a magnetic zeolite, with a structure of cancrinite, from fly ash, red mud and steel slag, also considering an hydrothermal procedure at 374 ºC in presence of NaOH.

Table 2.4 Raw Materials Used for Synthesis Zeolite

Name of raw materials	Types of zeolite synthesized
Rice husk ash	Analcime, Y
Fly Ash	X-type Zeolite
Waste Basalt Powder	X-type Zeolite
Paper Industry Sludge	A-type zeolite, P-type zeolite
Spent catalytic cracking catalyst	A-type zeolite
Waste Perlite	Na-P1
SiO_2 Sinter and Perlite glass	Zeolite Y, P, and gmelinite
Lithium Slag	NaX-1
Brazilian chrysotile and rice husk	NaA
Coal Fly Ash	hydroxysodalite or Na-P1

2.3.3. Methods Used for Synthesizing Zeolites

Zeolites can be made from a variety of natural and synthetic source materials. However, from an economic standpoint, all raw materials are not ideal for zeolite synthesis. As a result, raw materials should have some characteristics. Numerous physicochemical and solvothermal approaches, such as the hydrothermal method, have been used and developed to synthetized zeolites. (Sugano et al., 2005), alkali-fusion method (Wajima), sol-gel method (Tsujiguchi et al., 2014), and alkali-leaching method (Shoppert et al., 2017). However, the choice

of the synthesis approach depends on which type of zeolite will produce. Each method has some advantages and few limitations.

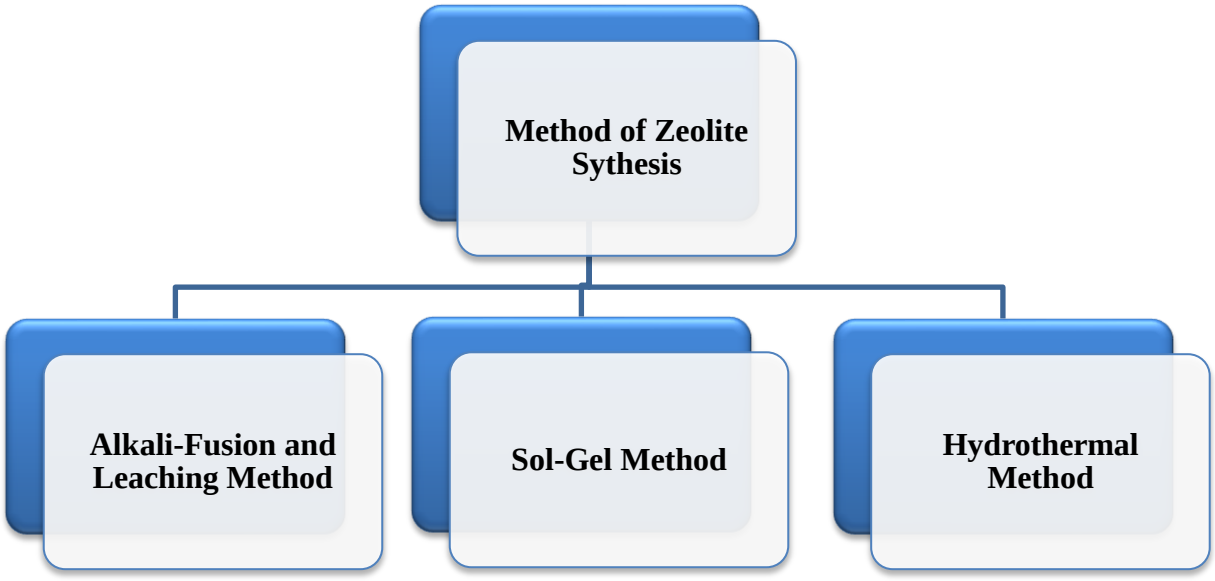

FIGURE 2.2 Methods for Synthesizing Zeolite

A. Alkali-Fusion and Leaching Method

The alkali fusion approach in zeolite synthesis refers to a generic method of decomposing silica or alumina-rich materials in the presence of alkali, which acts as an activator for the formation of soluble aluminate and silicate salts. Alkali (e.g., NaOH) is also utilized in solvothermal procedures, however there are several differences between solvothermal and alkali fused approaches. Alkali is used to prevent multiphase and fused in solid-state with raw materials before moving to any solvent in the alkali fusion approach, whereas in the solvothermal approach, alkali is used in terms of solution state and acts as a mineralizer of the reaction media. Inside the alkali-fusion technique, the raw material is first fused with alkali (e.g., NaOH) before being subjected to a hydrothermal treatment (Belviso et al., 2017). At the hydrothermal treatment, the fused product combined with water and treat with the proper conditions like heating with suitable temperature for the crystallization to form zeolite (Christidis et al., 2008).

Factors affecting the alkali-fusion strategies are: (i) silicon aluminum ratio of the raw material, (ii) concentrating the reacting alkali medium, (iii) temperature, and (iv) crystallization rate (H. Ma et al., 2010). It was observed that alkali activator has a significant impact at the synthesis of

synthetic zeolite (H. Ma, et al., 2010). In addition, Takaaki Wajima illustrated the alkali fusion approach to synthesize zeolite-A, zeolite-X and hydroxysodalite from the BFS (Wajima). In a preceding study, (Chen et al., 2012) suggested the hydrothermal reaction with alkali fusion to make zeolite X from lithium slag. The zeolite was found to have exceptional characteristics. Furthermore, in most of the processes, the alkali fusion approach is combined with a synthetic zeolite hydrothermal technique. Excessive temperatures, duration, and pressures are required for both strategies. Commercial chemicals that are high in alumina silicate, natural resources in the earth's crust, and industrial by-products are the main sources for zeolite production. Specific forms of zeolite products, such as zeolite-X, zeolite-P, hydroxysodalite, tobermorite, and nepheline, can be obtained under varied experimental settings. The benefits of this technology include the ability to employ low-grade raw materials without purification and the production of anhydrous zeolite with high purity. While it still has the issues of excessive energy intake and the related cost.

Any other technique of leaching that keeps the silica-alumina ratio out of the leachates containing NaOH solution is known as alkali leaching. The following elements influence the alkali leaching technique: I desalination rate, (ii) leachate free solid product silica-alumina ratio, (iii) fusion temperature, (iv) leaching agent concentration, and (v) crystallization rate (Melian-Cabrera et al., 2006). Several investigators have stated different zeolites synthesis through alkali leaching method. For instance, (El-Naggar et al., 2008) synthesized the pure zeolites by alkaline leaching technique from the silica extract which become acquired from the fly ash. The main benefit of this technique is to get a perfectly efficient product. However, this technique typically suffers from the necessity for multiple steps; it takes a long time and is costly.

B. Sol-Gel Method

The sol-gel approach is used to synthesized zeolites by first creating an amorphous gel from an interaction between aluminate and silicate or silica sol. Metal salts (metal aluminate and metal silicate or silica sol) or metal alkoxides are the most common starting ingredients for zeolites. Metal alkoxides are sometimes employed to improve self-assembling functionality because their organic components can mix in micelles and their hydrolytic inertness rises with the size of the organic components (steric effect) and the number of alcohol groups in the ligand increases (chelate or cage effect). Extra hydrothermal treatment is necessary to obtain any crystalline

phase. This treatment can be performed via way of means of both conventional or microwave heating. There are numerous elements that could impact the overall performance of this approach. They are: (i) hydrolysis rate, (ii) temperature, (iii) heating rate and (iv) pH (Han et al., 2007; Serrano et al., 1995). There are many reports in this approach. For example, Han et al.(Han, et al., 2007) Using a template-free approach, the hierarchical porous zeolite materials were prepared. The fundamental advantage of this method is that it no longer demands the use of specialized and expensive equipment. (Wittayakun et al., 2008).

C. Solvothermal Method

The term "solvothermal synthetic technique" refers to the use of a solvent in the synthesis of zeolites. Water is the most important solvent in many ways, thus it has its own unique term to describe its use: "hydrothermal." Many organic solvents, such as alcohols (e.g., methanol, ethanol, pentanol), ethylene glycol, hydrocarbons, and pyridine, have been effectively utilized for zeolite production (Kovo et al., 2009). The solvent utilized in this method can be nonpolar, hydrophobic, or hydrophilic polar. When an ionic solvent (ionic liquids) is used, this phrase is referred to as ionothermal. As a result, all hydrothermal and ionothermal procedures are basically solvothermal approaches, although not all solvothermal methods are. Nonetheless, the essential difference between solvents remains molecular in both solvothermal and hydrothermal synthesis methods, as well as ionic in ionothermal synthesis. The ionic nature of ionic liquids examines certain characteristics such as low vapor pressures (Luo et al., 2019).

Ionothermal synthesis is a type of solvothermal synthesis in which the solvents utilized are mostly ionic chemicals rather than molecular in nature like solvothermal synthesis. Ionic liquids are the solvents utilized in the Ionothermal process of zeolite synthesis, and their ionic character affects several properties, such as low vapor pressures (Kovo, et al., 2009).

Solvothermal techniques currently rely on a variety of factors in addition to temperature and pressure, such as reactant sources, composition, silica and alkali ratio, aging duration, alkalinity, stirring settings, inorganic cations, seeding time, and solvent (Abdullahi et al., 2017). As a result, by properly altering the settings, this process allows for easy and unique control of the final zeolite product's size, form distribution, and crystalline. Attempts to synthesize zeolite using a solvothermal technique have been made before. (Cui et al.) evolved zeolite omega from magadiite with properly crystal structure and excessive purity through solvothermal approach.

Despite the accomplishment of various tasks in certain areas, it suffers from the use of specialized organic solvents that may be environmentally hazardous, as well as active and time-consuming procedures (Chen, et al., 2012). However, this approach is getting famous day through day.

D. Hydrothermal Conventional Method

Hydrothermal treatment is the most conventional and broadly carried out approach for synthesizing zeolite and is taken into consideration to be the earliest synthesis approach, main to excessive percentage (88–90%) product yields. It is a treatment that includes excessive temperature and pressure in the presence of water that acts not only as a solvent, however additionally aids in shifting pressure. It is a reaction mediator, able to changing the physical and chemical properties of reagents or products, and it possesses the capacity to be an accelerator in chemical reactions (Ji et al., 2018; Johnson et al., 2014; Zhou et al., 2009).

Hydrothermal synthesis can be categorized into subcritical and supercritical synthetic reactions based on reaction temperature. The temperature in subcritical synthesis is 100-240 °C, whereas in supercritical synthesis, the temperature can reach 1000 °C and the pressure can exceed 3000 bar.

The hydrothermal synthesis process is often used on a combination in a sealed vessel with heat treatment. Furthermore, other approaches fused with hydrothermal treatment, such as (I) microwave-assisted synthesis, and (II) sonochemical-assistance.

I. Microwave-Assisted Method

Microwave (MW) is a type of electromagnetic wave (0.3-300 GHz). Many chemical reactions, including organic and inorganic synthesis, selective adsorptions, oxidation-reductions, and polymerizations, have lately benefited from microwave dielectric heating.(Lorentzen et al., 1996). In general, microwave-assisted synthesis is faster, cleaner, and more energy efficient than traditional approaches. In 1988, Mobil Oil Corp. received the first patent for the microwave synthesis of zeolites, for the zeolites NaA (ETA) and ZSM-5 (MFI). The exposure of gels to microwave radiation was discovered to dramatically speed up the crystallization process. A variety of zeolites have been synthesized via MW-assisted hydrothermal synthesis thus far

(Bunmai et al., 2018; Qiu et al., 2018; Tayraukham et al., 2020; Vichaphund et al., 2019), such as zeolite A (LTA), faujasite (FAU), sodalite (SOD), analcime (ANA), beta (BEA), ZSM-5 (MFI), silicalite-1 (MFI), A1PO4-5 (AFI), VPI-5 (VFI), and cloverite (-CLO). The shape of zeolites can be effectively controlled using this technology. In addition, the synthesis of substituted zeolites has been reported to benefit via MW-assisted hydrothermal synthesis.

For almost a decade, the microwave-assisted technique has been widely used in zeolite synthesis due to its ability to create extremely pure compounds in a short amount of time. With microwave aid, the time it took to synthesize zeolite was cut in half, to only 9 hours (Ji, et al., 2018).

Microwave irradiation accelerates the annihilation of ordinary hydrogen (H) bonding in water, causing ion oscillation and dipole rotation, resulting in isolated, so-called active water molecules that respond to the composition gel's rapid dissolution. The coordination transition of the alumina octahedral to the tetrahedral layer, which is more reactive and critical in the development of zeolite materials, is favored when the microwave behavior is coupled with the hydration of shell water molecules. As a result, thinner membranes result, which affects the permeability properties of zeolite.(Zhou, et al., 2009).

II. Sonochemical-Assisted Method

The homogeneous mixture is treated with intense ultrasound radiation (20 kHz–10 MHz) before hydrothermal treatment in the sonochemical-assisted approach. Due to sonochemical effects from acoustic frequency, zeolite nucleation and formation were superior, and this method reduced the synthesis time from 24 to 16 hours. For optimal zeolite formation, the reactants are frequently enclosed inside a Teflon-coated Autoclave with hydrothermal synthesis pressure (up to 15 bars). Crystal nucleation and crystallization do not always occur in solution; instead, they can happen on gels that are present in the mixes. (Jusoh et al., 2017).

2.4. Zeolite Characterization

Zeolite characterization used to identify the crystalline product by comparing its properties to those of known standards. X-Ray diffraction, Scanning electron microscopy, Fourier Transform Infrared Spectrometry, particle size distribution, Brunauer-Emmett-Teller and thermo gravimetric analysis are methods used to describe a particular type of zeolite.

2.4.1. X-Ray diffraction (XRD)

The use of X-ray diffraction (XRD) to identify and characterize zeolites at various phases of their syntheses, modifications, and employment as catalysts is critical. X-ray diffraction is often used to detect the presence of crystalline zeolite and quantify the amount present. The elastic scattering theory underpins the X-ray diffract meter. All varieties of zeolites have different diffraction patterns. The goal of XRD patterns is to figure out the unit cell characteristics and consequently the unit cell volume (Von-Kiti, 2017). Cu-K radiations are used in powder X-ray diffraction experiments to estimate zeolite crystallinity. XRD may be used to identify phases as well. The zeolite sample is exposed to an x-ray beam ray during this action. The emergent rays' intensity is measured as a function of deflection angle 2θ.

Using Bragg's law

$$n\lambda = 2d \sin\theta \quad \ldots\ldots 2.6$$

Where n is an integer, λ is the wavelength, d is the lattice spacing and θ is the deflection angle

For crystals with cubic symmetry e.g. FAU, the size of the unit cell a_0 can be determined from the angular positions of the reflection.

$$a_0 = \frac{\lambda\sqrt{h^2 + k^2 + l^2}}{2\sin\theta} \quad \ldots\ldots 2.7$$

h k l is an orientation indicated by the Miller's indices

2.4.2. Fourier Transform Infrared Spectrometry (FTIR)

The FTIR detects vibrations induced by internal tetrahedral framework stretching as well as vibrations caused by exterior tetrahedral connections. The spectrometer has a detector, a beam splitter, and two mirrors, one fixed and one moving. The beam splitter separates the beam into two halves, one for the fixed mirror and the other for the moving mirror, using radiation from the IR source. The diffuse reflectance principle is used to run FTIR. A spectrum of absorbance and reflectance properties is emitted by an incident beam. Radiation that passes through the sample is recorded by detector. Radiations can be read as energy signals due to calibrations on the detector.

2.4.3. Scanning Electron Microscopy (SEM)

SEM is a versatile advanced apparatus that is mostly used to examine material surface phenomena. It has contributed significantly to our understanding of zeolite materials. The morphology of the zeolites is determined using SEM. The zeolites investigated with this device range in size from 20nm to 20m. The following data was acquired from the SEM image of the material: Topography describes an object's surface properties, such as texture, smoothness, and roughness, while morphology describes its shape and size. Crystal form, which includes zeolite type, crystal form, and size, exterior surface roughness, and phase purity, which includes the existence of different zeolite types. The crystal size is a guess of the crystallite size and or the aggregate particle size (Robson, 2001).

An electron gun, electron lenses, scan coils, and detectors are the main components of a SEM. A cathode or filament, commonly constructed of tungsten, generates an electron stream in the electron cannon. The electrons in the filament escape at a high voltage. The electron lenses determine the final size of the beam. The beam is scanned across the sample or target using scan coils. The electrons interact with electrons in the inner atomic shells when it hit the target. The detection of back scattered and secondary electrons that escape from the sample. If no detection is made, the image will be black (Ohrman, 2000).

2.4.4. Atomic Absorption Spectrometry (AAS)

Atomic absorption spectrometry (AAS) uses feature wavelengths of electromagnetic radiation from a light source to detect elements in both liquid and solid samples. Individual elements absorb wavelengths differently, and the absorbances of those elements are evaluated relative to standards. In effect, AAS takes use of the many wavelengths of radiation that can be absorbed by using different atoms. Analytes are atomized first in AAS to allow their characteristic wavelengths to be released and monitored. Excitation occurs when electrons in atoms jump up one energy level while taking in a specific amount of energy. This energy is a function of the element and correlates to a specific wavelength. Specific elements will be recognized and their concentrations measured depending on the light wavelength and intensity.

2.4.5. Particle Size Analysis (PSA)

The random changes in the intensity of light scattered from a suspension or solution can be used to measure particle size. Dynamic light scattering (DLS) is the most frequent name for this technology, although it's also known as photon correlation spectroscopy (PCS) and quasi-elastic light scattering (QELS). The mean value from the intensity distribution (called the Z average) and the polydispersity index (PDI) to define the distribution width are often the key results from DLS (Varenne et al., 2016). The intensity can be converted to a volume or numerical distribution. The sample in the cell is illuminated by light from the laser light source. The dispersed light signal is gathered using one of two detectors at a scattering angle of 90 ° (right angle) or 173 ° (back angle). The availability of two detectors gives you more options when it comes to measuring circumstances. A number of liquids can be used to disperse particles. To interpret the measurement findings, only the liquid refractive index and viscosity must be known. Due to the particle's randomly shifting relative position, the resultant optical signal shows random alterations.(Thomas, 1987).

$$D_z = \frac{\sum S_i}{\sum \left({S_i}/{D_i} \right)} \quad \ldots \quad 2.8$$

Here, S_i is the scattered intensity from particle *i* and D_i is the diameter of particle *i*. Note that the result is in the form of a harmonic mean. Since this mean is calculated from the intensity weighted distribution, leading to the statement that the Z-average size is the intensity weighted harmonic mean size.

2.4.6. Brunauer-Emmett-Teller (BET)

The Brunauer-Emmett-Teller (BET) theory aims to explain the physical adsorption of gas molecules on a solid surface and serves as the foundation for an important evaluation method for the size of a material's unique surface area. The Langmuir idea connects the monolayer adsorption of gas molecules onto a solid surface, also known as adsorbates, to the gas strain of a medium above the solid surface at a constant temperature. The adherence of atoms or molecules of gas to a surface is known as adsorption. Adsorption should not be confused with absorption, which occurs when a fluid passes through a liquid or solid. The amount of gas adsorbed depends

on the exposed surface are but also on the temperature, gas pressure and strength of interaction between the gas and solid.

Because of its excellent purity and strong interaction with most materials, nitrogen is commonly utilized in BET surface area analysis. Due to the weak contact between gaseous and solid phases, the surface is chilled with liquid N_2 to get detectable levels of adsorption. The sample compartment is then gradually filled with known amounts of nitrogen gas. Partially vacuum circumstances are used to achieve relative pressures lower than atmospheric pressure. There is no additional adsorption after the saturation pressure, regardless of how high the pressure is raised. Pressure transducers with high precision and accuracy detect pressure changes caused by the adsorption process. After the adsorption layers have developed, the sample is taken out of the nitrogen atmosphere and heated, causing the adsorbed nitrogen to be released and quantified. The information gathered is represented by a BET isotherm, which displays the amount of gas adsorbed as a function of relative pressure.

The BET Equation uses the information from the isotherm to determine the surface area of the sample, where w is the weight of nitrogen adsorbed at a given relative pressure (P/Po), V_m is monolayer capacity, which is the volume of gas adsorbed at standard temperature and pressure (STP), and C is constant. STP is defined as 273 K and 1 atm

$$\frac{1}{w(^{p_o}/_{p}-1)} = \frac{1}{V_m * c} + \frac{c-1}{V_m c}(^{p}/_{p_o}) \quad \ldots\ldots 2.9$$

2.4.7. Thermo Gravimetric Analysis (TGA/DTG)

TGA is a fundamental technique in thermal analysis. While a substance is subjected to a controlled temperature program in a technique, its mass is measured as a function of temperature or time. Physical processes like as phase transitions, absorption, and desorption, as well as chemical phenomena such as chemisorption, thermal breakdown, and solid-gas interactions, are all revealed by this measurement (e.g., oxidation or reduction).DTG stands for difference thermo gravimetric ratio of dm (weight loss or gain) at heating/cooling/isotherm, with dm over T or time (-dm/dt) as the interpretation. In the vast majority of cases, succeeding decomposition processes result in overlapping stages of breakdown. Without the first derivative, a reliable qualitative and

quantitative evaluation of the TG curve is difficult in most circumstances (i.e. DTG curve). The rate of mass loss (dm/dT in mg/min unit) is determined by the DTG peak height at any temperature. In overlapping reactions, T on set, T final, and T peak (the temperature of the maximum mass loss rate) can be precisely measured using the DTG curve.

Many researchers investigated the thermal decomposition behaviors and kinetics of plastics (PE) in a non-catalytic and catalytic co-pyrolysis over zeolite based catalyst by using a thermogravimetric analyzer (TGA). (Raveh-Amit et al., 2022) studied catalytic pyrolysis of HDPE on decomposition efficiency and kinetics. The pyrolysis initiation temperature was significantly decreased in the presence of the zeolite catalyst. In the case of treating 5 g of HDPE, the use of 10% of zeolite Y lowered the initial decomposition temperature of the pyrolysis from 475 ^{o}C to 430 ^{o}C. (Covarrubias et al., 2010) investigated Catalytic degradation of polyethylene using nanosized ZSM-5 zeolite and Na Y zeolite. Adding the ZSM-5 catalyst to the system the degradation process was dramatically shifted to lower temperatures. Increasing dosage of catalyst decreased the degradation process which was improved specially in T Onset decreasing 24 ^{o}C using nanosized ZSM-5 zeolite. Temperature reduction of 27 ^{o}C was observed by nanosized Na Y zeolite catalytic degradation on the T Onset. (Neves et al., 2007) investigated Catalytic degradation of polyethylene to evaluation of the effect of dealuminated Y zeolites using thermal analysis. The ultrastable Y zeolite (USY) reduces significantly the activation energy during the thermal process, and the dealuminated Y zeolites reduce even more the activation energy resulting in a more rapid degradation.

CHAPTER 3

3. METHODOLOGY

3.1. Overall Research Framework

This research was carried out to valorize silica enriched byproduct for partial replacement of cement clinker and synthesis of zeolite based catalyst. The research methodology of the whole study is summarized as shown in Figure 3.1

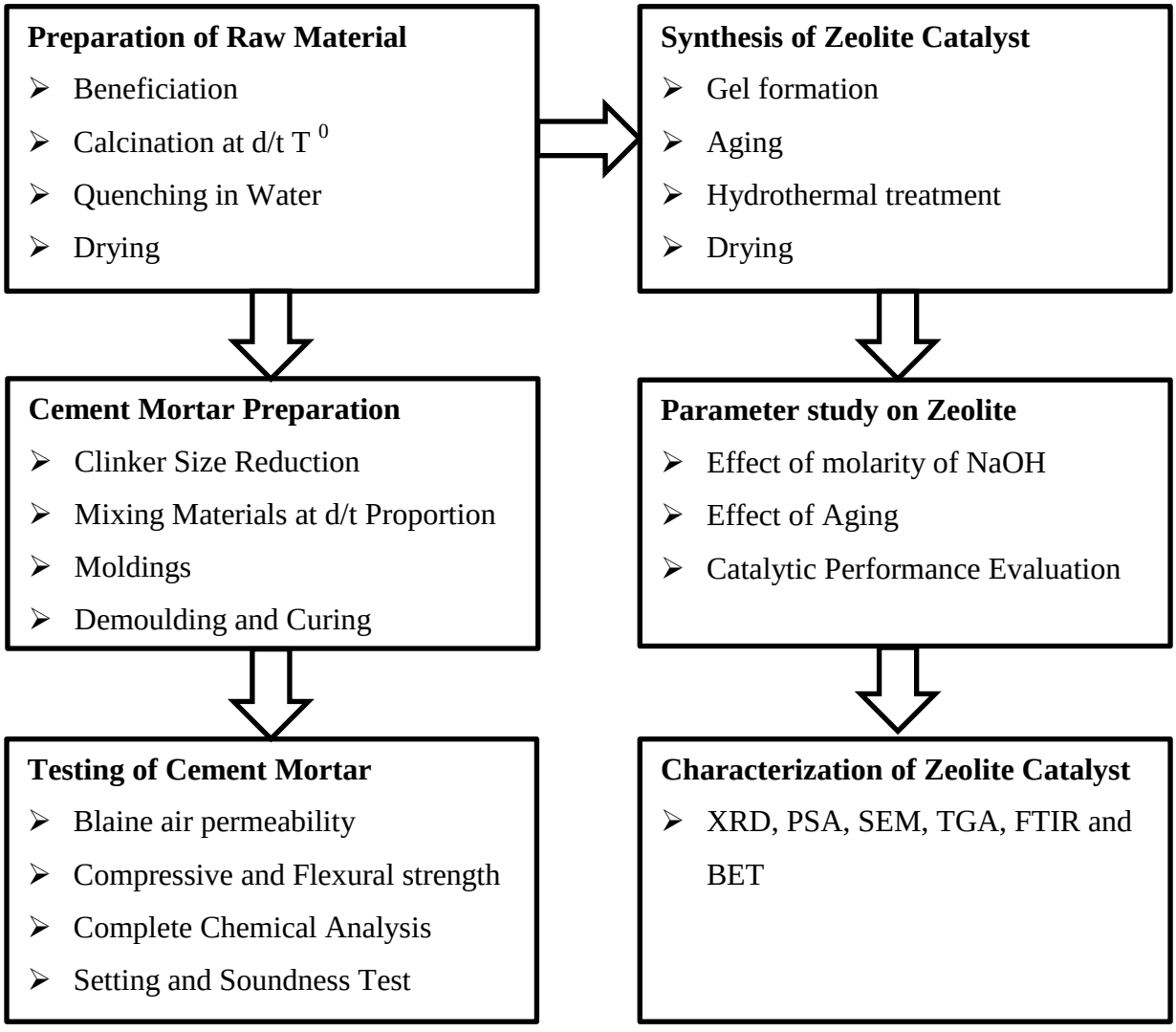

FIGURE 3.1 Overall Flow of Research Methodology

3.2. Materials and Equipment

3.2.1. Materials and Chemicals

Various types of raw materials, equipment's and chemicals were used so that the experiments can be carried out efficiently. Awash Melkassa chemical factory silica enriched byproduct was selected for partial replacement of cement clinker as well as synthesis of zeolite based catalyst.

Table 3.1 Material used Throughout the Experiments

Materials	Function of Materials
Different Size Beaker	Were used for holding and mixing specimen
Analytical Balance	Was used to measured different sample weight
Different Sieve	Were used to separate CFW powder in different size
Crucibles	Were used to hold a sample for calcination process
Muffle Furnace	Was used to calcine a given sample of CFW
Digital pH Meter	Was used to measure a pH of sample
Flocculating Unit	Was used to facilitate bonding between particles
Hydrothermal Autoclave Reactor	Was used for gel formation and crystallization process
Round Bottom Flask	Was used to hold mother liquor
Drying Oven	Was used to dry samples
Auto Mixer	Was used for mixing cement cast
Prism Mold	Was used for molding cement mortar
Jolting Machine	Was used to compact cement mortar prism and remove bubble and gases in cast
Curing Chamber	Was used to store cement cast molded

Table 3.2 Chemical used Throughout the Experiments

Chemical	Function of chemicals
NaOH (99%w/w)	Was used to gel formation with CFW in hydrothermal reactor
HCl (37%v/v)	Was used to remove metals and impurities in CFW
HNO_3 (72% v/v)	Was used for washing of hydrothermal autoclave reactor and neutralize basic environment in hydrothermal autoclave reactor
Distilled Water	Was used for chemical reaction, washing purpose and mixing aggregate in cement cast
Standard Sand	Was used to assess and avoid effect on reported cement strength generated by clinker
Clinker	Was used for preparation of cement cast
Gypsum	Was used for regulating the setting time of cement and controls the rate of hardening of the cement

3.3. Preliminary Test

Awash Melkassa chemical factory waste was used for synthesis of zeolite based catalysts. Raw silica enrich byproducts of factory has showed a full crystallized structure which is supported by crystallographic arrangement by XRD analysis. Uniform crystallization temperature was set to 110 ^{o}C as Control factor(Adane, 2020). Different molarity of NaOH was used with in standard Na_2O/SiO_2 allowable for synthesis of zeolite Y. Different aging of gel and crystallization time was used as variable factor. Effect of the three variables was studied Preliminary experimental data and methodology that was conducted is summarized in Table 3.3 and Figure 3.2.

Table 3.3 Preliminary Experimental Data for Synthesis of Zeolite Y

Exp No	Mass of CFW (gm)	Calcination Condition @ 675 ^{o}C	Molarity of NaOH (M)	Volume of Water (ml)	Mass of NaOH (gm)	Aging Time(hr) @ 30 ^{o}C	Crystallization Time(hr) @ 110 ^{o}C
1	10	Not calcinated	3.1	43.1	5.5	24	24
2	15	Not calcinated	3.7	54.5	8.07	No	36
3	15	Not calcinated	3.7	54.5	8.07	8	24
4	15	Not calcinated	3.7	54.5	8.07	12	24
5	15	Not calcinated	3.7	54.5	8.07	24	24
6	25	Not calcinated	4.4	63	11.2	No	24
7	25	Not calcinated	4.4	63	11.2	8	24
8	25	Not calcinated	4.4	63	11.2	24	24
9	25	Not calcinated	4.4	63	11.2	48	24
10	25	Not calcinated	5.5	50.4	11.2	24	24
11	25	Calcinated	3.7	54.5	8.07	12	24
12	25	calcinated	4.4	63	11.2	12	24
13	25	calcinated	5.5	50.4	11.2	12	24

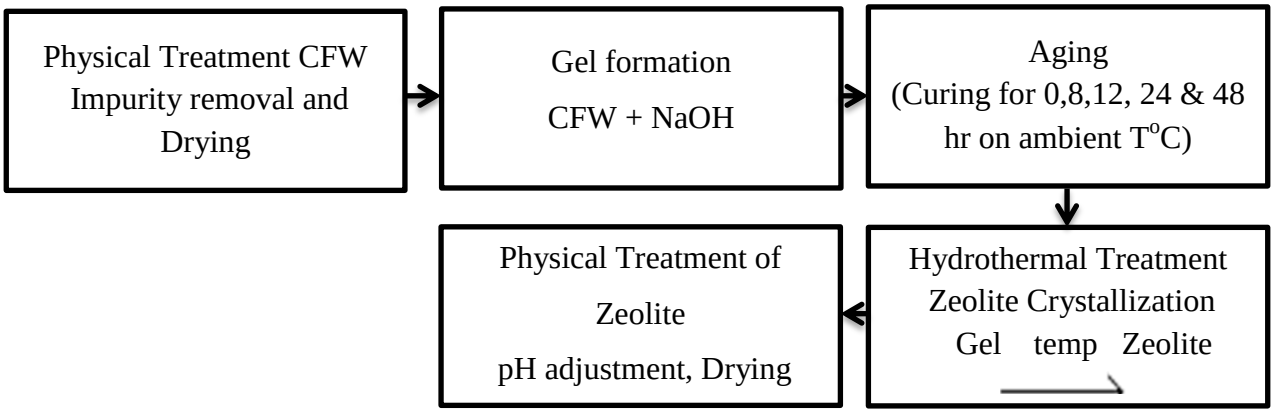

FIGURE 3.2 Overall Flow Diagram for Preliminary Production of Zeolite Using Conventional Hydrothermal Synthesis Method

Although different trial have been conducted, it wasn't possible to synthesis zeolite based catalysts. Experimental trial 11 and raw CFW XRD pattern of zeolite synthesis are represented in Figure 3.3 (a). This was due to the crystalline structure of CFW which doesn't allow formulation of complex. The synthesized sample was characterized by XRD. It hasn't reformed from the original material even with NaOH attack. This showed the CFW is highly crystalized that it isn't ready to react with other compounds. The catalysts activity of synthesized sample was studied by TGA analysis as represented on Figure 3.3 (b).

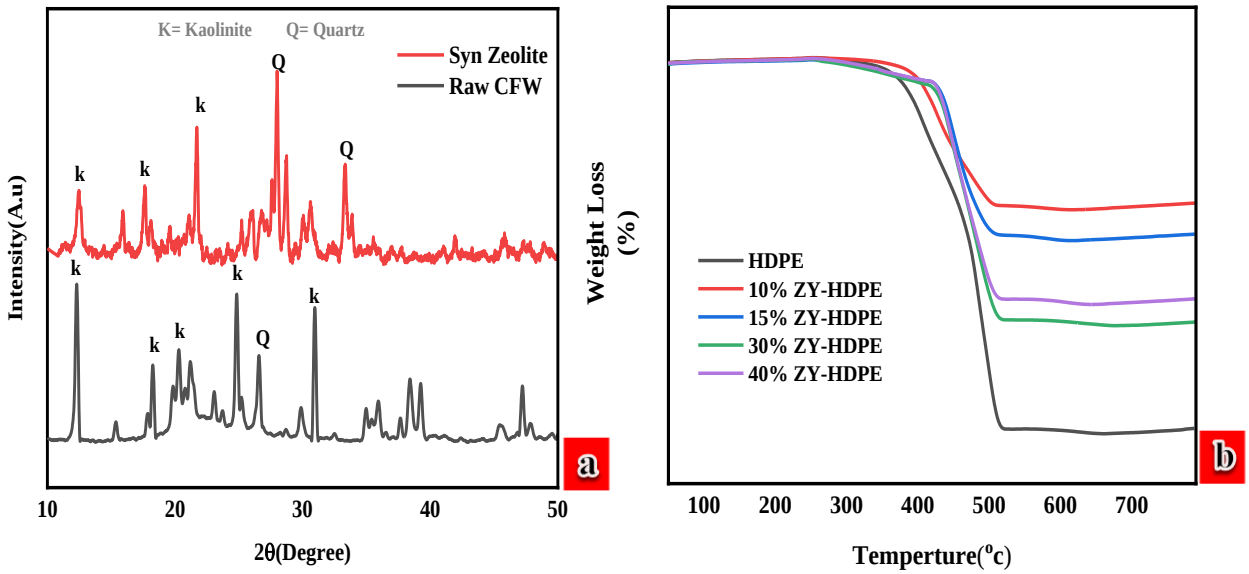

FIGURE 3.3 XRD of Synthesized Sample Vs. Raw CFW (a) and Thermal Degradation Of HDPE by Synthesized Sample (b)

It was concluded that the raw CFW can't be used for synthesis of zeolite based catalysts because of highly crystallite nature of waste that disable it to react with NaOH to form zeolite based catalysts. In addition, From the TGA analysis it has showed increasing thermal stability of polymer by delaying the rate of degradation. This indicates the formation of ultra-stable composite which enhance the stability of HDPE. Although zeolite based catalysts expected to fasten the rate of degradation of polymer, the synthesized sample delays the rate of degradation of polymer. It was concluded the crystalline nature of CFW has been a challenge to achieve our goal. Therefore methodology adjustment was done, where crystalline nature of CFW modified. Hence newly developed method of amorphous silica enriched CFW preparation was developed.

3.4. Amorphous Silica Preparation

3.4.1. Beneficiation of CFW

The beneficiation was carried out; as such at the beginning, 1000 gm of raw CFW was measured and put on 4 beakers with 2 liter capacity. 700ml of 1M HCl was poured on every 1000 gm of CFW. It was soaked for 24hrs at ambient temperature. During soaking time, the impurities in CFW had been seen floated. Floating dirt was removed by simple filtration using filter paper. The slurry remaining at the bottom was then soaked in a bucket of distilled water for 2 hour at ambient temperature. These processes had been proceeding several times until clean water was seen. It took 1 day to achieve impurities removal. The mixture was decanted several times to urge obviate of the sand, stony particles, heavy impurities and soluble salts presented. The slurry was dried in an oven at 110 ^{o}C for 24 hour to remove the water contents. Then the dried sample was grind using mortar and pestle. After grinding, the samples were sieved under dry conditions, the size fraction of less than 230 meshes or 63 microns collected and the remaining (Oversized) samples were recycled for same size reduction process.

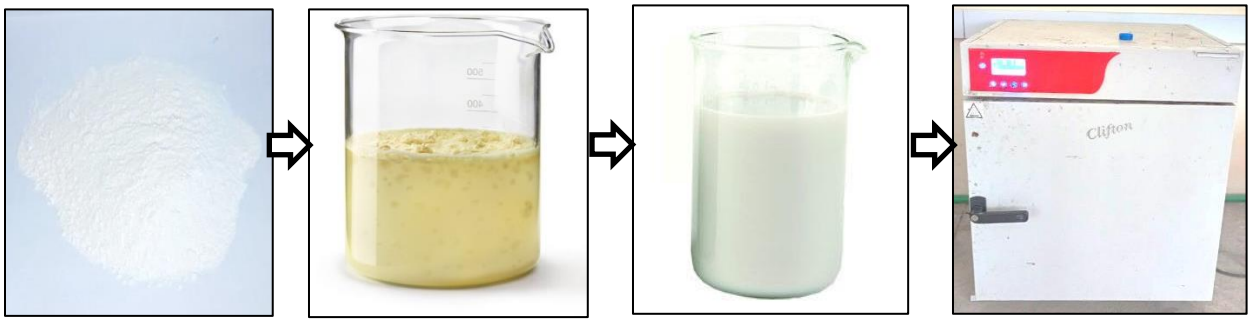

FIGURE 3.4 Diagrammatic Representation of CFW Beneficiation

3.4.2. Calcination and Quenching of CFW

The nature of CFW was seen to be high crystallized arrangement which indicated The Si-O or Al-O structures in CFW are inactive in nature from preliminary test. In order to apply this CFW to any application it was need to change crystallized structure to amorphous structure which will activate Si-O or Al-O structures. Since CFW resemble kaolin structure, calcination was expected

to change the structure of CFW to resemble Meta kaolinite. After beneficiation of CFW it was calcine at different temperatures (500, 600, 650 and 675 ^{o}C). During calcination, the main reaction which occurred is the breaking off the kaolinite structure. The heating reaction breaks off -OH chain from the mineral, and collapsing the kaolinite structure, resulting in an amorphous alumina silicate structure ($Al_2O_3.2SiO_2$) known as Meta kaolinite. Although the calcination temperature that change kaolinite to Meta kaolinite doesn't alter beneficiated CFW crystallography as expected to be. Therefore a different approach was followed to achieve the amorphous product. A new approach was developed to alter the crystallography of CFW. Supper cooling of calcinated CFW was undertaken in cooled water (10 ^{o}C) for 4 hour. This involves quench cooling of calcinated CFW. This behavior of CFW was characterized by using XRD which show the crystallographic arrangement of CFW. This result also can be supported by microstructural analysis using FTIR.

FIGURE 3.5 Diagrammatic Representation of Activated CFW Preparation

3.5. Experimental Procedure for Cement Clinker Replacement and Measurement

3.5.1. Milling Clinker

Cement clinker was collected from National cement located in Dira Dawa, 515 Kilometers from Addis Ababa, Ethiopia. Quantity of cement clinker having the same chemical composition was collected from the factory. Chemical composition of sample clinker was tested by complete chemical analysis method. Clinker with 5% gypsum was Grinded at different time lap by ball mill. During grinding of different specimens, fineness of samples was tested by blaine air permeability apparatus frequently. Grinding quenched at desired point. 3 Sample with different fineness ranging from 1200 – 3615 cm^2/g has been prepared.

3.5.2. Dry Mixing

Cement clinker and gypsum with desired fineness was mixed manually with different proportion of activated CFW with uniform fineness. Reference (0% CFW), 5% activated CFW replacement, 10% activated CFW replacement and 15% activated CFW replacement were mixed on clinker and gypsum. Details of the CFW-added mixes (Samples 2–13) are given in Table 3.4.

Table 3.4 Mixed Ratio of Activated CFW with Cement Clinker and Gypsum

Sample Number	Cement content (%)(cement clinker, gypsum, CFW)
1(Reference)	C95G5CFW0
2	C90G5CFWA5
3	C85G5CFWA10
4	C80G5CFWA15
5	C90G5CFWB5
6	C85G5CFWB10
7	C80G5CFWB15
8	C90G5CFWC5
9	C85G5CFWC10
10	C80G5CFWC15
11	C90G5CFWD5
12	C85G5CFWD10
13	C80G5CFWD15

Note: CFWA – Calcinated CFW at 500 ^{o}C and quenched at 500 ^{o}C C - Cement Clinker

CFWB – Calcinated CFW at 600 ^{o}C and quenched at 600 ^{o}C G – Gypsum

CFWC – Calcinated CFW at 650 ^{o}C and quenched at 650 ^{o}C

CFWD - Calcinated CFW at 675 ^{o}C and quenched at 675 ^{o}C

3.5.3. Mold Preparation

Standard sand, gypsum, dry mixture and distilled water were weighed and then mixed in the automatic mixing machine with different proposition as shown on table 3.4. Constant parameter were applied to all the sample which are 1350 gm of standard sand, 225gm of distilled water and 22.5 gm of gypsum as control factor for the mold preparation.

The mortar was then placed on a mold with dimensions of 40 × 40 × 160 mm. The bubbles and gases were removed by vibration using a jolting machine for 2 minutes. The prism mold was placed in a moist curing chamber for 24 hour with a temperature of 20 °C and a humidity level of more than 95% to avoid any evaporation of water. After 24 hour, the cubes were hardened and then removed from molds and placed in an accelerated water curing tank for 2 days and 28 days. Then the cube were removed from water bath to the flexural and compressive strength testing machine according to different periods , then cube were placed on the resting point on the machine and were operated at low speed and reading were taken.

Cement Paste on Prism Mold **Cement Paste on Jolting Machine** **Final Cement Mold**

FIGURE 3.6 Diagrammatic Representation of Cement Mold Preparation

3.5.4. Blaine Air Permittivity Test

The fineness is expressed as a percentage of the total surface area of the cement.an automatic blaine apparatus was used. Glass U-tube manometer with valve, steel stand, stainless steel test cell with disk and plunger, rubber aspirator bulb, filter paper disks, manometric liquid, and brush are all included in the kit. The temperature was set to 27 ^{o}C, with a relative humidity of 65%. First, filter paper was placed in the cell, and 2.8 gm of cement clinker was weighed. Another filter paper was placed on top of it, and the plunger was used to compress it. The cell was then mounted on top of the U-tube manometer. The air in the manometer was removed using the aspirator bulb through the side tube until reached oil level 1. As the oil began to fall, the side valve was closed and the oil was monitored. The time it took for the oil to fall from level 2 to level 3 was monitored. The time for the standard cement sample is T_O and the time for the observing sample is T_S, both were recorded electronically. The blaine air permittivity fineness of cement blend was measured automatically with the software and its final result was displayed on screen.

3.5.5. Flexural Strength and Compressive Strength Test

The bending strength of typical beam specimens with dimensions was determined. Flexural strength (sometimes known as the modulus of rupture) is a bending tensile strength measurement. The flexural strength of the beams was determined using three-point loading according to the criteria of BS 1881: part 118 at 2 and 28 days (1983). The samples were put through a three-point bending test, with a single focused force applied in the middle of the span and increased uniformly until failure. The distance between the support points was 100 mm, and the beam specimen's entire length was 160 mm. As required by BS 1881: part 119, test cubes were crushed to determine the compressive strength of test samples (1983). Compressive strength refers to a material's or structure's ability to support loads that tend to shrink in size. The compressive strength tests were carried out on base cement samples using a standard process given in IS: 14858(2000) and calibrated to a precision of 1% as required by 1828. (class1). The compressive strength test was carried out using a compressive test machine at a relative load rate of 2 kN/s until the cube fractured. For ordinary Portland cement (OPC), compressive strength is ranging between 33 – 53MPa at 28 days and 10 -23MPa at 2days of curing after casting.

3.5.6. Soundness Test

Lechatelier's device was used to determine the soundness of cement. Calculate the water required to get the typical consistency of cement before doing the test (P). To get a standard consistency paste, 0.78 times the amount of water was added to the cement (0.78P). The Lechatelier mold was lightly oiled before being placed on a glass plate. The cement paste was put into the mold, which was then sealed with a lightly oiled glass plate and a weight to prevent it from falling out. The entire assembly was then immersed in a water bath at 27 ^{o}C for 24 hours. The whole apparatus was then taken from the water, and the distance between two indication points was calculated using a measuring scale and recorded as L_1. For the second time, the entire assembly was immersed in a water bath at boiling point for three hours. After 3 hours, the assembly was withdrawn from the bath, and the distance between two indicator points was measured and recorded as L_2.

Expansion = B – A…….....3.

Where, A is the measurement taken after 24hours of immersion in water at 27 ± 2 ^{o}C and B is the measurement taken after 3hours of immersion in water at boiling temperature

Therefore the value we calculated by subtracting distance between expansion on room temperature and boiling point temperature was taken as the expansion of cement that undergo after hardening.

3.5.7. Setting Time Test

The setting time is calculated by watching the needle penetrate a standard consistency cement paste until it reaches a certain value. The paste was made with 500 gram of cement clinker blend. The required amount of water was 0.87 P, where P stands for water consistency. Distilled water was used. Cement clinker and water was mixed to form a Paste. Gauging time was maintained between 3-5 minutes. Before any sign of setting appears, the gauging was completed. The counting of the gauging time began when water was added to the dry cement. The mixture was filled smoothly on mold. The mold beneath the needle-bearing rod (Needle for determining the initial setting time) was placed the needle slightly lower until it contacted with the sample block's surface, then swiftly released it to allow it to pierce the block. The needle was penetrated initially the test block entirely. This method was repeated until the needle was unable to pierce the block

to a depth of 5.0 ± 0.5 mm from the mold's bottom. The time between when water was added to the cement and when the needle failed to pierce the test block to a depth of 5.0 ± 0.5 mm from the bottom of the mold was the initial setting time. The time between when water is introduced to the cement and when the needle failed to produce an impression on the surface of the test block was the final setting time.

3.6. Experimental Procedure for Synthesis of Zeolite Based Catalyst

The methodology utilized in this study for the synthesis of Zeolite Y from activated CFW was conventional hydrothermal synthesis method. Aluminosilicate zeolites are usually synthesized under hydrothermal conditions because, it has some advantages prescribed by different researchers which include, the high reactivity of reactants, low energy consumption, low air pollution, easy to regulate the solution, formational of metastable phases, and unique condensed phases. Numerical Calculation for synthesis of zeolite catalyst is presented on appendix D. To synthesize zeolite based catalyst from Activated CFW there was variety of individual process steps were followed:

3.6.1. Gel Formation

Here the mass of sodium hydroxide and volume of water required for gellating of Activated CFW was calculated. At this stage, gelation was achieved with a desired molar composition using the following equations.

The Silica/Alumina (SiO_2/Al_2O_3) ratio used in this work is obtained from AAS analysis of samples, while the ratio of Sodium oxide to Silica (Na_2O/SiO_2) and that of water to Sodium oxide (H_2O/Na_2O) were found from standard constant for zeolite formation. 10 gm of activated CFW had been put in a conical flask and mix with 23.76 ml of deionized water until the activated CFW was dissolved completely. 10.56 gm of NaOH was added to the solution and stirred vigorously by flocculating unit before the remaining 23.76 ml of deionized water was added. The content was continuously stirred with flocculating unit for 30 minute(Adane, 2020).

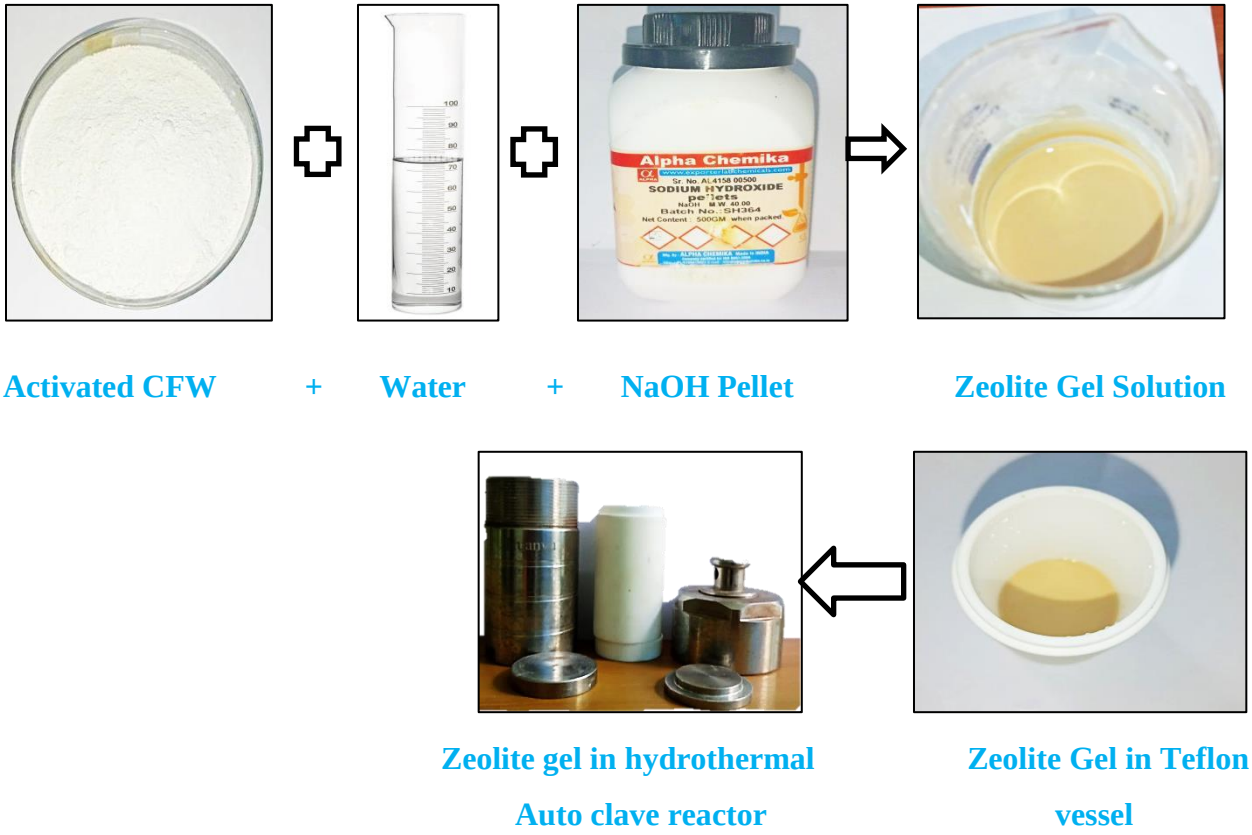

FIGURE 3.7 Diagrammatic Representation of Zeolite Gel Formation

The resulting gel was put in a Teflon bottle (Model: ZHT-172C), sealed and left to age for 0, 12, 24 and 48 hour at room temperature.

$$NaOH\ (s) + H_2O\ (l) + 2Al_2Si_2O_7\ (s) \rightarrow Na_2O.Al_2O_3.SiO_2.H_2O\ (aq) \quad \text{.....3.1}$$

The molecular formula of zeolite Y synthesized from Awash Melkassa chemical factory waste with a batch molar composition of the gel was 13.2 Na_2O. Al_2O_3. 11SiO_2. 263H_2O

3.6.2. Crystallization

The enclosed solution in Teflon autoclave was placed in electric oven for 1 days and 110 ^oC temperature to be crystallized(Adane, 2020). The hydrothermal treatments take place where there was multiphase reaction-crystallization process. Zeolite based catalyst was synthesized with excess sodium hydroxide and precipitate.

3.6.3. Physical Treatment of Zeolite Based Catalyst

The precipitate was separated from the solution by filtration. The zeolite based catalyst filtrate was washed thoroughly several times, to remove excess sodium hydroxide, using deionized water. The pH was monitored, while washing, using pH-mV meter to obtain neutral pH. The precipitated solid after washing was dried overnight 110 ^{o}C temperature (Adane, 2020) and the crystals were pulverized in a mortar and pestle to obtain a smooth and evenly distributed powder.

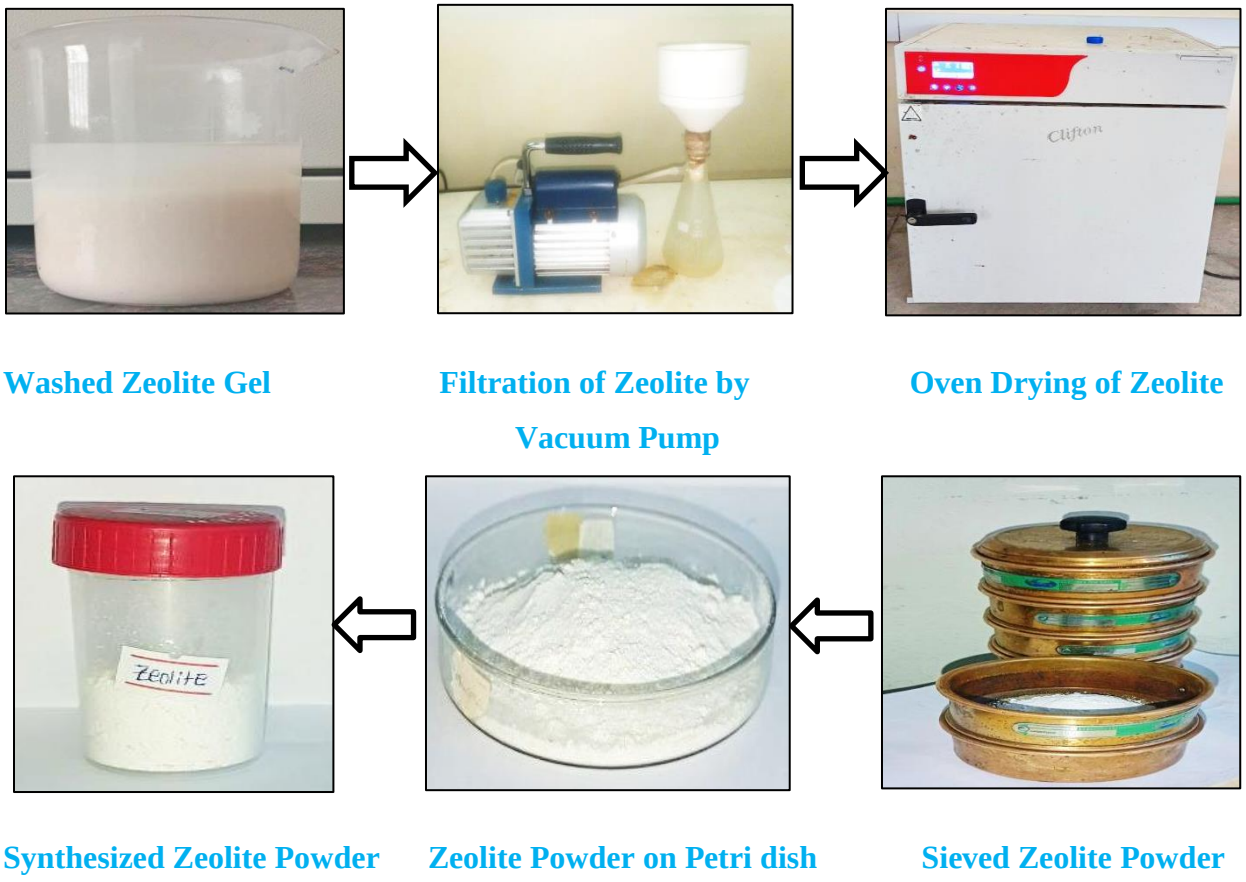

FIGURE 3.8 Diagrammatic Representative of Physical Treatment of Synthesized Zeolite

3.7. Characterization of Raw Materials and Products

3.7.1. Atomic Absorption Spectrometry (AAS)

In this study the chemical composition analysis of CFW and synthesized zeolite based catalyst were done by atomic absorption spectrometer (AAS) spectry AA-20 plus model at Geological survey of Ethiopia. Apart from the AAS, the $LiBO_2$ Fusion, HF attack, Gravimetric, Colorimetric

were carried out for all samples to perform the complete silica analysis at Geological Survey of Ethiopia.

3.7.2. X-ray Diffraction (XRD)

The analysis of the silica enriched byproduct, Activated silica enriched byproduct powder samples was carried out using the Shimadzu XRD-7000 X-ray diffractometer with Cu-K radiation in this work. At room temperature, the instrument measurement conditions were voltage = 40 kV, current = 30 mA, with a step size of 0.020. The scan range was set to 5 to 80 ^{o} with a scan speed of 3 ^{o}/min in continuous scan mode for the zeolite powder samples. 0.4 gm of powder sample was placed in an aluminum holder to prepare samples for X-ray examination. To absorb the X-ray radiation on a regular basis, the sample holder surface should be smoothed. Within the XRD machine, the diffraction pattern was depicted by generating a scan with continuous scanning mode for peak intensity (Irel) as the Y-axis versus 2Ɵ as the X-axis.

3.7.3. Scanning Electron Microscopy (SEM)

The crystallite size and morphology examination of the silica enriched byproduct, activated silica enriched byproduct, and zeolite based catalyst produced from Awash Melkassa chemical industrial waste was carried out in high vacuum using a JEOL JCM-6000 Plus (Washington, DC, USA). The test was conducted at room temperature with an applied voltage of 10-20 kV. This detector gathered 40 signals from secondary and backscattered electrons at the same time. Although sample coating is important in many SEM examinations, this analysis was performed under high vacuum without it. Small amount of sample powder was poured on the carbon tape which is attached to the holder. The excess powder was then blown away using an air gun to ensure that no small powder particles remained on the tape. It was then placed in the SEM chamber for analysis. The material was photographed with a magnification of X1000-X6000.

3.7.4. Fourier Transform Infrared Spectrometry (FTIR)

The JASCO FT/IR-6600typeA was used to analyze the internal and exterior chemical bonding (Functional Groups) linkages of the silica enriched byproduct, activated silica enriched byproduct, and zeolite based catalyst manufactured from Awash Melkassa chemical industry waste. At room temperature, the instruments measuring conditions for each test ranged from 500

to 4000 cm^{-1} with a resolution of 4 cm^{-1}. The sample for FTIR analysis was made by weighing 1 gram of material and 100 gm of potassium bromide (KBr) powder into an agate mortar. Using an agate mortar and pestle, combine the powders until the sample was evenly distributed and the mixture has the consistency of fine powder. Then the test was ruined by loading the sample on to the FTIR instrument. The FTIR pattern was plotted within the FTIR machine by generating the transmittance peaks (%) as the Y-axis versus wavenumber (cm^{-1}) as the X-axis.

3.7.5. Particle Size Analysis (PSA)

The ZEN1690/ Nano S90 model Zeta sizer Nano particle analyzer was used determine particle size. Particle size can be determined by measuring the random changes in the intensity of light scattered from a suspension or solution. Dynamic light scattering (DLS) is the most frequent name for this technology, although it's also known as photon correlation spectroscopy (PCS) and quasi-elastic light scattering (QELS). It is the only technique presented in this document that is unique. The mean value from the intensity distribution (called the Z average) and the polydispersity index (pdI) to represent the distribution width are often the key results from DLS (Varenne, et al., 2016). In order to compare to other methodologies, you can convert an intensity to a volume or numerical distribution. The sample in the cell is illuminated by light from the laser light source. The dispersed light signal is gathered using detectors at a scattering angle of 90 ° (right angle) or 173 ° (back angle). The availability of two detectors gives you more options when it comes to measuring circumstances. A number of liquids can be used to disperse particles. To interpret the measurement findings, only the liquid refractive index and viscosity must be known. Due to the particle's randomly shifting relative position, the resultant optical signal shows random alterations.(Thomas, 1987).

$$\boldsymbol{D_z} = \frac{\sum \boldsymbol{S_i}}{\sum\left(\boldsymbol{S_i}/\boldsymbol{D_i}\right)} \quad \text{3.1}$$

Here, S_i is the scattered intensity from particle *i* and D_i is the diameter of particle *i*. Note that the result is in the form of a harmonic mean. Since this mean is calculated from the intensity weighted distribution, leading to the statement that the Z-average size is the intensity weighted harmonic mean size.

3.7.6. Brunauer-Emmett-Teller (BET)

Quantachrome Instruments version 11.0 BET (Brunaure Emmett Teller) apparatus was used to determine surface area and pore volume. The sample must be degassed to remove any water or other impurities before the surface area can be accurately determined. Samples are degassed at high temperatures in a vacuum. To shorten degassing time, the highest temperature possible is usually chosen that does not alter the sample's structure. It was degassed the sample for 8 hours to guarantee that unwanted vapors and gases were removed from the surface. 0.5 gm of sample was used in the BET to determine the surface area. The BET machine degasses and analyzes samples placed in glass cells. Glass rods were put into the cell to limit the quantity of dead space. The diameter of a sample cell was 6 mm. powder sample was inserted in cell. The cell was linked to the machine's outgas port and put into heating mantles. After the sample was degassed, the cell was delivered to the analysis port. Using liquid nitrogen dewars, the sample was chilled and held at a constant temperature. To ensure that the contact between the gas molecules and the sample's surface was strong enough to allow for considerable adsorption, a low temperature had to be maintained. The adsorbate, in this case nitrogen gas, was pumped into the sample cell using a calibrated piston. The dead volume in the sample cell must be calibrated before and after each measurement. Helium gas was used for a blank run because it did not adsorb onto the material.

3.8. Performance Evaluation of Synthesized Zeolite Based Catalyst Using TGA

The DTG-60H model Shimadzu instrument was used to test the thermal stability of the synthetic zeolite based catalyst manufactured from Awash Melkassa chemical factory waste as well as the thermal deterioration of the composite made from the synthesis zeolite based catalyst and HDPE. For each test, the instrument used a non-isothermal temperature program that ranged from 30 °C to 800 °C at a heating rate of 20 °C/min and a nitrogen purge rate of 50 ml/min. 10 mg amounts of sample was weighted and place them in a platinum crucible. Then, the sample was placed onto the TGA instrument and starts the test. The % mass loss in (mg) is represented as the Y-axis versus temperature (^{o}C) as X-axis on TGA curve in the TGA machine.

The catalyst activity of the synthesized zeolite-based catalyst on high-density polyethylene (HDPE) collected from municipal solid waste was investigated using thermo gravimetric analysis (TGA). The HDPE was cleaned with distilled water. Before TGA analysis, the obtained

materials were manually chopped to minimize particle size. The reduced sized HDPE was sieved to get considerably particle size less than 25Mesh (700 µm) for homogeneity. Because the size difference between synthetic zeolite based catalyst and reduced HDPE is directly related to the density of samples, it is difficult to blend them together. Because the synthesized zeolite based catalyst was very fine, it kept setting down when blended to HDPE. As a result, temperatures higher than the HDPE glass transition were required. With the use of heating at 180 ^{o}C in the melting blending process, a composite mixture of HDPE and zeolite-based catalyst was created. For the thermo gravimetric analysis, the composite mixture HDPE/catalyst and HDPE were created with varied proportions. The catalyst proportions in the Polyethylene Zeolite based catalyst mixture were 10, 15, 30, and 40%, according to specified literature (Caldeira et al., 2017). HDPE of 10, 9, 8.5, 7 and 6mg has been combined with 0, 1, 1.5, 3 and 4 mg of zeolite respectively in focused on to put together 10, 15, 30 and 40 mass % HDPE-Z combination composite. The composite mixture was feed to DTG-60H Shimadzu device on platinum crucible at 20 ^{o}C/min of heating rate below 50ml/min purge rate of nitrogen atmosphere with temperature range of 30 ^{o}C – 800 ^{o}C. Blank reference was used with 10 mg of HDPE of 0% Z for TGA analysis with the same conditions as above composite mixtures.

CHAPTER 4

4. RESULTS AND DISCUSSION

4.1. Raw material characterization

4.1.1. Silica Enriched CFW

The raw CFW was collected from Awash Melkassa chemical factory. The waste collected is generated from aluminum sulfate manufacturing process. The raw material used for the production is kaolin. The waste generated is expected to be de aluminized kaolinite due to dealuminization process takes place for aluminum extraction from kaolin for aluminum sulphate production. The chemical composition analysis was done by atomic absorption spectrometer (AAS) spectry AA-20 plus model at Geological survey of Ethiopia. Table 4.1 indicates the composition of SiO_2 content is the highest percentage present in CFW followed by aluminum oxide. This sample has resemblance with kaolinite chemical composition but with less percentage of aluminum oxide.

Table 4.1 Awash Melkassa Chemical Factory Waste (CFW) Mineral Composition (%)

	SiO_2	$A1_2O_3$	Fe_2O_3	CaO	Na_2O	MgO	K_2O	P_2O_5	TiO_2	H_2O	LOI
CFW	65.44	16.57	0.48	<0.01	<0.01	<0.01	1.60	0.19	<0.01	1.22	14.73

Powdered X-ray diffraction (XRD) of Awash Melkassa factory waste was used to determine the sample crystallite throughout this work. The identification of the mineral compositing component of CFW is done by matching the peak intensity position (2θ) in the sample X-ray diffraction-gram with the peak position value of the diffraction intensity (2θ) standards contained in the Joint Committee for Powder Diffraction Standards (JCPDS). Although there is no standard distinct diffraction intensity (2θ) for the particular sample, it is approximated to resemble Kaolinite crystallography arrangement structure which can be found at appendix F. Therefore, the Crystallographic arrangement XRD result matched with standard kaolinite in the Joint Committee for Powder Diffraction Standards (JCPDS). The crystalline phases of raw CFW

revealed by the X-ray diffractogram pattern indicated mainly the presence of kaolinite and quartz as showed in Figure 4.1

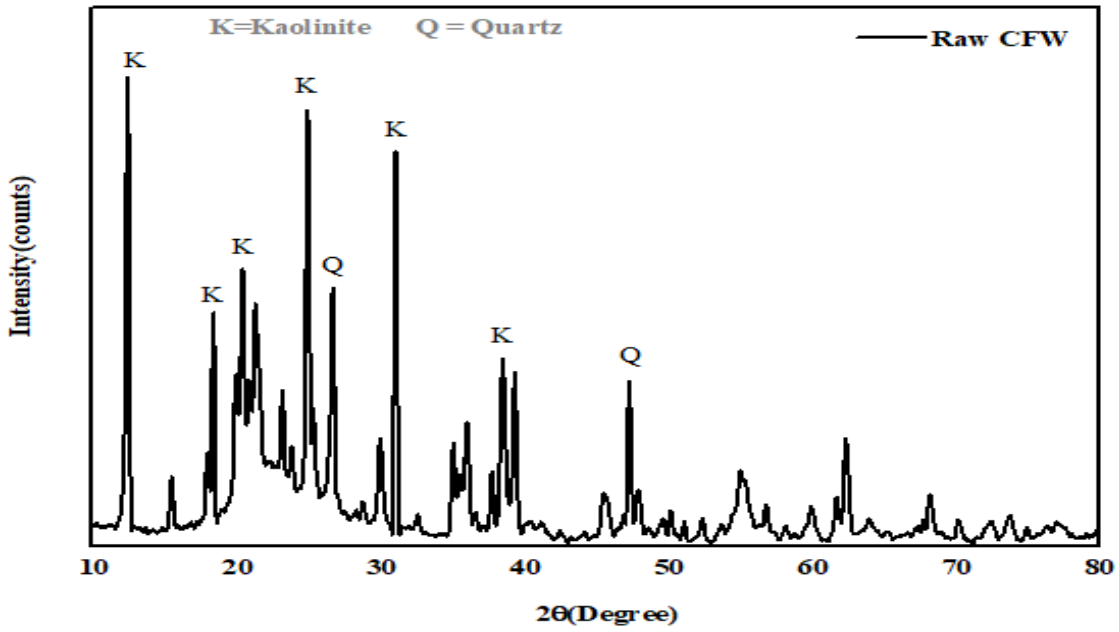

FIGURE 4.1 XRD Pattern of Powder Raw CFW

As shown in the Figure 4.1, the raw CFW has many sharp peaks, which contains the kaolinite and the quartz. The x-ray diffraction analysis of the peaks shows a sharp peak with high intensity at 2Θ = 12.3 ^{o}. This is the main peak used in identification of kaolinite clay. Beside the kaolinite the 2Θ angle at 26.6 ^{o} profiles, correspond to that of quartz. Kaolinite and quartz are the dominant characteristics of natural kaolin which resembles CFW (Treacy et al., 2007).

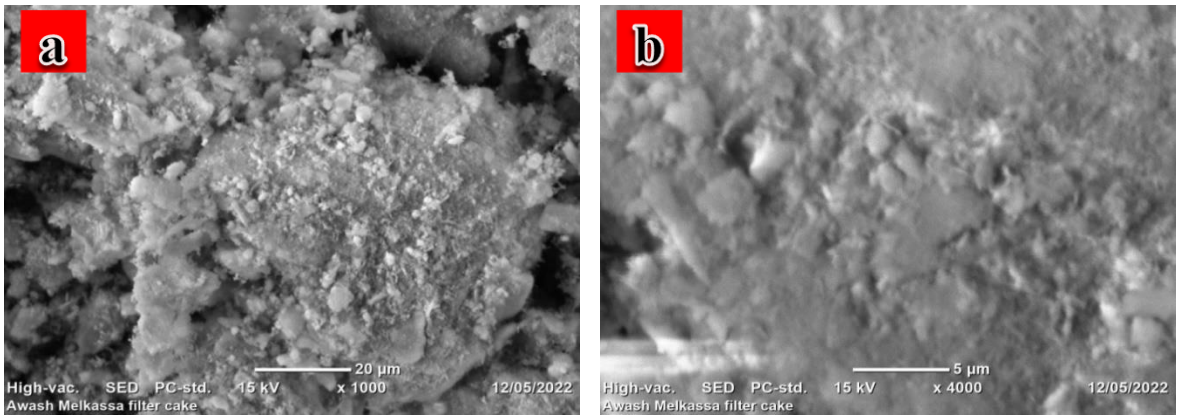

FIGURE 4.2 SEM Image of General Morphology of CFW with 20µm magnification (a) and 5µm magnification (b)

Figure 4.2 shows SEM image of untreated CFW morphology. The images has unstructured in nature, irregular in shape with uneven edge agglomerate and porous in the surface. The same phenomena was reported in physico-chemical characteristics of kaolin clay by (Yahaya et al., 2017). It also showed agglomeration of the particles. The pore holes are not observed continuously on the surface of CFW. This indicates may be the CFW, a clear layered rectangular shapes observed that indicate the natural kaolinite, is double layer Alumino-silicate clay (Olaremu, 2015).

4.1.2. Activated CFW

Specific calcination temperature at which the crystalline CFW changed to amorphous CFW were investigated at different temperature ranging from 500 to 675 ^{o}C. When CFW was calcined and quenched by air, air quenched chemical factory waste (AQCFW), it didn't change the crystalline structure to amorphous. Therefore, a new developed approach was followed to prepare amorphous silica enriched CFW. The developed method was calcination of CFW at different temperatures followed by immediate quenching in water. This method altered the crystallography structure of CFW as it is validated by crystallographic arrangement XRD analysis in Figure 4.3.

Table 4.2 Calcination and Quenching Temperature

Sample Name	Calcination Temperature	Quenching Temperature
CFW-500 ^{o}C/ CFWA	500 ^{o}C	10 ^{o}C
CFW-600 ^{o}C/CFWB	600 ^{o}C	10 ^{o}C
CFWC-650 ^{o}C/CFWC	650 ^{o}C	10 ^{o}C
CFWD-675 ^{0}C/CFWD	675 ^{0}C	10 ^{o}C
CFW-600 ^{o}C & Air Quench/AQCFW	600 ^{o}C	Room Temperature

Calcine CFW possesses a crystal- like short-range molecular arrangement, but lacking a long-range order. Upon cooling of the calcinated CFW below the freezing point, molecular motion is slowed down. If cooling of the calcinated CFW takes place fast enough, the molecules are not able to rearrange into a crystalline lattice; therefore, they are stack in a more disordered state and crystallization can't be reversed. Therefore the CFW was transformed to activate CFW that is ready for reaction with cement clinker as well as sodium hydroxide in the case of hydrothermal treatment. CFW calcination and quenching Process condition are summarized on Table 4.2.

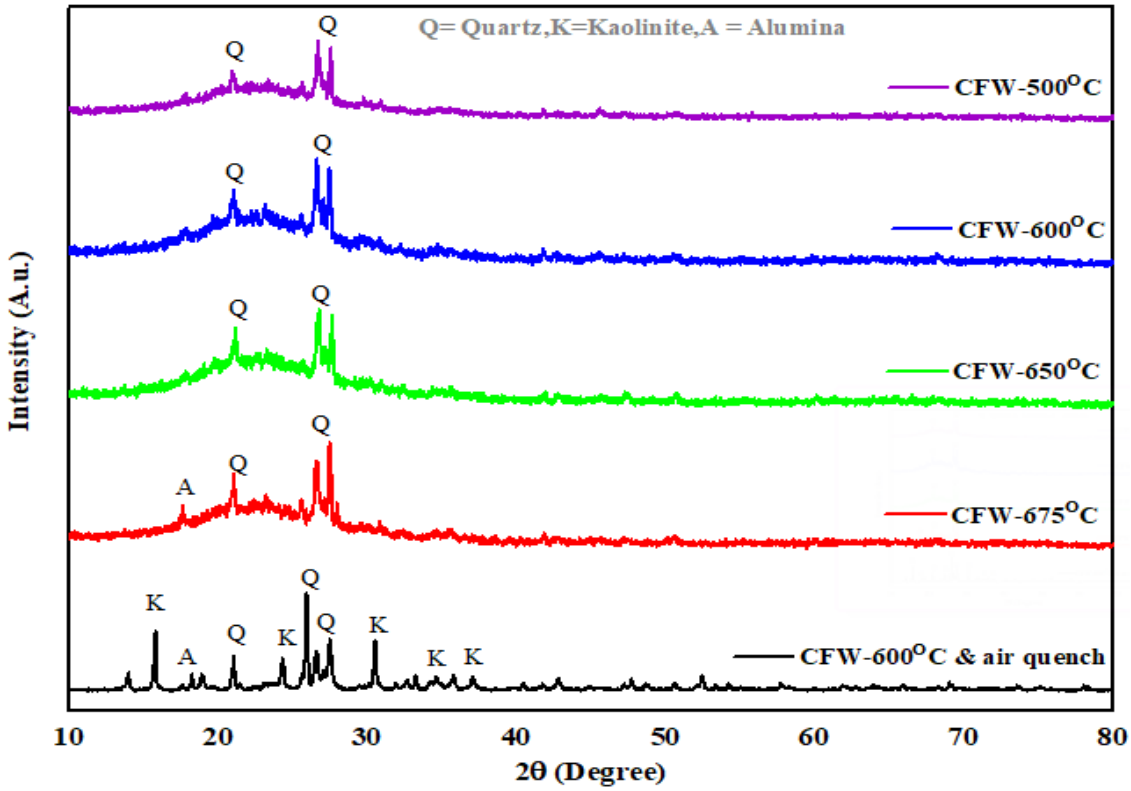

FIGURE 4.3 XRD Pattern of Activated CFWs at Various Temperature

Different amorphous materials have been prepared by different calcination temperature and quenching. The peaks at 2Θ = 15.8, 13, 30.4,35 and 37.4 ^{o} disappeared but the peak at 2Θ = 21.01 and 26.67 ^{o} was not affected by the thermal and quenching treatment, attributed to the presence of quartz. The major peak present in activated CFW is attributed to due to quartz. Previous work indicates crystallized silica is thermally stable even after calcination at 1050 ^{o}C (Edomwonyi-Otu et al., 2013).

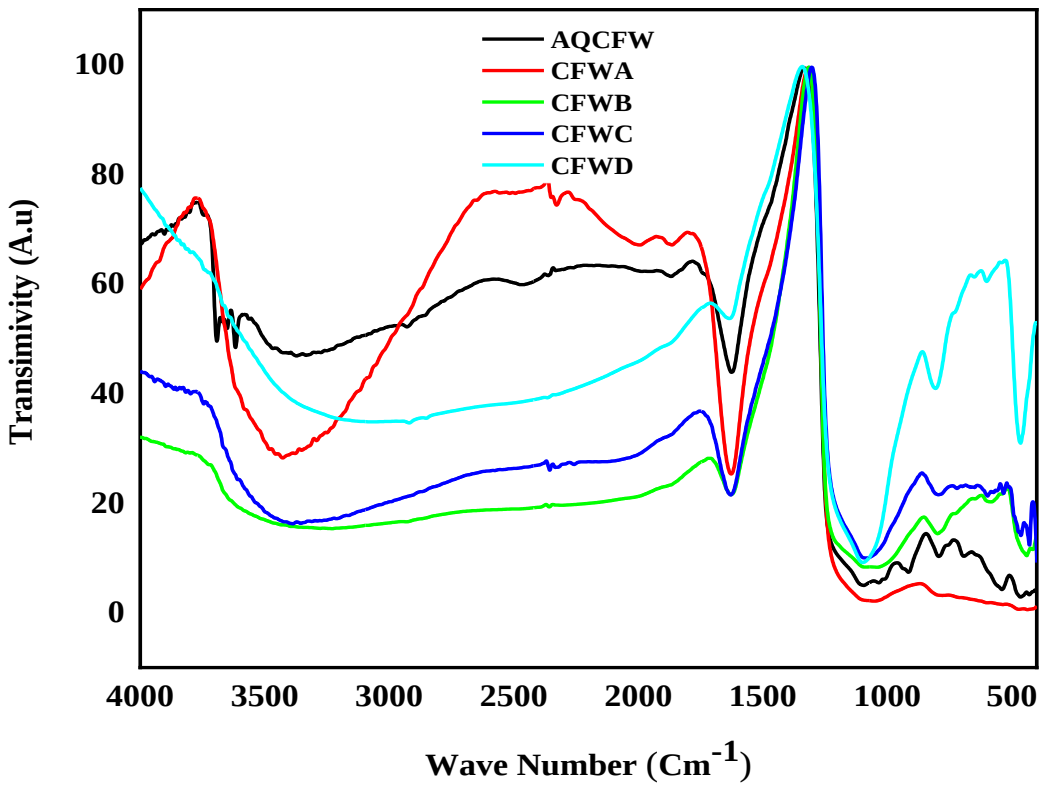

FIGURE 4.4 Micromolecular Arrangement of Activated Replacement and Calcinated CFW

(Figure 4.4) shows the FT-IR spectra of calcinated CFW and activated CFW crystals respectively, both were characterized by different vibration belong to Si-O, Al (VI)-O, Al (VI)-OH and Si-O-Al bonds. Bands around 3620 cm^{-1} related to Al (VI)-OH stretching vibration. With quenching of CFW these band disappear and 4-coordination vibration of Al (IV)-O appear at around 805 cm^{-1} band. The broad bands in the region of 3400- 1630 cm^{-1} are character of stretching and deformation vibrations of O-H and H–O–H groups from the weakly bound water molecules, which are reduced in infrared spectra of CFWA, CFWB, CFWC and CFWD. The band at 1630 cm^{-1} showed in decrease on transimitivty with increasing amorphous nature (Mohkami et al., 2011). The broad bands at about 3400 cm^{-1} and 1630 cm^{-1} show adsorbed atmospheric water. These bands start to decrease Transimivity with increasing calcination temperature. It is due to decreasing in amount of adsorbed water in CFW and owing to the weak bonding at higher temperature. This might cause weak vibrations at higher temperature resulting in less intense peak in calcinated CFW. The Si–O stretching vibration at 1090 cm^{-1} , Si–O–Al vibration at 805 cm^{-1} and Si–O bending vibration at about 470 cm^{-1} also present IR spectrum.

The band centered at 1090 cm^{-1} in the IR spectrum, corresponding to the Si–O-Si or Si-O-Al bond became broad due to decreasing of crystallite structure during quenching and formation of metakaolin like structure. It was observed that the peak on AQCFW, which is calcinated and air quenching sample showed a sharper peak at 1090 cm^{-1} band than other activated CFW. This is due to the crystallite structure of AQCFW sample exhibit high crystallite, which is supported by XRD crystallographic structure analyses.

4.1.3 Crystallinity Difference

From Origin software analysis, the FWHM of the samples AQCFW, CFWA, CFWB, CFWC and CFWD were calculated using fitting method. Crystallinity index is the ratio of the crystalline peaks to the sum of crystalline and amorphous peaks. Amorphous peaks are the noise in XRD data, whereas, the sum of crystalline and amorphous, represents the whole XRD profile

$$\text{Crystallinity}(D) = \frac{K * \lambda}{FWHM * Cos(2\theta)} * 2 \quad \ldots\ldots 4.1$$

$$\text{D Average} = \frac{\sum \text{D}}{\text{n}} \quad \ldots\ldots 4.2$$

$$\text{Crystallinty} = \frac{\text{Area of crystalline peaks}}{\text{Area of all peaks (Crystalline + Amorphous)}} * 100\% \quad \ldots\ldots 4.3$$

$$\text{Amorphous \%} = 100\% - \text{Crystalline \%} \quad \ldots\ldots 4.4$$

Table 4.3 Summarized Amorphous and Crystalline Percentage of Samples

Sample	Amorphous (%)	Crystalline (%)
CFW – 500 ^{o}C/CFWA	88.00	11.9
CFW – 600 ^{o}C/CFWB	89.5	10.5
CFW – 650 ^{o}C/CFWC	87.6	12.3
CFW – 675 ^{o}C/CFWD	86.6	13.4
AQCFW	24.57	75.43

Numerical Calculation for crystalline and amorphous percentage of samples is represented on appendix B. The crystalline percentage of the calcinated and quenched samples showed less than a 15% crystallite. All the activated CFW can be taken as amorphous phase kaolinite. Table 4.3 showed that CFWB (calcination at 600 ^{o}C then quenched at 10 ^{o}C) have the smallest Crystallite percentage which indicates it is more amorphous compare to the other forms. The lowest value also indicates it is more ready for any kind of reaction to take place. This can be taken as the optimum activated CFW for both synthesis of Zeolite based catalyst and cement clinker replacement material. It consist silica and alumina in active form and react with $Ca(OH)_2$ to form C-S-H gel which will enhance strength as well as react with NaOH for synthesis of zeolite based catalyst.

4.2. Product Characterization of Cement Mortar

4.2.1. Chemical Analysis

The CO_2 emission reduced and energy save from CFW replacement material is calculated in detailed on appendix A. With the save energy by CFW replacement material the cost of clinker production reduced is also calculated on appendix A.

The procedures for the chemical examination of cement and lime by wet chemistry are specified in ISO 29581. Table 4.4 shows the average values of three different cement clinker samples. In chemical analysis of cement clinker compound analysis were carried out to figure out compounds like SiO_2, $A1_2O_3$, Fe_2O_3, CaO and other component. CaO, SiO_2, Al_2O_3 and Fe_2O_3 are the major component of cement clinker, it accounts for more than 95% and MgO, TiO_2, P_2O_5 and alkalis are the minor components in initial less than 3%.

Table 4.4 Clinker Oxides Composition (%)

	SiO_2	**$A1_2O_3$**	**Fe_2O_3**	**CaO**	**F- CaO**	**MgO**	**SO_3**	**LOI**
Clinker	21.43	5.67	3.32	65.81	1.05	1.59	0.64	0.42
Standard	20.5-22	5.0-5.5	3.3-3.9	65-66.5	<2.20	1.0-2.0	0.5-0.8	0.3-0.5

The major components are not present in individual oxide, but exist as compound formed by two or more oxides C_3S, C_2S, C_3A and C_4AF are the composition minerals of the clinker. Using bogus equation we can calculate the mineral composition of cement clinker on appendix C.

Lime Saturation Factor (LSF) is the ratio of the actual amount of CaO in raw meal/clinker to the theoretical lime required by the major oxides (SiO_2, Al_2O_3 and Fe_2O_3) in the raw mix or clinker. The LSF notion refers to the amount of lime in the cement compared to the amount of lime necessary to generate C_3A, C_3S, and C_4AF in the clinker. It controls the clinker's Alite (C_3S) to Belite (C_2S) ratio. In the clinker, a higher Alite to Belite ratio indicates a better LSF. The standard LSF for all cement is well below 100%. The LSF was found to be 0 .954.

Silica Modulus (SM) is the ratio of content of SiO_2 to the Al_2O_3 and Fe_2O_3. The ratio of solid to melt content is denoted by the letter SM. The SM of cement indicates the amount of SiO_2 it contains. A greater SM makes cement raw material burning more difficult. The typical SM in cement is between 2.3 and 2.5. The SM was found to be 2.39.

Alumina ratio (AR): is the content Al_2O_3 to Fe_2O_3 ratio. AR denotes the temperature at which liquid formation begins, the type of liquid that forms, and the color of the clinker that forms. This regulates the C_3A/C_4AF ratio in the cement. The typical AR in cement is between 1.5 and 2.5. The AR was found to be 1.71.

The mechanism of the lime – CFW reaction in Portland cement is yet unknown. Within 24 hours, the reaction usually starts, producing considerable amounts of secondary aqueous calcium silicate and significantly enhancing the microstructure. The predicted chemical reactions are represented on appendix C.

4.2.2. Flexural and Compressive Strength

Mortar samples of 2 and 28 days were tested for its flexural strength and compressive strength having different percentage of activated CFW as a replacement of cement. The level of replacement of cement by different Activated CFW was 5%, 10% and 15%, three sample of each replacement were tested for flexural strength and mean of these three samples is the flexure strength of mortar. In this research the mixing ratio was 1: 2: 4 and have a constant (w/c) ratio of 0.55. Reference mixture samples without any activated CFW were used as benchmark samples.

After the flexure strength of mortar was identified. The cement piece was fed to compressive strength machine to be tested for compressive strength. Six sample of each replacement were tested for compressive strength and mean of these six samples is compressive strength.

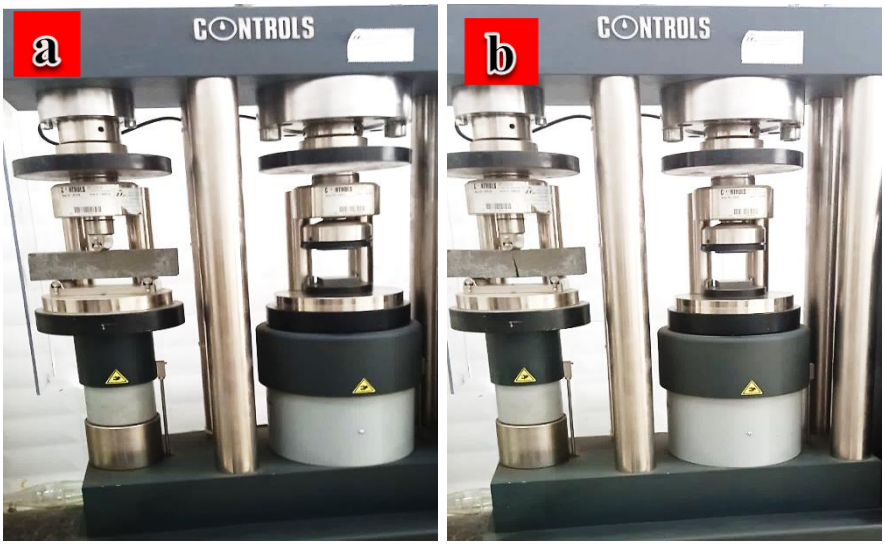

FIGURE 4.5 Cement Mortar in Compressive Strength Machine (a) and Cement Mortar Failure (b)

There are 2 types of OPC, which are distinguished by 2 day compressive strength. R type OPC and N type OPC. For N type OPC, the 2 day curing compressive strength should be greater than 10 MPa, while R type OPC should be greater than 20MPa. The strength development is related with the chemo-physical properties of the activated CFW replacement in addition to clinker property. In 2 days cured mortar the replacement act as filler partially filling void between cement grains. The reactivity of activated CFW was very slow at the beginning of hydration since it had decreased the compressive strength compare with the bench mark sample although the decrement isn't significant. CFWB with 5 and 10% can be used for production of R type OPC as well as CFWD with 5% replacement. The rest replacement can be used for production of N type OPC. It can be concluded that the activated CFW used act as filler in the beginning of hydration.

The clinker replacement material with great flexural strength results were obtained at later aging. After 28 days of curing, the CFWB partial replacement sample showed a substantial

increase in compressive and flexural strength of material compared to other samples. This suggested the presence of an active silica alumina component in the replacement that reacts with clinker to hold the hydrate in place. Amorphous silica can help convert C_3A hydration products like C_3AH_6 and C-A-S-H gel into more stable forms (Zheng, et al., 2021). Additional C-S-H and C-A-S-H gels are formed when amorphous silica aluminum reacts with the remaining free lime and unreacted $Ca(OH)_2$. The reaction with C_3A to form another C-A-S-H gel is the other predicted reaction. During hydration, amorphous silica dissolves and forms the silica anion. The anion produced is thought to be adsorbed on the surface of C_3A. Other ions generated during C_3A dissolution, such as Ca^{2+} and $Al(OH)_4$, react with adsorbed silica anion to form new C-A-S-H gels. The hydration reaction is what causes the amorphous CFW replacement material to increase the strength of cement mortar.

Table 4.5 represents all the results of flexural and compressive strength and figures 4.6(a__b) shows its graphical representation. Except CFWA all replacement material obey the standard strength development of OPC cement with 28 days curing which should be greater than 42.5 MPa. CFWA clinker replacement material showed retardation effect on compressive strength because it hasn't participated in the hydration reaction. It has affect the amount of clinker should be used instead of the replacement which retards the hydration of cement. This showed there is less amount of activated silica alumina material in the sample. This is also supported by crystallographic XRD analysis showing less amorphous phase than other replacement material used.

Table 4.5 Flexural and Compressive Strength (MPa) After 2 and 28 Days of Curing

Cement content (%)(clinker, gypsum, CFW, Sand & Water)	2 day		28 day	
	Mean Flexural Strength (MPa)	Mean Compressive Strength (MPa)	Mean Flexural Strength (MPa)	Mean Compressive Strength (MPa)
C95G5CFW0SW	5.32	22.55	8.3	45.13
C90G5CFWA5SW	4.87	19.33	7.91	40.85
C85G5CFWA10SW	4.62	16.51	7.84	39.42
C80G5CFWA15SW	3.77	15.34	7.02	37.1
C90G5CFWB5SW	4.27	21.84	8.1	43.2
C85G5CFWB10SW	5.37	23.92	9.6	58.3
C80G5CFWB15SW	4.06	18.41	9.2	54.3
C90G5CFWC5SW	5.03	19.62	8.5	46.18
C85G5CFWC10SW	4.93	18.05	9.1	51.35
C80G5CFWC15SW	3.85	13.96	8.9	49.22
C90G5CFWD5SW	4.37	21.62	8.04	42.97
C85G5CFWD10SW	3.99	17.23	7.73	49.83
C80G5CFWD15SW	4.96	16.99	7.3	43.53

Note S – Sand and W – Water

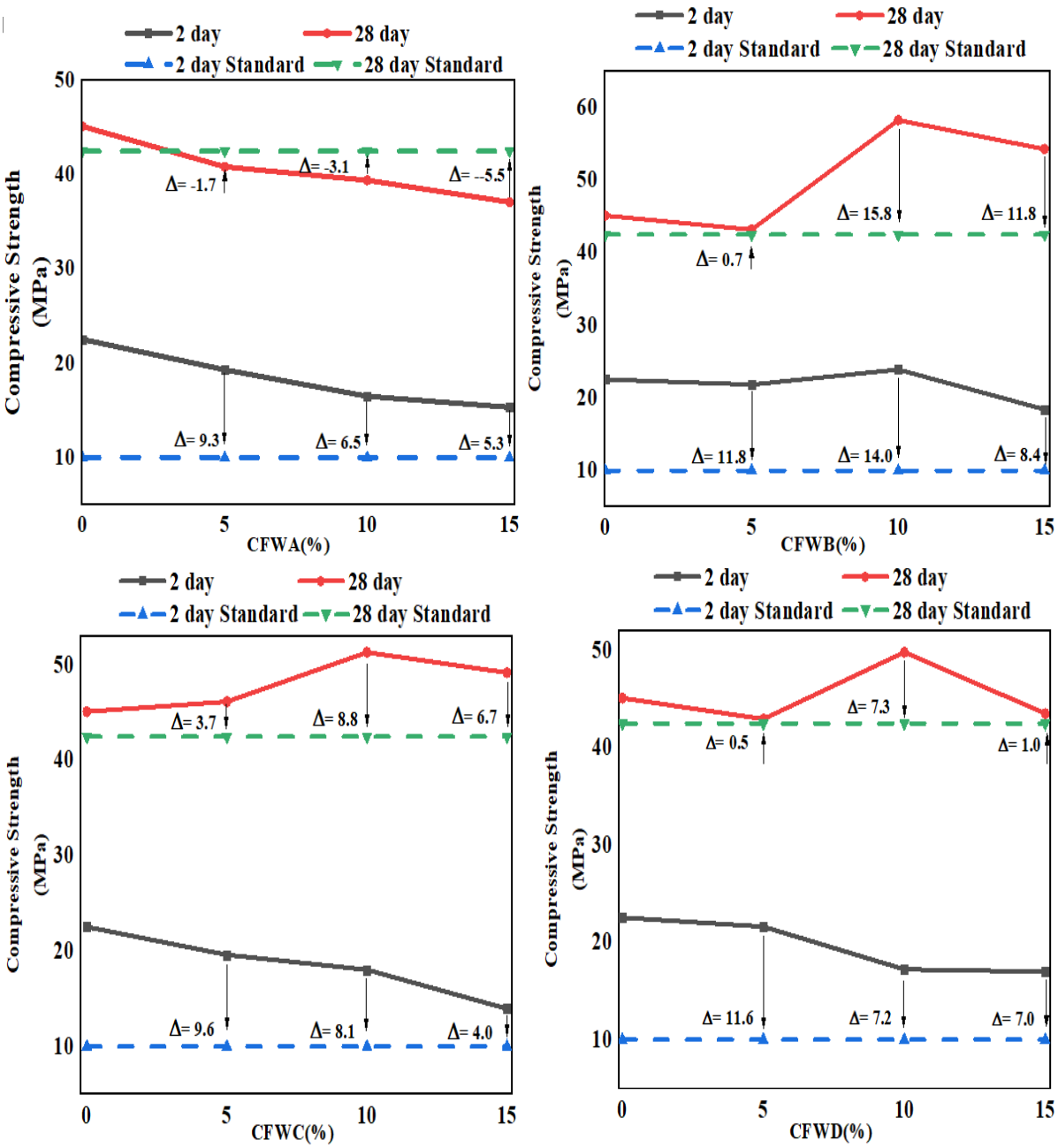

FIGURE 4.6 Effect of Different Clinker Replacements on Compressive Strength of Cement

Strength Activity Index

The pozzolanic properties of various substances can be analyzed using strength activity index (SAI) method (Mohammad Razaul, 2017). Majority SAI values at the ages of 2 and 28 days were

found higher than the minimum requirement of 75% as specified in ASTM C618(ASTM, 2010) Strength activity index is defined as:

$$\text{Strength activity index} = \frac{R}{O} * 100 \quad \text{eqn 4.8}$$

Where R is average compressive strength of CFW based mortar cube; and O is average compressive strength of reference mortar cube.

Table 4.6 Strength Activity Index Results

	SAI (%)	
Mix designation	**2 day**	**28 day**
C90G5CFWA5SW	85.72	90.51
C85G5CFWA10SW	**73.21**	87.34
C80G5CFWA15SW	**68.03**	82.20
C90G5CFWB5SW	96.85	95.72
C85G5CFWB10SW	106.07	129.18
C80G5CFWB15SW	81.64	120.31
C90G5CFWC5SW	87.01	102.32
C85G5CFWC10SW	80.04	113.78
C80G5CFWC15SW	**61.91**	109.06
C90G5CFWD5SW	95.87	95.21
C85G5CFWD10SW	76.41	110.41
C80G5CFWD15SW	75.34	96.45

Note: The values shown in bold represent sample not satisfying values of SAI as per ASTM C618(ASTM, 2010).

It was seen that majority of cement with replacement has achieved the standard strength activity index except 10%, 15% of CFWA replacement and 15% of CFWC replacement. These indicate the replacement chosen can be approved for replacement material with in standard.

4.2.3. Blaine Air Permittivity Test

Compressive strength test with different fineness of 3615, 2590 and 1200 cm^2/gm and different proportion of cement clinker replacement of 5%, 10% and 15% of CFWB was carried out on. With different fineness, compressive strength test was carried out on cubes cast from every proportions of cement prepared as per BS 1881: Part 108,111,116:1983 at the ages of 2 and 28 days.

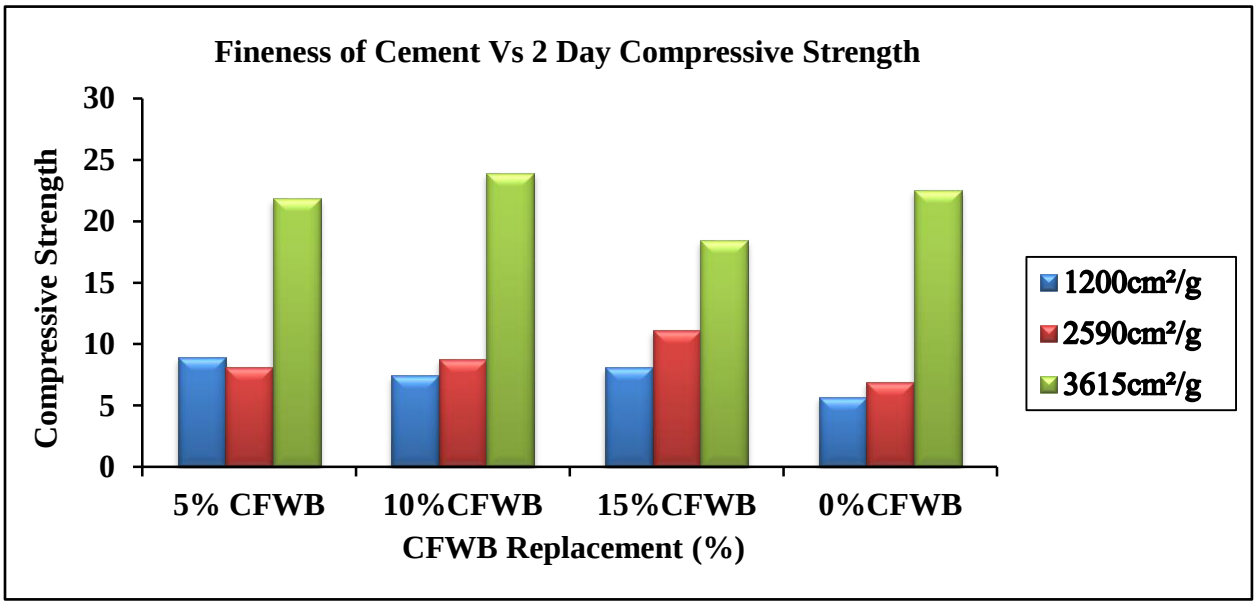

FIGURE 4.7 Effect of Fineness of Cement on 2 Day Aging of Compressive Strength

Figure 4.7 shows a nonlinear connection between cement clinker surface area and mortar. strength for 2 days curing. When compared to a blank cement mortar, replacement cement mortar demonstrated an increase in compressive strength with a difference in fineness. In general, cement clinker replacement with CFWB with fineness of 3615 cm^2/gm resulted in better compressive strength for both early and later aging. This suggests that increasing fineness is

linked to the amount of surface area accessible in direct contact with water. Later on, the rates of hydration and the development of associated strength are improved. It was also discovered that increasing clinker surface area enhances reactivity with SiO_2 and $A1_2O_3$ of silica enriched replacement CFW with the clinker to facilitate heat of hydration and contact with water during the hydration process.

10% replacement showed better compressive strength on 3615 cm^2/gm fineness for early aging. It also obeys the standard strength class of 42.5R cement. 5% of cement replacement with 2590 and 1200 cm^2/gm have showed greater compressive strength than other replacement and blank cement mortars for early aging.

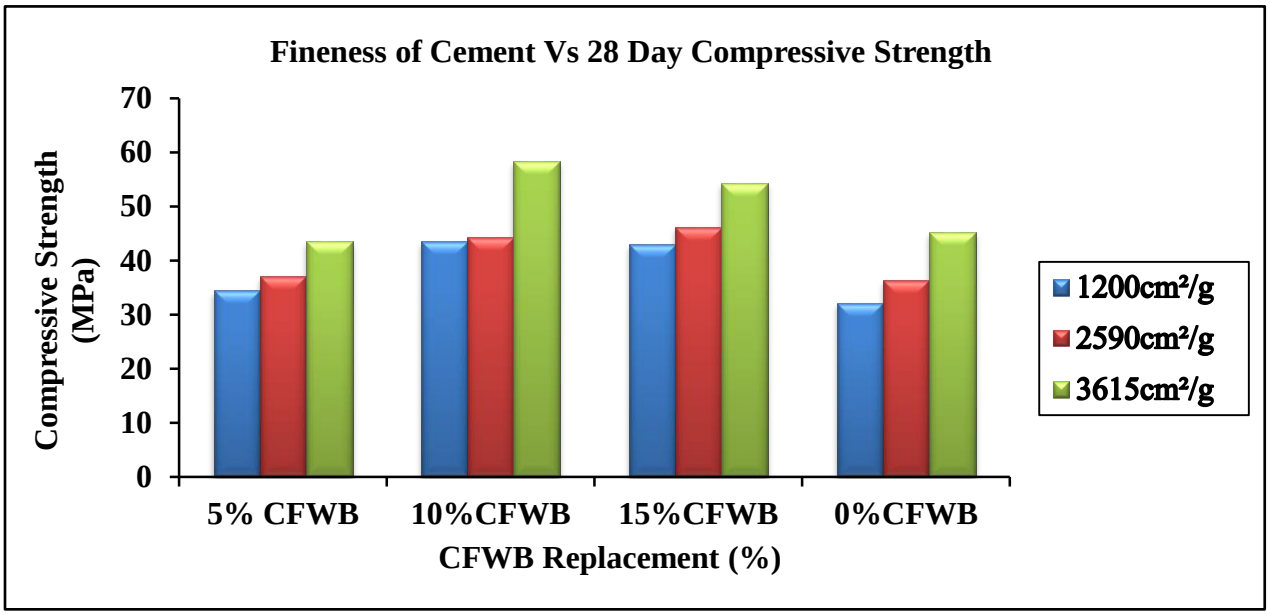

FIGURE 4.8 Effect of Fineness of Cement on 28 Day Aging of Compressive Strength

Figure 4.8 shows a nonlinear connection between cement clinker surface area and mortar strength for 28 days curing. Fineness has a greater impact at an early age, and it has less of an impact as become later aged. This is due to the fact that finer cement (due to its larger surface area) reacts more readily with water at early ages. The effect of fineness on cement is also linked to increased cohesiveness and less bleeding. The cement crystals are surrounded by a dense calcium-silicate-hydrates (C-S-H) gel as it age, which prevents water diffusion and hence slows the hydration process. Although fineness has little effect on the compressive strength of cement as it ages.

4.2.4. Setting time and Soundness of Cement

Initial and final setting times of optimum cement replacement and Reference mixture samples without any CFW was used as benchmark samples , which are determined using the Vicat needle test, are used as a quality control measure for cement characterization(ČSN, 2017; Standard, 2005) and specified as a requirement in related standards (EN, 2011). Table 4.3 shows a comparison of the initial setting time, total setting time, and expansion of cements with and without CFW. The following parameters influence the setting time: water/cement (w/c) ratio, temperature and relative humidity, cement fineness, and chemical composition. (Wijaya et al., 2016). In this scenario, the water/cement (w/c) ratio, temperature, relative humidity, and cement fineness were all kept constant. As a result, the chemical composition of cement paste is the only element that influences its setting time. When compared to a blank sample, the initial setting time increases as the CFW content is introduced. Aluminum oxide (Al_2O_3) causes cement paste to set quickly.(Arimanwa et al., 2016). Cement sample with replacement contained highest quantity of Al_2O_3 resulting in the fastest initial set of the cement paste compare with benchmark.

Free lime can be present due to surplus lime in the kiln's raw material or insufficient burning or cooling. This hard-burnt lime hydrates slowly, and because slaked lime has a bigger volume than free calcium oxide, it expands. These phenomena were observed on the blank sample, generating greater expansion than the replacement material, despite the fact that the expansion of cement paste was reduced by 12.5% when activated CFW was added. This suggests that the current free lime reacts with the amorphous silica alumina on CFW, as revealed in the chemical study above. It also satisfied the standard soundness of cement paste with 0.5 mm. Although the presence of magnesia on CFW, it isn’t responsible for any kind of unsoundness to occur on cement paste. This showed the minority component on CFW have insignificant effect on cement clinker replacement.

Table 4.7 Setting Time and Soundness of Cement

	Setting Time		Expansion Test (mm)
	Initial Setting time (min)	Final setting time (min)	
C85G5CFWB10	93.0	140	0.5
Blank Sample	80.0	160	2.61
Standard	≥75	≤600	≤10

4.3. Product Characterization of Zeolite Based Catalyst

4.3.1. Effect of Synthesis Condition on Crystallographic Arrangement of Zeolite Catalyst

Powder X-ray diffraction was used to determine the sample crystallinity. The formation of zeolite from Awash Melkassa chemical factory waste was confirmed by comparing its XRD pattern to document by International Zeolite Association (IZA) powder pattern identification diffractograms table indicating a FAU structure, According to Treacy and Higgins within a range of 2θ = 5-50 ^{o}. The synthesized zeolite exhibited similar crystalline structure to standard zeolite Y although intensity of peak is lower. The first peak for standard zeolite Y appear 6 – 7 ^{o} (Treacy, et al., 2007). It has been reported that zeolite P appear as a second phase in zeolite Y synthesized (Salman, 2007). The major peak 2Θ expected on standard zeolite Y is 6.31, 10.31, 12.01, 15.92, 17.91 and 24.52 ^{o}. The first three strongest peak for each zeolite was observed at 2θ = 6.34, 12.64 and 15.80, then 2θ = 6.33, 26.8 and 31.2 ^{o}, finally, 2θ = 6.25, 26.70 and 31.06 ^{o}, with approximately similar d-spacing shown (Table4.9)

Effects of Gel Aging Time on Zeolite Synthesis

During the study of gel aging time effects on zeolite synthesis, the zeolite crystallizations temperature and Na_2O/SiO_2 were made constant at 110 ^{o}C and 0.6, respectively(Adane, 2020). Figure 4.10 shows XRD patterns of the sample which were prepared at different aging time of 12, 24, 36, 48 hour and with no aging time. On the figure, the aging time of 12, and 0 hour were

matched with that of Y standards from International Zeolite Association (IZA) powder pattern identification diffractograms table by (Treacy, et al., 2007) indicating a FAU structure except the first major peak on zeolite Y haven't appeared in 0 hour aging of gel. However, 24 hour aging time sample pattern were transformed more off to zeolite ZSM -5. The ZSM - 5 XRD pattern also confirmed with the same way as zeolite Y confirmed. The spectrum of the 12 hour aging sample was similar to that of standard zeolite Y from (IZA), with the exception of some quartz impurity (Środoń et al., 2001), other peaks indicated that the Y type zeolite was obtained. The presence of impurities may be caused by incomplete transformation of CFW into full developed amorphous CFW phase during physical treatment which is also supported on XRD pattern of activated CFW. With increasing aging time at room temperature zeolite P and ZSM -5 are formed with a high background noise indicating that the sample still contained an amount of amorphous material. The XRD patter of zeolite prepared within 12 hour aging time has showed similar index of XRD patterns of standard zeolite NaY, all diffraction planes (hkl) correspond to NaY phases were 111,311,331, 551 and 733 in good agreement with Joint Committee for Powder Diffraction Standards (JCPDS) those reported in the literature (Treacy, et al., 2007) which can be found at appendix F.

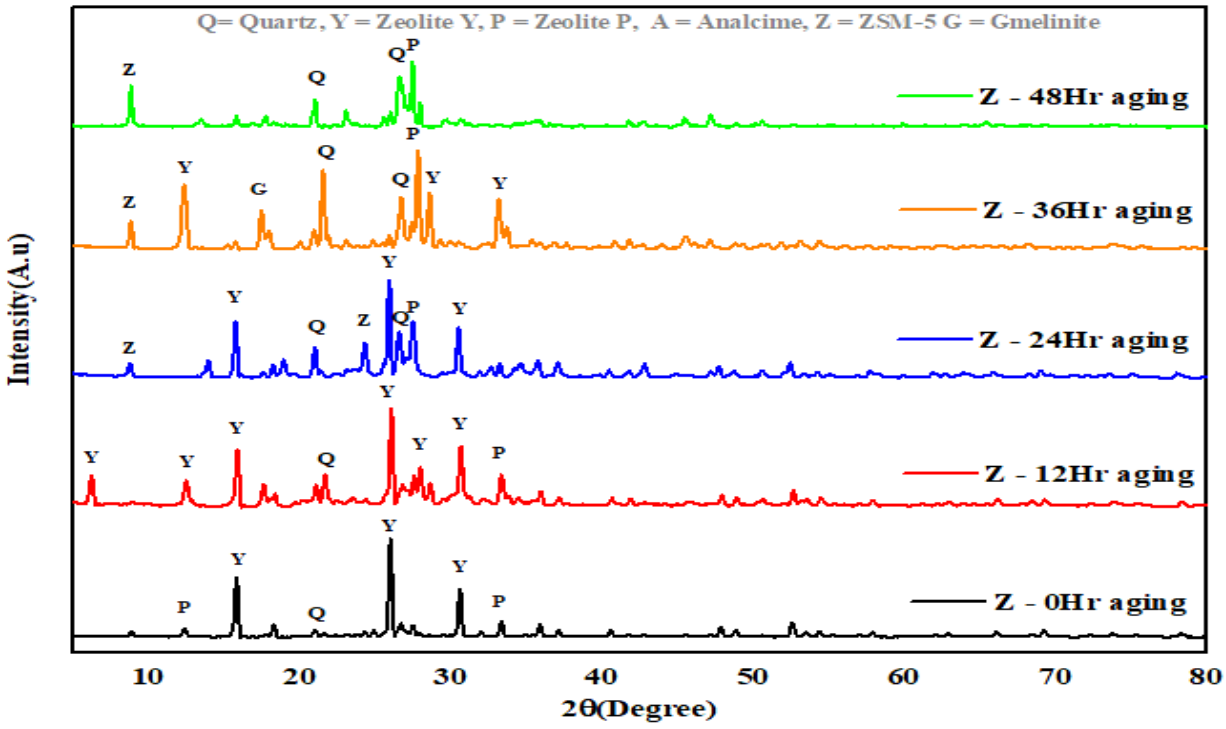

FIGURE 4.9 XRD patterns of Zeolite Synthesized with Different Aging Times

Effect of Composition on Zeolite Synthesis

During the study of molarity effects on zeolite synthesis, the zeolite aging time and crystallization temperature were made constant at 12 hour and 110 ^{o}C. 0.6, 0.7, 0.8 and 0.9 Na_2O/SiO_2 was used. It was observed that the intensity of the primary peak at 6.24 ^{o} didn't appear on 0.6 Na_2O/SiO_2 ratio. This is due to the low crystalline phase of the zeolite Y within the synthesized samples which may be attributed to factor like the presence of impurities within the alumina and silica used. This shows that zeolite manufacturing is promoted with a better NaOH concentration. Increasing the alkalinity during synthesis of zeolite will lessen the dissolution time of the silica and alumina within the activated CFW. Hence, the reactivity was improved in addition to the de-polymerization of silica species. This is due to the fact that when NaOH comes in contact with the activated CFW, it produces OH^- ions. The release of those OH^- ions in the solution, favors the breakdown of Si-O-Si, Si-O-Al and Al-O-Al bonds in the activated CFW. As a result, free silicon and aluminum ions are released into the solution to form Si-OH and Al-OH bonds which are essential for the zeolite Y. 80, 62, 55 and 40% of synthesized zeolite Y percentage was calculated with different Na_2O/SiO_2 ratio of 0.9, 0.8, 0.7 and 0.6 respectively.

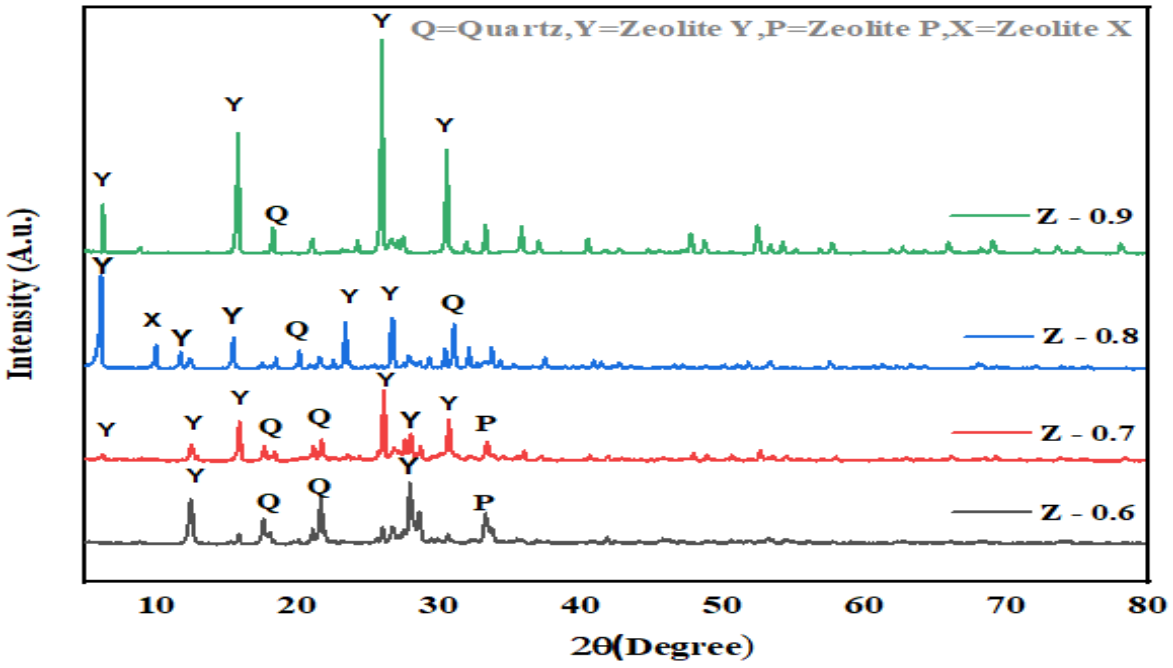

FIGURE 4.10 XRD Patterns of Zeolite Synthesized with Different Na_2O/SiO_2 Ratio

Table 4.8 Comparison of Lattice Spacing, between the Developed Zeolite Y from Awash Melkassa CFW and Standard Zeolite NaY from International Zeolite Association (IZA)

Zeolite Y Prepared from Chemical Factory Waste		Standard Zeolite Y (IZA) By Treacy and Higgins	
2Ɵ (degree)	d, spacing (A^o)	2Ɵ (degree)	d, spacing (A^o)
6.34	13.93	6.31	14.00
12.64	7.22	12.10	7.31
15.80	5.60	15.92	5.56
26.14	3.41	26.24	3.40
27.72	3.17	27.52	3.24
30.56	2.92	30.16	2.96
33.52	2.67	33.66	2.66

The synthesized zeolite was characterized using PSA to determine the size of the particles appropriately at a temperature of 25 ± 2 °C. Water dispersant with refractive index of 1.330 and viscosity of 0.8872 Cp was used. Size distribution by intensity percentage was drawn with counting rate of 233 and measuring position of 0.65 mm. It has showed 100% intensity was recorded at 73.22 nm size of zeolite. It was concluded that zeolite synthesized from Awash Melkassa chemical factory waste by this method is nano size particle.

4.3.2. Micro molecular Arrangement of Zeolite Based Catalyst

The FTIR spectra were obtained in the region of 400–4000 cm^{-1} to characterize the vibrations structure of sample. ZY1, ZY2 and ZY3 represented zeolite synthesized with 0.9, 0.8 and 0.7 Na_2O/SiO_2 ratio. The band at 3400 cm^{-1} corresponds to Si–OH, Si–OH–Al or OH hydroxyl groups. 2000-2360 cm^{-1} stretching corresponds to Si-H (silane). The water-bending vibration at 1620 cm^{-1} indicates the presence of adsorbed water in zeolites. The band at 590 cm^{-1} is assigned

to the double ring external linkage band (Yin et al., 2012). The band at 940 cm^{-1} and 710 cm^{-1} represents the Si–O, SiO–Al, Al–OH asymmetric and symmetric stretching vibrations corresponding to the internal TO_4 structure (T = Si, Al), while the bands at shoulder 1097 and 710 cm^{-1} represent the asymmetric and symmetrical stretching vibrations corresponding to the external TO_4 structure (T=Si, Al), respectively(Yin, et al., 2012).

Table 4.9 General Infrared Assignment to Zeolite

Internal Tetrahedral	Assignment (cm^{-1})	External linkages	Assignment (cm^{-1})
Asymmetric stretch	1250-950	Double ring	650-500
Symmetric stretch	720-650	Pore opening	420-300
T-O bend	500-420	Symmetric stretch	820-750
		Asymmetric stretch	1150-1050

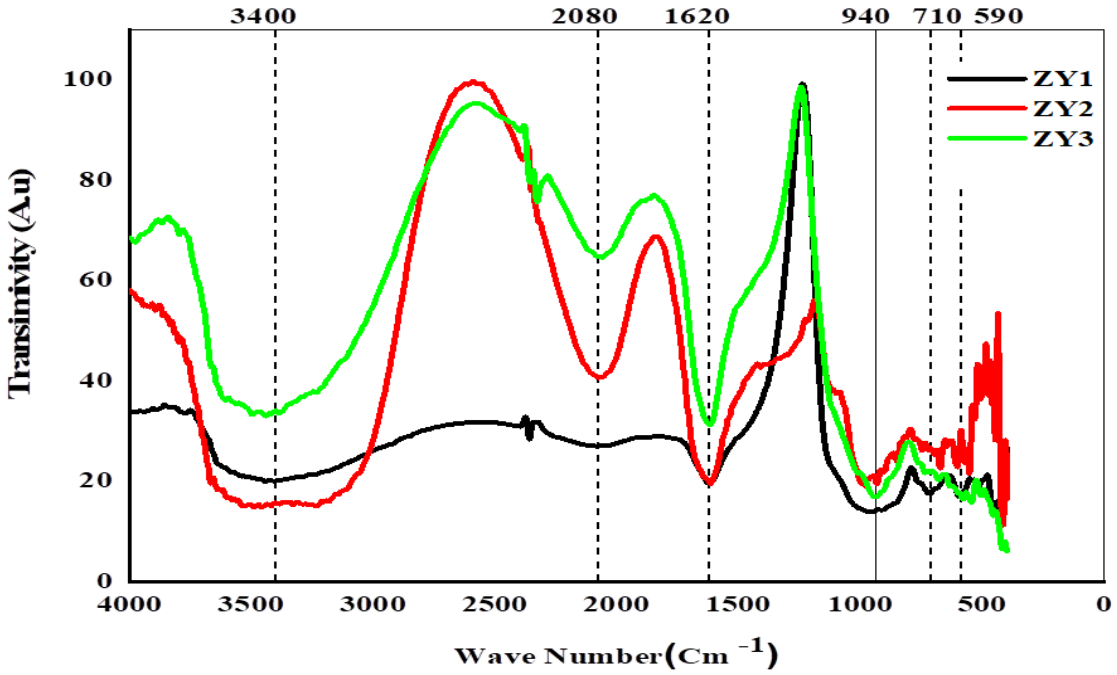

FIGURE 4.11 Micromolecular Arrangement of Zeolite by FTIR

broad band at 3400 cm^{-1} was due to the hydrogen bonding of water with OH groups, the bands in the hydroxyl spectral region (3,000– 4,000 cm^{-1}) are generally structure less and broad. Band 2080 cm^{-1} starts to become weak peak with increasing molarity of NaOH. With increasing the molarity of NaOH the Si-H bond become weak. Band 1620 cm^{-1} broadens with increasing molarity of NaOH where the absorbed water disappears with Na attachment increment. Shoulder band 1030 cm^{-1} showed asymmetric stretching vibration absorption band of Si-O(Na) in zeolite, Which happen to be present on different molarity of NaOH attachment on zeolite. The Si–O, SiO–Al, Al–OH asymmetric and symmetric stretching vibrations corresponding to the internal TO_4 structure (T = Si, Al) are represented by bands at 940 cm^{-1} and 710 cm^{-1} on all type of zeolite synthesized, respectively, whereas the external TO_4 structure (T=Si, Al) is represented by bands at 1097 and 710 cm^{-1}. It can be conclude the result presented in figure 4.12 shows that FTIR spectrum of the synthesized zeolite ties with the typical absorption peaks of the standard zeolite(Garcia et al., 2016)

4.3.3. Morphology of Zeolite Based Catalyst

SEM was used to characterize the general features of zeolite based catalyst crystals. For this work, morphology was studied by using Scanning Electron Microscopy from JEOL, JCM-6000 Plus (Washington D.C, USA) with applied potential 15 kV.

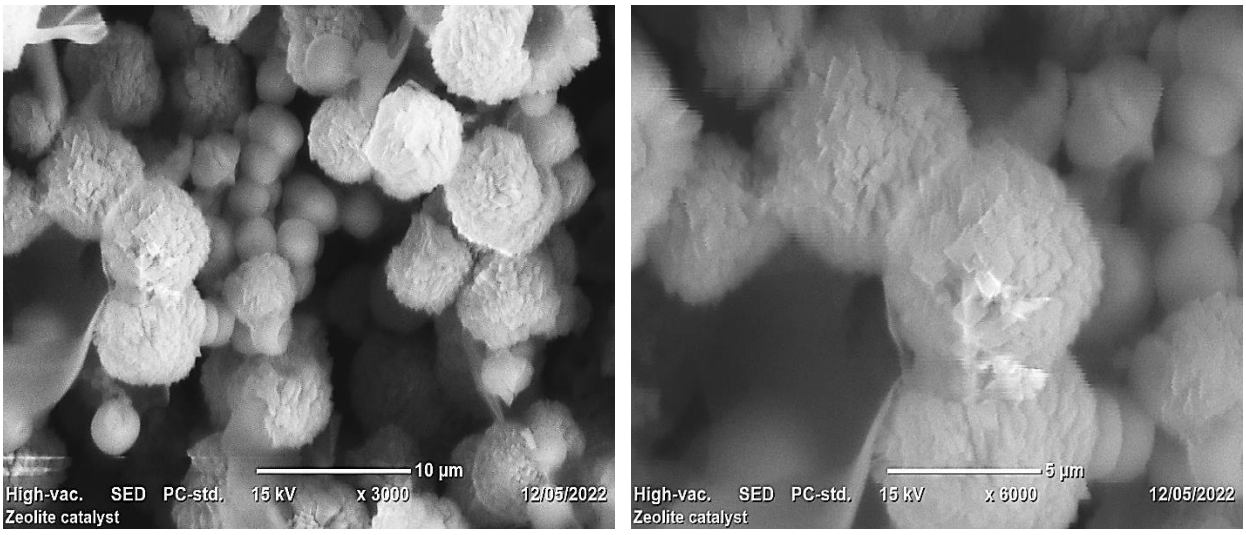

FIGURE 4.12 SEM Image of General Morphology Synthesised Zeolite Based Catalyst

Figure 4.13 is the SEM image of the developed zeolite Y with some secondary phase of Zeolite P. it was observed that a cubic shaped with in spherical. The cubic structure showed zeolite Y morphology. Similar report had been done by (ROUQUEROL, 1999). This is in agreement with XRD analysis result. Similar phase transformation of zeolite P and Y was studied (Azizi et al., 2013).

4.3.4. Surface Area and Pore Volume analysis using BET

To calculate the BET (Brunaure Emmett Teller) surface area and pore volume, nitrogen adsorption–desorption was performed using Quantachrome Instruments version 11.0. The pore volume and surface area are also measured. This equation is used to compute BET surface area.

$$S_A = \frac{V_m}{22400} * a_m * N * 10^{-20} \dots \dots \dots \dots \dots \dots \dots \dots \dots \dots \dots \dots \dots \dots \dots \dots \dots \dots \dots . \dots \dots \dots \dots . \dots eqn\ 4.9$$

Where S_A is surface area m^2/gm, V_m is volume of monolayer m^3, a_m is area occupied by one molecular of nitrogen in monolayer is 0.162 nm^2, N: Avogadro's number $6.02*10^{23}$ molecules /mole.

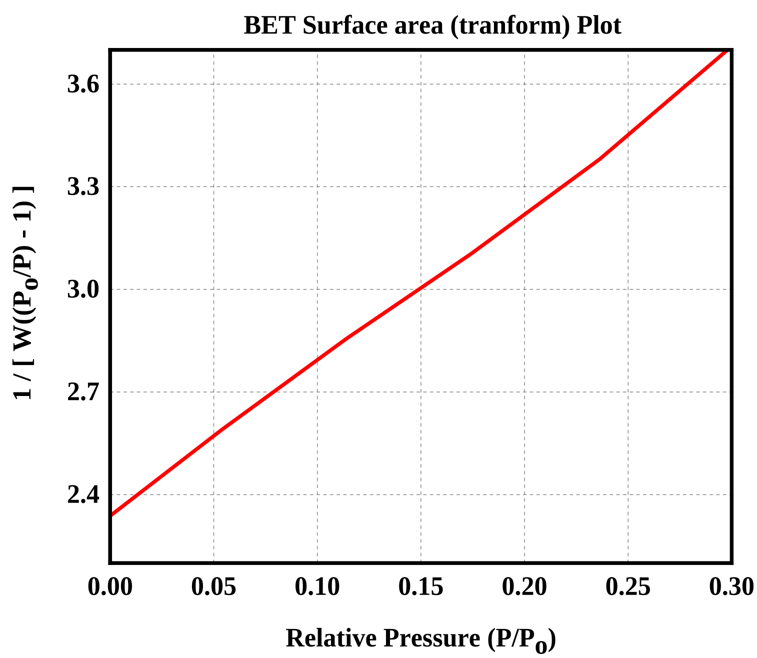

FIGURE 4.13 BET Surface Area Plot of Synthesized Zeolite

Table 4.10 Computing Surface Area and Pore Volume of Synthesized Zeolite with Previous Works

	Synthesized Nano Zeolite Y	**Nano Zeolite Y (Ahmedzeki et al., 2016)**	**Nano Zeolite Y (Rahman et al., 2012)**
BET Surface Area (m^2/g)	509.46	499.43	621.18
Porous Volume cm^3/g	0.074	0.38	0.33
Porous Diameter Å	18.47	18.68	21.22

Figure 4.13 showed the BET surface area was found to be 509.46 m^2/g. Surface area and porous size are important in the catalysis. Frequently high specific surface area associated with high activity. Surface area and porous size are important in the catalysis. Frequently high specific surface area associated with high activity. The actives sites are formed typically in the surface of the catalyst, so, if the material has more porosity, it has more surface area to form the actives sites and this usually leads to higher activity of the catalyst. Increasing the surface area of a reactant increases the frequency of collisions and increases the reaction rate. Therefore the synthesized zeolite based catalyst having larger surface area have enhanced the catalysts activity as it is confirmed by TGA analysis.

4.3.5. Performance Evaluation of Synthesized Zeolite Based Catalyst Using TGA

The DTG-60H Shimadzu equipment with platinum crucible was used in this study to examine the zeolite Y catalyst's performance in HDPE catalytic cracking. TGA curves show the instances of mass loss in comparison to polymer decomposition, which is linked to evaporation or volatilization of lighter products. Figure 4.14 shows the thermo gravimetric curves for thermal and catalytic cracking of HDPE at a heating rate of 20 $^oC\ min^{-1}$. The introduction of zeolite catalysts facilitate polymer degradation, which resulted in the shattering of C-C bonds in the polymer components. This breaking produces heat and hydrocarbon radicals, which undergo gradual changes. Heating plastic above 300 °C causes a free radical chain reaction, which causes

the material to depolymerize. At the start of the TGA curve, every dosage of zeolite catalyst resulted in a considerable improvement in HDPE rate of decomposition. 30% zeolite catalyst dosage produced the lowest on set temperature. This could be owing to the presence of enough catalytic active site at larger concentrations, causing HDPE cracking to begin at a lower temperature.

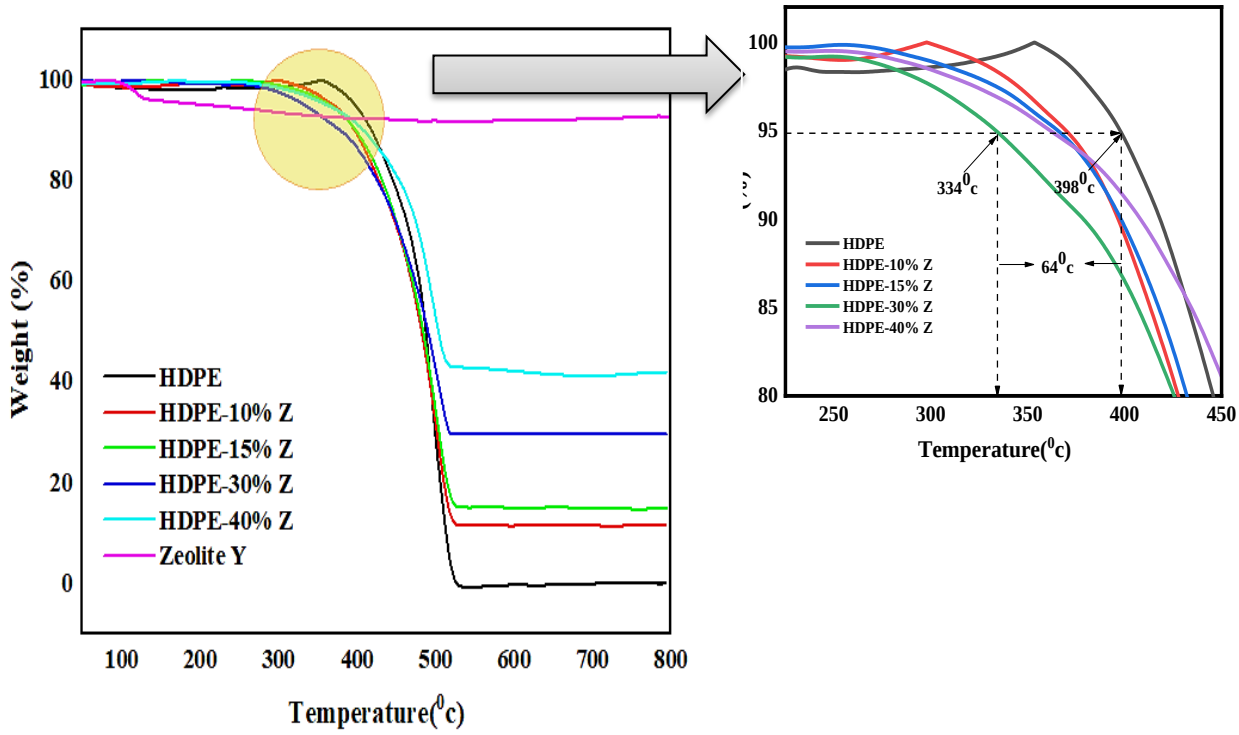

FIGURE 4.14 Normalized TGA curves of the polymer (HDPE) weight loss vs. temperature for: Zeolite, HDPE, HDPE-10Z, HDPE-15Z, HDPE-30Z and HDPE-40Z

Thermal stability of synthesized zeolite has been studied. Weight loss was recorded from 120 ^{o}C, these was due to water molecule desorption on synthesized catalysts. The presence of impurities except Quartz in the Zeolite catalyst was not observed. It can be concluded that synthesized zeolite was highly stable which doesn't decompose up to 800 ^{o}C. The thermo gravimetric profile obtained for synthesis zeolite is shown in figure 4.14 along with thermal catalytic degradation of HDPE.

In case of HDPE-30Z the degradation temperature dropped from 398 ^{o}C to 334 ^{o}C at 95% weight (T_5), which implies that breakdown temperature reduced by 64 ^{o}C compared to pure HDPE. When compared to pure HDPE, each of the catalyst dosages reduced the final decomposition

temperature of all HDPE. TGA residual analysis results for 10%, 15%, 30%, and 40% HDPE-Z were 11.53 %, 14.88%, 29.63 % and 41.89 %, respectively, as shown in Table 4.10. These small variations could be the result of measurement errors during HDPE-Z sampling for TGA analysis.

Table 4.11 TGA Values Obtained in the Degradation of HDPE with Zeolites, Under Heating Rate of 20 ^{o}C min^{-1}

Sample	T^{o} Onset	T^{o} Peak	T^{o} Final	Residual mass%	Mass loss%
HDPE	431	489	530	0.14	99.86
HDPE-10%Z	416	503	533	11.53	88.47
HDPE-15%Z	408	501	529	14.88	85.12
HDPE-30%Z	396	503	521	29.63	70.37
HDPE-40%Z	432	498	525	41.89	58.11

CONCLUSION AND RECOMMENDATION

Conclusion

Amorphous silica has been successfully achieved by newly adopted procedure of calcination with immediate quenching of silica enriched Awash Melkassa chemical factory byproduct. Highly amorphous silica has been achieved at 600 ^{o}C calcination and immediate quenching as witnessed by XRD result.

With the successful achievement of amorphous silica, cement clinker can be partially replaced (5, 10 and 15) wt% by Awash Melkassa CFW. The blaine air permittivity, chemical analysis, compressive strength, flexural strength, setting time and soundness results were with fulfill the minimum standard of OPC cement. Initial setting time increase when cement clinker is partially replaced by activated CFW as compared to standard OPC. This is due to the presence of aluminum oxide (Al_2O_3) which encourages rapid setting of cement paste. The replacement of clinker with activated Awash Melkassa CFW has successfully enhanced property of cement produced. Maximum compressive strength has been achieved by 10% CFWB replacement with 120% strength index. Fineness of clinker blend had showed significant effect on 2days curing of cement rather than 28 days curing.

A nano zeolite Y with 73.22 nm particle size and 509.46 m^2 BET specific surface area has been synthesized successfully from silica enriched Awash Melkassa CFW. The result obtained showed that molarity of NaOH or ratio of Na_2O/SiO_2 has higher effect than gel aging time for zeolite Y synthesis. The synthesized catalysts facilitate the rate of decomposition temperature by adding different dosage of catalyst. The degradation temperature of HDPE dropped from 398 ^{o}C to 334 ^{o}C at 95% weight loss (T_5), with HDPE-30Z which implies that breakdown temperature reduced by 64 ^{o}C compared to pure HDPE.

Recommendation

Due to financial and time constraints, the scope of this work was limited. Based on the present study, some recommendations can be made for future work.

- Further calcination of CFW until the glass transition temperature of the waste can be identified and investment of preparing amorphous chemical factory waste by high temperature calcination.
- It is recommended to study using of raw CFW for partial replacement of cement clinker and effect of raw CFW on cement properties.
- Further studies on chloride resistance, sulfur attack resistance and resistance to acid attack need to be studied on cement replaced by activated CFW.
- It is recommended to study synergistic effect of raw CFW with Activated CFW in cement clinker replacement.
- It is recommended to use hydrothermal synthesis method with microwave assistance or sonochemical-assisted approach for synthesis of zeolite based catalysts from Awash Melkassa chemical factory byproduct.
- It is recommended that further study on the specific condition temperature and time of crystallization required for the development of Zeolite-Y from Awash Melkassa chemical factory byproduct.
- It is recommended to the performance of catalyst should be evaluated for various application

REFERENCE

Abdul-Wahab, S. A., Hassan, E. M., Al-Jabri, K. S., & Yetilmezsoy, K. (2019). Application of zeolite/kaolin combination for replacement of partial cement clinker to manufacture environmentally sustainable cement in Oman. Environmental Engineering Research, 24(2), 246-253.

Abdullahi, T., Harun, Z., & Othman, M. H. D. (2017). A review on sustainable synthesis of zeolite from kaolinite resources via hydrothermal process. Advanced Powder Technology, 28(8), 1827-1840.

Adane, T. (2020). Synthesis and Characterization of Zeolite Y Catalyst from Ethiopian Ansho Kaolin for Heavy Hydrocarbon Cracking. ASTU.

Ahmedzeki, N. S., Yilmaz, S., & Al-Tabbakh, B. A. (2016). Synthesis and characterization of nanocrystalline zeolite Y. Al-Khwarizmi Engineering Journal, 12(1), 79-89.

Ai, H. M., & Zhu, S. F. (2015). Study on the Calcinations of Recycled Cement Clinker Using Waste Concrete and Waste Clay Brick. Paper presented at the Key Engineering Materials.

Ali, M., Saidur, R., & Hossain, M. (2011). A review on emission analysis in cement industries. Renewable and Sustainable Energy Reviews, 15(5), 2252-2261.

Amin, N., Gul, S., Sultana, S., & Alam, S. (2021). Preparation and Characterization of Mesoporous Silica from Bagasse Bottom Ash from the Sugar Industry. Crystals, 11(8), 938.

Arimanwa, M., Onwuka, D., & Arimanwa, J. (2016). Effect of chemical composition of ordinary portland cement on the compressive strength of concrete. International refereed journal of Engineering and Science, 5, 20-31.

ASTM. (2010). Standard Specification for Coal Fly Ash and Raw or Calcined Natural Pozzolan for Use. Paper presented at the ASTM

Awadh, S. M., & Al-Owaidi, M. R. Iraqi Geological Journal.

Azizi, S. N., Alavi Daghigh, A., & Abrishamkar, M. (2013). Phase transformation of zeolite P to Y and analcime zeolites due to changing the time and temperature. Journal of Spectroscopy, 2013.

Barbosa, W. d. S. Influence of the physical-chemical characteristics of the clinker phases on the rheological behavior of cement pastes.

Belviso, C. (2018). State-of-the-art applications of fly ash from coal and biomass: A focus on zeolite synthesis processes and issues. Progress in Energy and Combustion Science, 65, 109-135.

Belviso, C., Cavalcante, F., Niceforo, G., & Lettino, A. (2017). Sodalite, faujasite and A-type zeolite from 2: 1dioctahedral and 2: 1: 1 trioctahedral clay minerals. A singular review of synthesis methods through laboratory trials at a low incubation temperature. Powder technology, 320, 483-497.

Benhelal, E., Zahedi, G., Shamsaei, E., & Bahadori, A. (2013). Global strategies and potentials to curb CO2 emissions in cement industry. Journal of cleaner production, 51, 142-161.

Bogue, R. H. (1955). The chemistry of Portland cement (Vol. 79): LWW.

Bukhari, S. S., Behin, J., Kazemian, H., & Rohani, S. (2015). Conversion of coal fly ash to zeolite utilizing microwave and ultrasound energies: A review. Fuel, 140, 250-266.

Bunmai, K., Osakoo, N., Deekamwong, K., Rongchapo, W., Keawkumay, C., Chanlek, N., . . . Wittayakun, J. (2018). Extraction of silica from cogon grass and utilization for synthesis of zeolite NaY by conventional and microwave-assisted hydrothermal methods. Journal of the Taiwan Institute of Chemical Engineers, 83, 152-158.

Caldeira, V. P., Santos, A. G., Oliveira, D. S., Lima, R. B., Souza, L. D., & Pergher, S. B. (2017). Polyethylene catalytic cracking by thermogravimetric analysis. Journal of Thermal Analysis and Calorimetry, 130(3), 1939-1951.

Cao, L., Shen, W., Huang, J., Yang, Y., Zhang, D., Huang, X., . . . Ji, X. (2019). Process to utilize crushed steel slag in cement industry directly: Multi-phased clinker sintering technology. Journal of Cleaner Production, 217, 520-529.

Carmignano, O. R., Vieira, S. S., Teixeira, A. P. C., Lameiras, F. S., Brandão, P. R. G., & Lago, R. M. (2021). Iron ore tailings: characterization and applications. Journal of the Brazilian Chemical Society, 32, 1895-1911.

Chen, D., Hu, X., Shi, L., Cui, Q., Wang, H., & Yao, H. (2012). Synthesis and characterization of zeolite X from lithium slag. Applied Clay Science, 59, 148-151.

Chindaprasirt, P., & Rattanasak, U. (2020). Eco-production of silica from sugarcane bagasse ash for use as a photochromic pigment filler. Scientific Reports, 10(1), 1-8.

Chinnam, R., Francis, A., Will, J., Bernardo, E., & Boccaccini, A. (2013). Functional glasses and glass-ceramics derived from iron rich waste and combination of industrial residues. Journal of Non-Crystalline Solids, 365, 63-74.

Christidis, G. E., & Papantoni, H. (2008). Synthesis of FAU type zeolite Y from natural raw materials: hydrothermal SiO2-Sinter and Perlite glass. The open mineralogy journal, 2(1).

Costa, F., & Ribeiro, D. (2021). Evaluation of phase formation and physical-mechanical properties of Portland cements produced with civil construction waste. Cement, 5, 100012.

Costa, J. A. S., & Paranhos, C. M. (2020). Mitigation of silica-rich wastes: an alternative to the synthesis eco-friendly silica-based mesoporous materials. Microporous and Mesoporous Materials, 309, 110570.

ČSN, E. (2017). 196-3 Methods of testing cement–Part 3: Determination of setting times and soundness. Praha: Czech office for standards, metrology and testing.

Cui, M., Wang, Y., Liu, X., Zhu, J., Sun, J., Lv, N., & Meng, C. (2014). Solvothermal conversion of magadiite into zeolite omega in a glycerol–water system. Journal of Chemical Technology & Biotechnology, 89(3), 419-424.

Darweesh, H. H. M. (2020). A Low Temperature Manufactured Portland Cement Clinker from Pulverized Waste of Fly Ash. zeolites, 6, 10.

Dikshit, P., Sawarkar, N., Kaushal, A., & Khatik, S. (2001). Recycling of silica rich industry waste ash for economising use of phosphatic fertilizers in typic haplustert of Jabalpur. Indian Journal of Agricultural Research, 35(2), 108-111.

Dong, Y., Di, J., Yang, Z., Zhang, Y., Wang, X., Guo, X., . . . Jiang, G. (2020). Study on the effectiveness of sulfate-reducing bacteria combined with coal gangue in repairing acid mine drainage containing Fe and Mn. Energies, 13(4), 995.

Edomwonyi-Otu, L., Aderemi, B. O., Ahmed, A. S., Coville, N. J., & Maaza, M. (2013). Influence of thermal treatment on kankara kaolinite. Opticon1826(15).

El-Diadamony, H., Amer, A. A., Sokkary, T. M., & El-Hoseny, S. (2018). Hydration and characteristics of metakaolin pozzolanic cement pastes. HBRC journal, 14(2), 150-158.

El-Naggar, M., El-Kamash, A., El-Dessouky, M., & Ghonaim, A. (2008). Two-step method for preparation of NaA-X zeolite blend from fly ash for removal of cesium ions. Journal of Hazardous Materials, 154(1-3), 963-972.

Elmrabet, R., Hmidani, Y., Mariouch, R., Elharfi, A., & Elyoubi, M. (2021). Influence of raw meal composition on clinker reactivity and cement proprieties. Materials Today: Proceedings.

EN, B. S. (2011). 197-1. Cement–Part 1: Composition, specifications and conformity criteria for common cements. London: European Committee For Standardisation.

Fruijtier-Pölloth, C. (2009). The safety of synthetic zeolites used in detergents. Archives of toxicology, 83(1), 23-35.

Gajić, G., Mitrović, M., & Pavlović, P. (2019). Ecorestoration of fly ash deposits by native plant species at thermal power stations in Serbia Phytomanagement of polluted sites (pp. 113-177): Elsevier.

Gao, T., Dai, T., Shen, L., & Jiang, L. (2021). Benefits of using steel slag in cement clinker production for environmental conservation and economic revenue generation. Journal of Cleaner Production, 282, 124538.

Garcia, G., Cardenas, E., Cabrera, S., Hedlund, J., & Mouzon, J. (2016). Synthesis of zeolite Y from diatomite as silica source. Microporous and Mesoporous materials, 219, 29-37.

Giergiczny, Z. (2019). Fly ash and slag. Cement and Concrete Research, 124, 105826.

Gil, A., & Korili, S. (2016). Management and valorization of aluminum saline slags: current status and future trends. Chemical Engineering Journal, 289, 74-84.

Guo, B., Qiao, G., Han, P., Li, Z., & Fu, Q. (2022). Effect of natural carbonation on chloride binding behaviours in OPC paste investigated by a thermodynamic model. Journal of Building Engineering, 104021.

Guo, Z., Hao, Y., Tian, H., Bai, X., Wu, B., Liu, S., . . . Lin, S. (2021). Field measurements on emission characteristics, chemical profiles, and emission factors of size-segregated PM from cement plants in China. Science of The Total Environment, 151822.

Han, W., Jia, Y., Xiong, G., & Yang, W. (2007). Synthesis of hierarchical porous materials with ZSM-5 structures via template-free sol–gel method. Science and Technology of Advanced materials, 8(1-2), 101-105.

Hartmann, A., Petrov, V., Buhl, J.-C., Rübner, K., Lindemann, M., Prinz, C., & Zimathies, A. (2014). Zeolite synthesis under insertion of silica rich filtration residues from industrial wastewater reconditioning. Advances in Chemical Engineering and Science 4 (2014), Nr. 2, 4(2), 120-134.

Höller, H., & Wirsching, U. (1985). Zeolite formation from fly ash. Fortschritte der mineralogie, 63(1), 21-43.

JeyaSundar, P. G. S. A., Ali, A., & Zhang, Z. (2020). Waste treatment approaches for environmental sustainability Microorganisms for Sustainable Environment and Health (pp. 119-135): Elsevier.

Ji, M., Gao, X., Wang, X., Zhang, Y., Jiang, J., & Gu, X. (2018). An ensemble synthesis strategy for fabrication of hollow fiber T-type zeolite membrane modules. Journal of membrane science, 563, 460-469.

Johnson, E., & Arshad, S. E. (2014). Hydrothermally synthesized zeolites based on kaolinite: A review. Applied Clay Science, 97, 215-221.

Jusoh, N., Yeong, Y. F., Mohamad, M., Lau, K. K., & Shariff, A. M. (2017). Rapid-synthesis of zeolite T via sonochemical-assisted hydrothermal growth method. Ultrasonics sonochemistry, 34, 273-280.

Kalpokaitė-Dičkuvienė, R., Baltušnikas, A., Levinskas, R., & Čėsnienė, J. (2019). Incinerator residual ash–metakaolin blended cements: effect on cement hydration and properties. Construction and Building Materials, 206, 297-306.

Kanyo, J. E., Schafföner, S., Uwanyuze, R. S., & Leary, K. S. (2020). An overview of ceramic molds for investment casting of nickel superalloys. Journal of the European Ceramic Society, 40(15), 4955-4973.

Karein, S. M. M., Ramezanianpour, A., Ebadi, T., Isapour, S., & Karakouzian, M. (2017). A new approach for application of silica fume in concrete: Wet granulation. Construction and Building Materials, 157, 573-581.

Kleib, J., Aouad, G., Abriak, N.-E., & Benzerzour, M. (2021). Production of Portland cement clinker from French Municipal Solid Waste Incineration Bottom Ash. Case Studies in Construction Materials, 15, e00629.

Kongnoo, A., Tontisirin, S., Worathanakul, P., & Phalakornkule, C. (2017). Surface characteristics and CO2 adsorption capacities of acid-activated zeolite 13X prepared from palm oil mill fly ash. Fuel, 193, 385-394.

Koshy, N., & Singh, D. (2016). Fly ash zeolites for water treatment applications. Journal of Environmental Chemical Engineering, 4(2), 1460-1472.

Kovo, A., Hernandez, O., & Holmes, S. (2009). Synthesis and characterization of zeolite Y and ZSM-5 from Nigerian Ahoko Kaolin using a novel, lower temperature, metakaolinization technique. Journal of Materials Chemistry, 19(34), 6207-6212.

Kusakabe, K., Kuroda, T., Murata, A., & Morooka, S. (1997). Formation of a Y-type zeolite membrane on a porous α-alumina tube for gas separation. Industrial & engineering chemistry research, 36(3), 649-655.

Łach, M., Grela, A., Komar, N., Mikuła, J., & Hebda, M. (2019). Calcined post-production waste as materials suitable for the hydrothermal synthesis of zeolites. Materials, 12(17), 2742.

Lee, Y.-R., Soe, J. T., Zhang, S., Ahn, J.-W., Park, M. B., & Ahn, W.-S. (2017). Synthesis of nanoporous materials via recycling coal fly ash and other solid wastes: A mini review. Chemical Engineering Journal, 317, 821-843.

Lemoine, G. (2013). Comparison of different types of zeolites used as solid acid catalysts in the transesterification reaction of Jatropha-type oil for biodiesel production. Worcester Polytechnic Institute.

Looms, J. S. (1988). Insulators for high voltages: IET.

Lorentzen, E. M., & Kingston, H. S. (1996). Comparison of microwave-assisted and conventional leaching using EPA method 3050B. Analytical Chemistry, 68(24), 4316-4320.

Ludwig, H.-M., & Zhang, W. (2015). Research review of cement clinker chemistry. Cement and Concrete Research, 78, 24-37.

Luo, Y., Raza, W., Yang, J., Li, L., & Lu, Y. (2019). Recent advances in acid-resistant zeolite T membranes for dehydration of organics. Chinese Journal of Chemical Engineering, 27(6), 1449-1457.

Ma, H., Yao, Q., Fu, Y., Ma, C., & Dong, X. (2010). Synthesis of zeolite of type A from bentonite by alkali fusion activation using Na2CO3. Industrial & engineering chemistry research, 49(2), 454-458.

Ma, L., Han, L., Chen, S., Hu, J., Chang, L., Bao, W., & Wang, J. (2019). Rapid synthesis of magnetic zeolite materials from fly ash and iron-containing wastes using supercritical water for elemental mercury removal from flue gas. Fuel Processing Technology, 189, 39-48.

Majchrzak-Kucęba, I., & Nowak, W. (2011). Characterization of MCM-41 mesoporous materials derived from polish fly ashes. International Journal of Mineral Processing, 101(1-4), 100-111.

Malekpour, A., Millani, M., & Kheirkhah, M. (2008). Synthesis and characterization of a NaA zeolite membrane and its applications for desalination of radioactive solutions. Desalination, 225(1-3), 199-208.

Melian-Cabrera, I., Espinosa, S., Groen, J., Kapteijn, F., & Moulijn, J. (2006). Utilizing full-exchange capacity of zeolites by alkaline leaching: Preparation of Fe-ZSM5 and application in N2O decomposition. Journal of Catalysis, 238(2), 250-259.

Miao, C., Liang, L., Zhang, F., Chen, S., Shang, K., Jiang, J., . . . Ouyang, J. (2022). Review of the fabrication and application of porous materials from silicon-rich industrial solid waste. International Journal of Minerals, Metallurgy and Materials, 29(3), 424-438.

Minachev, K. M., & Isakov, Y. I. (1973). Catalytic Properties of Zeolites—A General Review.

Mohammad Razaul, K. (2017). Feasibility assessment of palm oil clinker powder as supplementary cementitious material/Mohammad Razaul Karim. University of Malaya.

Mohd Nasir, N. A., Abu Bakar, N., Safiee, N. A., & Abdul Aziz, F. N. A. (2021). Permeation-durability properties of metakaolin blended concrete containing rubber. European Journal of Environmental and Civil Engineering, 1-16.

Mohkami, M., & Talaeipour, M. (2011). Investigation of the chemical structure of carboxylated and carboxymethylated fibers from waste paper via XRD and FTIR analysis. Bioresources, 6(2), 1988-2003.

Mrak, M., Winnefeld, F., Lothenbach, B., & Dolenec, S. (2021). EFFECT OF TEMPERATURE ON PHASE ASSEMBLAGE OF BELITE CALCIUM-SULFOALUMINATE CEMENT. Paper presented at the 14th STUDENTS'CONGRESS OF SCTM.

Neves, I. C., Botelho, G., Machado, A. V., & Rebelo, P. (2007). Catalytic degradation of polyethylene: An evaluation of the effect of dealuminated Y zeolites using thermal analysis. Materials chemistry and physics, 104(1), 5-9.

Nishi, Y., & Doering, R. (2000). Handbook of semiconductor manufacturing technology: CRC press.

Nisrinah, M. (2022). Synthesis of Silica from Rice Husk Ashes with Variation of Solvent (KOH) Concentration. Journal Of Natural Sciences And Mathematics Research, 3(2), 252-254.

Oertel, T., Hutter, F., Helbig, U., & Sextl, G. (2014). Amorphous silica in ultra-high performance concrete: First hour of hydration. Cement and Concrete Research, 58, 131-142.

Ohrman, O. (2000). Synthesis and Characterization of Zeolite Coatings on Monoliths Support. MSc Thesis, Lulea University of Technology.

Olaremu, A. G. (2015). Physico-chemical characterization of Akoko mined kaolin clay. Journal of Minerals and Materials characterization and Engineering, 3(05), 353.

Onwudili, J. A., Muhammad, C., & Williams, P. T. (2019). Influence of catalyst bed temperature and properties of zeolite catalysts on pyrolysis-catalysis of a simulated mixed plastics sample for

the production of upgraded fuels and chemicals. Journal of the Energy Institute, 92(5), 1337-1347.

Oruji, S., Khoshbin, R., & Karimzadeh, R. (2018). Preparation of hierarchical structure of Y zeolite with ultrasonic-assisted alkaline treatment method used in catalytic cracking of middle distillate cut: The effect of irradiation time. Fuel Processing Technology, 176, 283-295.

Özbay, E., Erdemir, M., & Durmuş, H. İ. (2016). Utilization and efficiency of ground granulated blast furnace slag on concrete properties–A review. Construction and Building Materials, 105, 423-434.

Ozdemir, O. D., & Piskin, S. (2019). A novel synthesis method of zeolite X from coal fly ash: alkaline fusion followed by ultrasonic-assisted synthesis method. Waste and Biomass Valorization, 10(1), 143-154.

Pandey, V. C. (2020). Chapter 3 - Scope of fly ash use in agriculture: prospects and challenges. In V. C. Pandey (Ed.), Phytomanagement of Fly Ash (pp. 63-101): Elsevier.

Panesar, D. K. (2019). Supplementary cementing materials Developments in the Formulation and Reinforcement of Concrete (pp. 55-85): Elsevier.

Papastamoulis, V., London, K., Crocker, R., & Patias, P. (2021). Transforming Construction Waste Analytics to Support Circular Economy and Carbon Footprint Reduction: Construction Waste Mapping Protocol CDWiMaP Handbook of Research on Driving Transformational Change in the Digital Built Environment (pp. 232-264): IGI Global.

Pedrolo, D. R. S., de Menezes Quines, L. K., de Souza, G., & Marcilio, N. R. (2017). Synthesis of zeolites from Brazilian coal ash and its application in SO2 adsorption. Journal of environmental chemical engineering, 5(5), 4788-4794.

Prošek, Z., Trejbal, J., Nežerka, V., Goliáš, V., Faltus, M., & Tesárek, P. (2020). Recovery of residual anhydrous clinker in finely ground recycled concrete. Resources, Conservation and Recycling, 155, 104640.

Purnomo, C. W., Salim, C., & Hinode, H. (2012). Synthesis of pure Na–X and Na–A zeolite from bagasse fly ash. Microporous and Mesoporous Materials, 162, 6-13.

Qiu, Q., Jiang, X., Lv, G., Chen, Z., Lu, S., Ni, M., . . . Deng, X. (2018). Adsorption of heavy metal ions using zeolite materials of municipal solid waste incineration fly ash modified by microwave-assisted hydrothermal treatment. Powder Technology, 335, 156-163.

Rahman, M., Awang, M., & Yusof, A. (2012). Preparation, characterization and application of zeolite-Y (Na-Y) for water filtration. Australian Journal of Basic and Applied Sciences, 6(1), 50-54.

Rajiman, R., Amin, M., Muttaqqi, M., Manurung, P., & Riadini, A. (2021). The Effect of Addition Basalt Stone and Coal as Substitution Material for Producing Cement Clinker. Sys Rev Pharm 2021; 12 (2): 456-466, 12(2), 456-466.

Ramachandra, T., & Shruthi, B. (2007). Spatial mapping of renewable energy potential. Renewable and sustainable energy reviews, 11(7), 1460-1480.

Raveh-Amit, H., Lemont, F., Bar-Nes, G., Klein-BenDavid, O., Banano, N., Gelfer, S., . . . Rousset, F. (2022). Catalytic pyrolysis of high-density polyethylene: decomposition efficiency and kinetics. Catalysts, 12(2), 140.

Rmaidh, S. A., & Awadh, S. M. (2021). Manufacture of Portland Cement from Claystone of Nfayil Formation Middle Miocene, in Southern Desert of Iraq. The Iraqi Geological Journal, 131-144.

Robson, H. (2001). Chapter 8 - Safety considerations for zeolite synthesis. In H. Robson & K. P. Lillerud (Eds.), Verified Syntheses of Zeolitic Materials (pp. 45-46). Amsterdam: Elsevier Science.

ROUQUEROL, F. (1999). Adsorption by clays, pillared layer structures and zeolites. Adsorption by powders and porous solids.

Rovani, S., Santos, J. J., Corio, P., & Fungaro, D. A. (2018). Highly pure silica nanoparticles with high adsorption capacity obtained from sugarcane waste ash. ACS omega, 3(3), 2618-2627.

Salman, N. (2007). Crystal chemical studies on the growth size problem of Y zeolite. Hannover: Gottfried Wilhelm Leibniz Universität Hannover.

Santos, B. P. S., Almeida, D., Maria de Fatima, V. M., & Henriques, C. A. (2018). Petrochemical feedstock from pyrolysis of waste polyethylene and polypropylene using different catalysts. Fuel, 215, 515-521.

Schraut, K. (2021). Portland cement clinker from reduced basic oxygen furnace slag.

Serrano, D., Uguina, M., Ovejero, G., Van Grieken, R., & Camacho, M. (1995). Synthesis of TS-1 by wetness impregnation of amorphous SiO2□ TiO2 solids prepared by the sol-gel method. Microporous materials, 4(4), 273-282.

Sha, W., O'Neill, E., & Guo, Z. (1999). Differential scanning calorimetry study of ordinary Portland cement. Cement and Concrete research, 29(9), 1487-1489.

Shoppert, A., Loginova, I., Chaikin, L., & Rogozhnikov, D. (2017). Alkali fusion-leaching method for comprehensive processing of fly ash. KnE Materials Science, 89-96.

Siddique, R., & Mehta, A. (2020). Utilization of industrial by-products and natural ashes in mortar and concrete development of sustainable construction materials Nonconventional and Vernacular Construction Materials (pp. 247-303): Elsevier.

Silveira, N. C., Martins, M. L., Bezerra, A., & Araújo, F. G. (2021). Red Mud from the Aluminium Industry: Production, Characteristics, and Alternative Applications in Construction Materials—A Review. Sustainability, 13(22), 12741.

Smirnov, A., Dobshits, L., & Anisimov, S. (2022). Influence of Superplasticizer and Silica Fume on the Structure Formation and Properties of Cement Stone Proceedings of FORM 2021 (pp. 111-121): Springer.

Sorrentino, F., Damidot, D., & Fentiman, C. (2021). Applications to Hydraulic Binders CaO-SiO2-AI2O3-Fe oxides chemical system (pp. 211-260): EDP Sciences.

Środoń, J., Drits, V. A., McCarty, D. K., Hsieh, J. C., & Eberl, D. D. (2001). Quantitative X-ray diffraction analysis of clay-bearing rocks from random preparations. Clays and Clay Minerals, 49(6), 514-528.

Standard, B. (2005). Methods of testing cement. Determination of strength.

Stutzman, P., Heckert, A., Tebbe, A., & Leigh, S. (2014). Uncertainty in Bogue-calculated phase composition of hydraulic cements. Cement and concrete research, 61, 40-48.

Sugano, Y., Sahara, R., Murakami, T., Narushima, T., Iguchi, Y., & Ouchi, C. (2005). Hydrothermal synthesis of zeolite A using blast furnace slag. ISIJ international, 45(6), 937-945.

Tadesse, T. M., & Subramanyam, B. (2018). Efficacy of filter cake and Triplex powders from Ethiopia applied to concrete arenas against Sitophilus zeamais. Journal of Stored Products Research, 76, 140-150.

Taher, M. A., & Damarany, B. K. (2019). Effect of partial substitution of raw gypsum with thermally treated phosphogypsum on the properties of Portland Pozzolanic Cement. Advanced Journal of Chemistry-Section A, 2(4), 296-315.

Tan, Y., Hameed, B., & Abdullah, A. (2020). Deoxygenation of pyrolysis vapour derived from durian shell using catalysts prepared from industrial wastes rich in Ca, Fe, Si and Al. Science of The Total Environment, 703, 134902.

Tang, Y., Fuh, J., Loh, H., Wong, Y., & Lu, L. (2003). Direct laser sintering of a silica sand. Materials & design, 24(8), 623-629.

Tawfik, T. A., Metwally, K. A., Zaki, W., & Faried, A. S. (2019). Hybrid effect of nanosilica and metakaolin on mechanical properties of cement mortar. Int. J. Eng. Res. Technol, 8(3).

Tayeh, B. A., Alyousef, R., Alabduljabbar, H., & Alaskar, A. (2021). Recycling of rice husk waste for a sustainable concrete: a critical review. Journal of Cleaner Production, 312, 127734.

Taylor, H. F. (1989). Modification of the Bogue calculation. Advances in Cement Research, 2(6), 73-77.

Taylor, H. F. W. Cement chemistry.

Tayraukham, P., Jantarit, N., Osakoo, N., & Wittayakun, J. (2020). Synthesis of Pure Phase NaP2 Zeolite from the Gel of NaY by Conventional and Microwave-Assisted Hydrothermal Methods. Crystals, 10(10), 951.

Thomas, J. C. (1987). The determination of log normal particle size distributions by dynamic light scattering. Journal of colloid and interface science, 117(1), 187-192.

Treacy, M. M., & Higgins, J. B. (2007). Collection of simulated XRD powder patterns for zeolites fifth (5th) revised edition: Elsevier.

Tripathi, D., Kumar, R., Mehta, P., & Singh, A. (2020). Silica fume mixed concrete in acidic environment. Materials Today: Proceedings, 27, 1001-1005.

Tsujiguchi, M., Kobashi, T., Utsumi, Y., Kakimori, N., & Nakahira, A. (2014). Synthesis of zeolite A from aluminoborosilicate glass used in glass substrates of liquid crystal display panels and evaluation of its cation exchange capacity. Journal of the American Ceramic Society, 97(1), 114-119.

Türköz, M., Umu, S. U., & Öztürk, O. (2021). Effect of Silica Fume as a Waste Material for Sustainable Environment on the Stabilization and Dynamic Behavior of Dispersive Soil. Sustainability, 13(8), 4321.

Varenne, F., Botton, J., Merlet, C., Hillaireau, H., Legrand, F.-X., Barratt, G., & Vauthier, C. (2016). Size of monodispersed nanomaterials evaluated by dynamic light scattering: Protocol

validated for measurements of 60 and 203 nm diameter nanomaterials is now extended to 100 and 400 nm. International journal of pharmaceutics, 515(1-2), 245-253.

Vichaphund, S., Sricharoenchaikul, V., & Atong, D. (2019). Selective aromatic formation from catalytic fast pyrolysis of Jatropha residues using ZSM-5 prepared by microwave-assisted synthesis. Journal of Analytical and Applied Pyrolysis, 141, 104628.

Von-Kiti, E. (2017). Synthesis and characterization of zeolites from bauxite and kaolin: application to the removal of heavy metals from mining wastewater.

Wajima, T. Immobilization of Carbon Dioxide using Blast Furnace Slag fused with NaOH.

Wang, G. C. (2016). 2 - Ferrous metal production and ferrous slags. In G. C. Wang (Ed.), The Utilization of Slag in Civil Infrastructure Construction (pp. 9-33): Woodhead Publishing.

Wang, J., Dai, Y., & Gao, L. (2009). Exergy analyses and parametric optimizations for different cogeneration power plants in cement industry. Applied Energy, 86(6), 941-948.

Wang, M., & Liu, X. (2021). Applications of red mud as an environmental remediation material: A review. Journal of Hazardous Materials, 408, 124420.

Wang, X., Hou, P., Yu, J., Zhou, X., & Cheng, X. (2020). The effects of silica fume on C3A hydration. Construction and Building Materials, 250, 118766.

Wang, Y.-S., Dai, J.-G., Wang, L., Tsang, D. C., & Poon, C. S. (2018). Influence of lead on stabilization/solidification by ordinary Portland cement and magnesium phosphate cement. Chemosphere, 190, 90-96.

Wen, X., Luo, Q., Hu, H., Wang, N., Chen, Y., Jin, J., . . . Fang, W. (2014). Comparison research on waste classification between China and the EU, Japan, and the USA. Journal of Material Cycles and Waste Management, 16(2), 321-334.

Wijaya, S. W., & Hardjito, D. (2016). Factors affecting the setting time of fly ash-based geopolymer. Paper presented at the Materials Science Forum.

Wittayakun, J., Khemthong, P., & Prayoonpokarach, S. (2008). Synthesis and characterization of zeolite NaY from rice husk silica. Korean Journal of Chemical Engineering, 25(4), 861-864.

Yahaya, S., Jikan, S. S., Badarulzaman, N. A., & Adamu, A. D. (2017). Effects of acid treatment on the SEM-EDX characteristics of kaolin clay. Traektoriâ Nauki= Path of Science, 3(9), 4001-4005.

Yilmaz, B., & Müller, U. (2009). Catalytic applications of zeolites in chemical industry. Topics in Catalysis, 52(6), 888-895.

Yin, H., Zhou, T., Liu, Y., Chai, Y., & Liu, C. (2012). Synthesis of high-quality nanocrystalline zeolite Y using pseudoboehmite as aluminum source. Journal of Porous Materials, 19(3), 277-281.

Yuanyuan, L., Min, L., & Peidong, S. (2021). A bibliometric review of studies on construction and demolition waste management by using CiteSpace. Energy and Buildings, 111822.

Zahiri, F., & Eskandari-Naddaf, H. (2019). Optimizing the compressive strength of concrete containing micro-silica, nano-silica, and polypropylene fibers using extreme vertices mixture design. Frontiers of Structural and Civil Engineering, 13(4), 821-830.

Zhang, J., Li, G., Ye, W., Chang, Y., Liu, Q., & Song, Z. (2018). Effects of ordinary Portland cement on the early properties and hydration of calcium sulfoaluminate cement. Construction and Building Materials, 186, 1144-1153.

Zhang, Y., & Ling, T.-C. (2020). Reactivity activation of waste coal gangue and its impact on the properties of cement-based materials–a review. Construction and Building Materials, 234, 117424.

Zhang, Z., Xiao, Y., Wang, B., Sun, Q., & Liu, H. (2017). Waste is a misplayed resource: synthesis of zeolites from fly ash for CO2 capture. Energy Procedia, 114, 2537-2544.

Zhao, J., Ni, K., Su, Y., & Shi, Y. (2021). An evaluation of iron ore tailings characteristics and iron ore tailings concrete properties. Construction and Building Materials, 286, 122968.

Zhao, S., & Zhang, Q. (2019). Effect of silica fume in concrete on mechanical properties and dynamic behaviors under impact loading. Materials, 12(19), 3263.

Zheng, D., Cui, H., Tang, W., Sang, G., & Lo, T. Y. (2021). Influence and mechanisms of active silica in solid waste on hydration of tricalcium aluminate in the resulting composite cement. Materials Today Communications, 27, 102262. doi: https://doi.org/10.1016/j.mtcomm.2021.102262

Zheng, D., Monasterio, M., Feng, W., Tang, W., Cui, H., & Dong, Z. (2021). Hydration Characteristics of tricalcium aluminate in the presence of nano-silica. Nanomaterials, 11(1), 199.

Zhou, H., Li, Y., Zhu, G., Liu, J., & Yang, W. (2009). Preparation of zeolite T membranes by microwave-assisted in situ nucleation and secondary growth. Materials Letters, 63(2), 255-257.

Zhu, J., Yang, K., Chen, Y., Fan, G., Zhang, L., Guo, B., . . . Zhao, R. (2021). Revealing the substitution preference of zinc in ordinary Portland cement clinker phases: A study from experiments and DFT calculations. Journal of Hazardous Materials, 409, 124504.

Zhu, Y., Shi, J., Shen, W., Chen, H., Dong, X., & Ruan, M. (2005). Preparation of novel hollow mesoporous silica spheres and their sustained-release property. Nanotechnology, 16(11), 2633.
Zhutovsky, S., & Shishkin, A. (2021). Recycling of hydrated Portland cement paste into new clinker. Construction and Building Materials, 280, 122510.
Zimmer, A., & Bragança, S. R. (2019). A review of waste glass as a raw material for whitewares. Journal of environmental management, 244, 161-171.

APPENDIX

Appendix A

Energy Analysis Predictions Calculation

The following assumptions are made to analyze the rotary kiln thermodynamically

a) The system is steady state, steady flow and open.

b) Ambient temperature are constant throughout the study i.e. $T_0 = 297K$.

c) The composition of raw material and coal material and feed rate of both are constant.

d) The velocity of atmospheric air is < 3 m/s.

e) The temperature of kiln shell is constant throughout the study.

f) Consider the gases inside the kiln as an ideal gas.

Specific consumption of energy for clinker production = 3735 KJ/Kg = $3.735*10^5$ KJ/Qtl

Let's calculate energy saved by 15 % replacement

For 15% replacement of CFW in 1Qtl clinker is = 0.15 Qtl CFW required = 0.85 Qtl clinker needed

1Qtl = $3.735*10^5$ KJ

0.85 Qtl = X

X= $3.17*10^5$KJ

The energy need for production of Activated CFW is 73.5 KJ/Qtl

The energy save by replacement per Qtl = ($3.735*10^5 – 3.17*10^5$) KJ/Qtl= $5.65*10^4$ KJ/Qtl

Cost Saved Calculation

$0.09 (4.65 ETB) is needed for 1 KWh energy consuming in Ethiopia

The energy save by replacement per Qtl = ($3.735*10^5 – 3.17*10^5$) KJ/Qtl= $5.65*10^4$ KJ/Qtl

For $5.65*10^4$ KJ/Qtl energy saved 15.69 KWh/Qtl can be reduced

73 Birr is saved for every Qtl cement clinker production

Potential waste per year = $5*10^4$ Qtl

Therefore for 15% replacement of clinker production = $71,568 (3.65 Million Birr) can be saved

CO_2 Emission Calculation

CO_2 emitted per ton cement production = 9 Qtl

Average cement production per year = $1.2*10^6$ ton

Estimated CO_2 emission per year = $1.08*10^7$ Qtl

Potential waste per year = $5*10^4$ Qtl

Replacement of cement clinker will save us 10^5 Qtl of CO_2 emissions to the environment

Appendix B

- **AQCFW**

Area of crystalline peaks = 4554.78

Area of all peaks (Crystalline + Amorphous) = 6039.68

Crystalline % = $\frac{\text{Area of crystalline peaks}}{\text{Area of all peaks (Crystalline + Amorphous)}} * 100\% = \frac{4554.78}{6039.68} * 100\% = 75.43\%$

Amorphous % = 100 % - Crystalline % = 100% - 75.43% = 24.57% ≈ 25%

- **CFWA**

Peak Position	FWHM	Crystallite size D(nm)	D (nm) average
23.11524	21.98203	0.368878735	2.631523894
26.9697	1.29498	6.308598743	

Area of crystalline peaks = 659.561

Area of all peaks (Crystalline + Amorphous) = 5535.62

Crystalline % = $\frac{\text{Area of crystalline peaks}}{\text{Area of all peaks (Crystalline + Amorphous)}} * 100\% = \frac{659.561}{5,535.62} * 100\% = 11.915\%$

Amorphous % = 100 % - Crystalline % = 100% - 11.915% = 88.085 % ≈ 88%

- **CFWB**

Peak Position	FWHM	Crystallite size D(nm)	D (nm) average
22.68787	0.15397	4.081133323	19.06016248
23.07424	1.34296	60.7833001	
26.58324	90.69427	0.900051797	
22.68787	7.7343	10.47616471	

Area of crystalline peaks = 587.2648

Area of all peaks (Crystalline + Amorphous) = 5,571.14

Crystalline % = $\frac{\text{Area of crystalline peaks}}{\text{Area of all peaks (Crystalline + Amorphous)}} * 100\% = \frac{587.2648}{5,571.14} * 100\% = 10.541\%$

Amorphous % = 100 % - Crystalline % = 100% - 10.541% =89.459% = 89.46%

- **CFWC**

Peak Position	FWHM	Crystallite size D(nm)	D (nm) average
23.13259	11.07992	0.731860391	8.795439725
26.73153	0.32068	25.4629448	
26.73153	42.63635	0.191513981	

Area of crystalline peaks = 688.6237

Area of all peaks (Crystalline + Amorphous) =5576.38

Crystalline % = $\frac{\text{Area of crystalline peaks}}{\text{Area of all peaks (Crystalline + Amorphous)}} * 100\% = \frac{688.6237}{5576.38} * 100\% = 12.35\%$

Amorphous % = 100% - Crystalline% = 100% - 12.35% = 87.65% ≈ 87.6%

- **CFWD**

Peak Position	FWHM	Crystallite size D(nm)	D (nm) average
21.02639	29.12041	0.27746613	20.56281741
23.07424	0.26305	30.71631802	
26.62002	0.33639	24.26818123	
27.5025	0.17505	46.72217373	
22.95895	9.76742	0.829947923	

Area of crystalline peaks = 676.0984

Area of all peaks (Crystalline + Amorphous) = 5,044.62

Crystalline % = $\frac{\text{Area of crystalline peaks}}{\text{Area of all peaks (Crystalline + Amorphous)}} * 100\% = \frac{676.0984}{5,044.62} * 100\% = 13.402\%$

Amorphous % = 100 % - Crystalline % = 100% - 13.402% = 86.597% = 86.6%

Appendix C

Mineral Composition of Clinker Calculation

C_3S = 4.071 (total CaO - free lime) - 7.600 SiO_2 - 6.718 $A1_2O_3$ - 1.430 Fe_2O_3

= 4.071(65.81-1.05)-7.600*21.43-6.718*5.67-1.430*3.32

= 57.93

Standard C_3S = 53 - 58

C_2S = 2.867 SiO_2- 0.7544 C_3S

= 2.867*21.43- 0.7544*57.93

= 18.06

Standard C_2S = 18 - 22

C_3A = 2.65 $A1_2O_3$- 1.692 Fe_2O_3

= 2.65*5.67-1.692*3.32

= 9.41

Standard C_3A = 8.0 – 9.5

C_4AF = 3.043 Fe_2O_3

= 3.043*3.32

= 10.10

Standard C_4AF = 10 – 11.5

$$\text{LSF} = \frac{CaO}{2.8 * \text{SiO}_2 + 1.2 * \text{Al}_2\text{O}_3 + 0.65 * \text{Fe}_2\text{O}_3}$$

$$\text{LSF} = \frac{65.81}{2.8 * 21.43 + 1.2 * 5.67 + 0.65 * 3.32} = \mathbf{0.954}$$

$$\text{SM} = \frac{\text{SiO}_2}{\text{Al}_2\text{O}_3 + \text{Fe}_2\text{O}_3}$$

$$\text{SM} = \frac{21.43}{5.67 + 3.32} = \mathbf{2.39}$$

$$\text{AR} = \frac{\text{Al}_2\text{O}_3}{\text{Fe}_2\text{O}_3}$$

$$\text{AR} = \frac{5.67}{3.32} = \mathbf{1.71}$$

The following is a simple explanation for reaction:-

$2(Al_2O_3.2SiO_2) + 7Ca(OH)_2 \rightarrow 3CaO.2SiO_2.3H_2O + 2(2CaO.Al_2O_3.SiO_2.2H_2O)$

CFW + Hydrated lime $\rightarrow 3CS_2H + 2C_2ASH$

When the above reaction is disintegrated in to the silica and alumina reaction, the CFW reaction results are as follows:-

$2SiO_2 + 3Ca(OH)_2 \rightarrow 3CaO.2SiO_2.3H_2O$ Silica reaction

120 222 336

$Al_2O_3 + 3Ca(OH)_2 + 3H_2O \rightarrow 3CaO.Al_2O_3.6H_2O$ Alumina reaction

102 222 54 378

From the silica reaction, 120 parts of SiO_2 react with 222 parts of $Ca(OH)_2$, i.e. 222/120=1.85

From the alumina reaction, 102 parts of Al_2O_3 react with 222 parts of $Ca(OH)_2$,i.e.222/102=2.18

The percent of $Ca(OH)_2$ that reacts with SiO_2 = (1.85/(1.85+2.18))*100 =46%

The percent of $Ca(OH)_2$ that reacts with Al_2O_3 = (2.18/ (1.85+2.18))*100 =54%

Appendix D

Silica Alumina Ratio Calculation

SiO_2 = 65.44

Al_2O_3 = 16.57

Let us take; - 10gm Activated CFW

For Silica

65.44 Wt.% SiO_2

X= $\frac{65.44*10}{100} = 6.544\text{gm } SiO_2$

Molecular mass of SiO_2 =60gm/mol

Therefore, no of moles of SiO_2 in 10gm Activated CFW is:

$n = \frac{m}{M} = \frac{6.544\text{gm}}{60\ gm/mol} = 0.109\text{mol } SiO_2$

For Alumina

16.57 Wt.% Al_2O_3

X = $\frac{16.57*10}{100} = 1.657\text{gm } Al_2O_3$

Molecular mass of Al_2O_3=102gm/mol

Therefore, no of moles of Al_2O_3 in 10gm Activated CFW is:

$n = \frac{m}{M} = \frac{1.6576\text{gm}}{102\text{gm/mol}} = 0.016\text{mol } Al_2O_3$

Thus $\frac{SiO_2}{Al_2O_3} = 6.71$

Gel Formation Calculation

$\frac{SiO_2}{Al_2O_3} = 6.71$ from AAS compositional analysis test results

$\frac{Na_2O}{SiO_2} = 0.8$, the ratio should be $0.6 - 0.8$ from standard

$\frac{H_2O}{Na_2O} = 30$, standared from the zeolite Y standard formula molecular composition

Calculation for batch composition

Molar mass of Syn-Z= (60*6.71) + 102+94 = 598.6gm/mole

Mole of Syn-Z in 10gm of Syn-Z

$$\frac{10gm}{598.6gm/mol} = 0.0167mole$$

Mole of SiO_2 in 10gm of Syn-Z

=0.0167*6.71=0.11mol

Calculation for Na_2O need in batch composition

$\frac{Na_2O}{SiO_2}$ is 0.8, from the standared formula (given)

$$\frac{Na_2O}{SiO_2} = 0.8$$

$Na_2O = 0.8*SiO_2 = 0.8*0.11 = 0.088$mole

From reaction

$2NaOH \rightarrow Na_2O + H_2O$

$2 \rightarrow 1$

$X \rightarrow 0.088$

NaOH = 0.264 mole of NaOH

Mass of NaOH $m = n * M$ = 0.264 mole*40 gm/mole = 10.56gm

Calculation for H_2O

$$\frac{H_2O}{Na_2O} = 30 - - - - - - given$$

$H_2O = 30*Na_2O = 30*0.088 = 2.64$ mole

From molar mass of water, mass of water was 2.64 mole *18gm/mole = 47.52 gm

Since density of water is 1gm/cm^3

1gm $\rightarrow cm^3$

47.52gm $\rightarrow$ 47.52 cm^3 = 47.52 ml of water was be added.

Formulating Molar Chemical Composition of Synthesized Zeolite Y

Mole of NaOH = 0.264 mole Mole of H_2O = 2.64 mole Mole of $Al_2Si_2O_7$ = 0.11 mole

$2NaOH \rightarrow Na_2O + H_2O$

2 → 1

26.4→ X,

X = 13.2 Mole of Na_2O

Finally, the synthesized Zeolite Y molar Chemical Composition from the above compositional calculation is as follows:

13.2 Na_2O. Al_2O_3. 11SiO_2. 263H_2O

Appendix E

Pictorial Presentation of the Zeolite Production Process

- **Beneficiation of Awash Melkassa chemical factory waste(CFW)**

Purpose:-to remove impurities such as soluble salt, quartz etc.

Figure a) Washing using HCl b) Washing using water c) Oven dried CFW

- **Calcination and Quenching of CFW**

Activating alumina and silica in the CFW by heat treatment using muffle furnace. It is also used to remove organic matters and crystal water. Immediate quenching is needed to convert the crystalline phase to amorphous.

Figure a) Calcination of CFW with Muffle Furnace b) Immediate Quenching with Water

- **Zeolite Formation Steps**

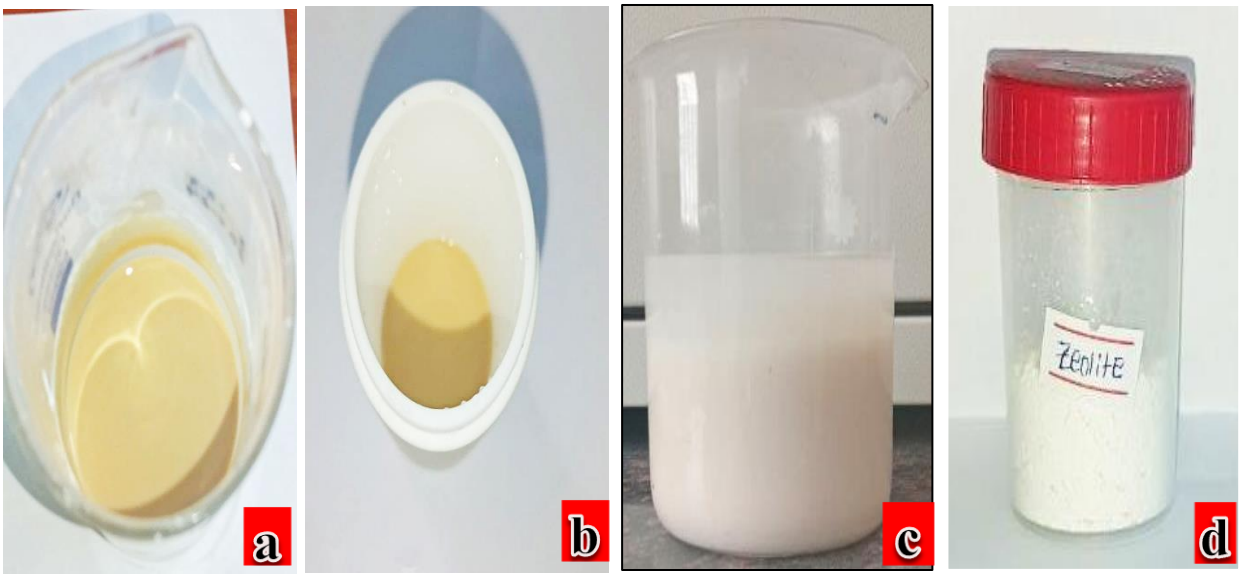

Figure a) Gel Formation (H_2O + NaOH + CFW),b) Zeolite Crystallization in Side Teflon, c) Washing Zeolite to Reduce pH Level to 8, d) Oven Dried Zeolite

Picture of laboratory equipment used in the preparation of Zeolite from CFW

Weigh Balance

Muffle Furnace

Drying Oven

Flocculator Unit

Hydrothermal Reactor

pH Meter

Picture of laboratory equipment used in the preparation of cement mortar

Weigh Balance

AutoMix

Compressing Machine

Blane Test Machine

Curing Chamber

Jolting Machine

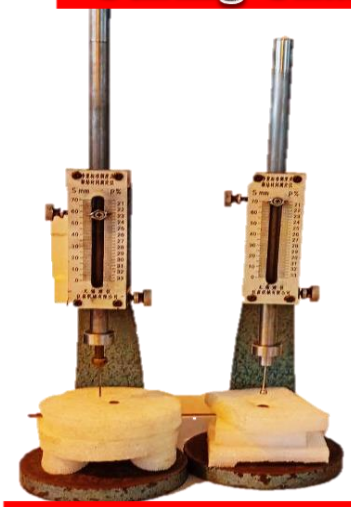

Vicat Set Test Apparatus

Le Chatelier Test Apparatus

Pictorial Presentation of preparation of cement mortar

- Preparation of dry cement materials with different proportion and mixing of the dry mixture with sand and water respectively.

- Preparing mold with the paste on 40*40*160 m^3 in rectangular Prism steel molds

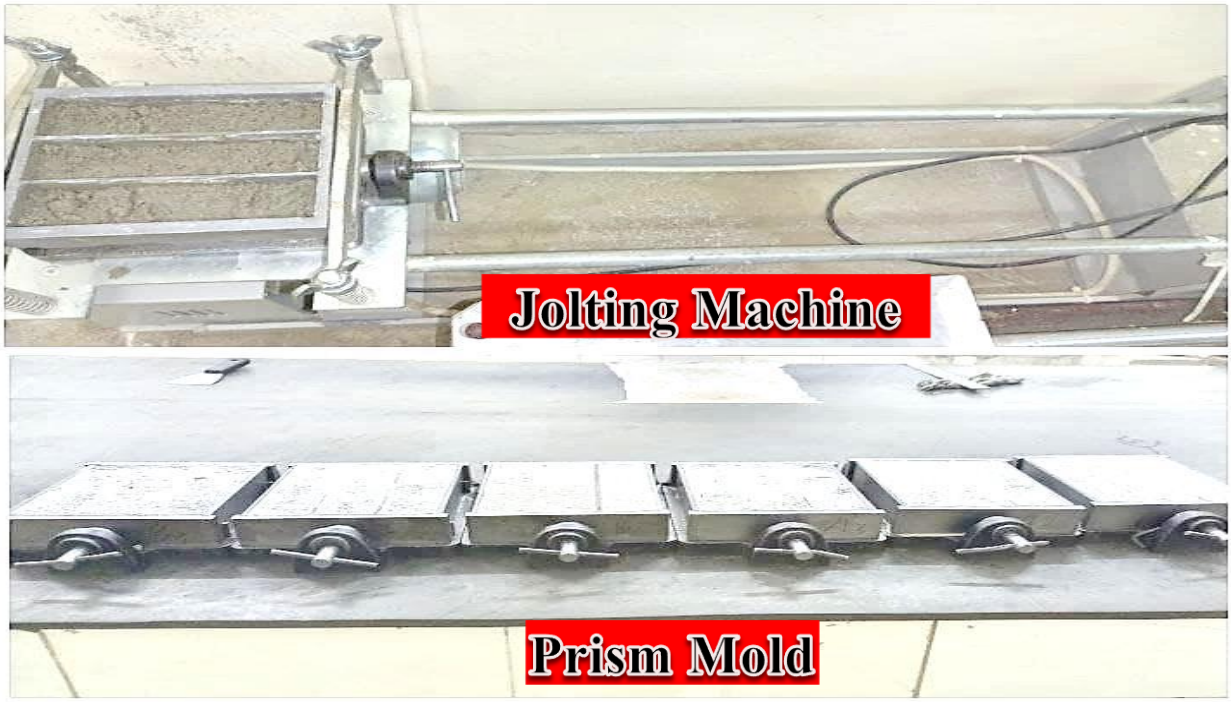

- After undergoing 24 hours of molding, it was placed in a submerged cure in water for 2 and 28 days. The Flexural and compressive strength test was performed at 2 and 28 days.

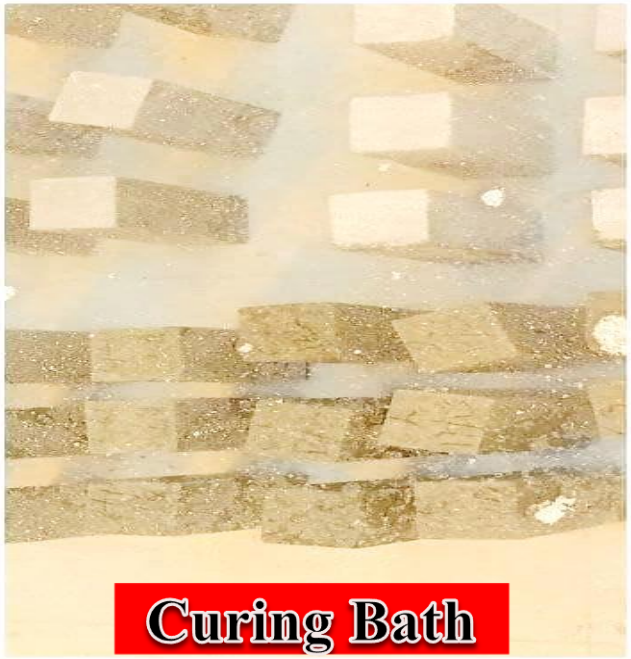

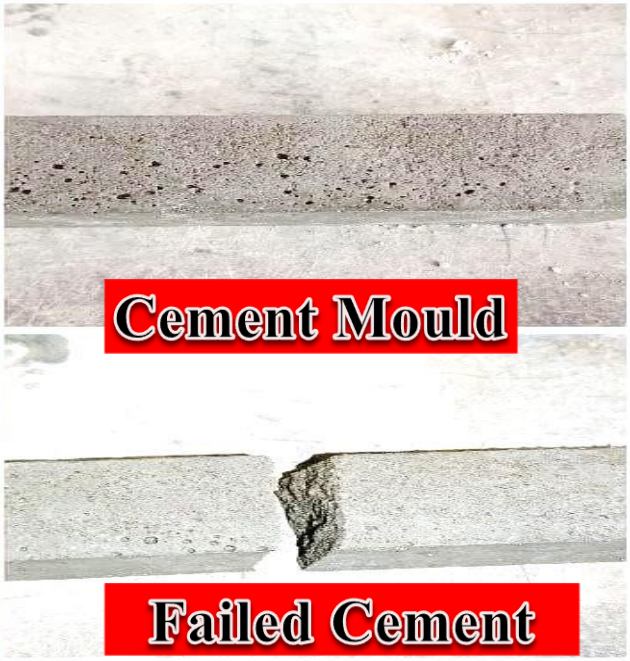

- A 500gm of cement paste was prepared on a mould then the mould placed under the rod bearing the needle(needle for determining the initial and final setting time)

Initial setting Time and Final setting Paste Paste

- 20 gm paste was prepared with 0.78P of water added. Paste was put on Lechatelier's device. It was immersed in water for 24 hour and measured the expansion, then again immersed in boiling water for 3hr and measured the expansion again finally values were subtracted to get Expansion of sample.

Cured Paste

Expanded Paste

Appendix F

- **Characterization results**

SEM Image of Cement with Replacements

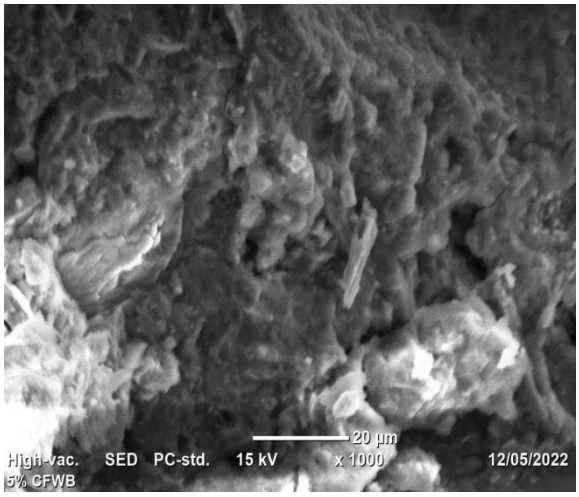

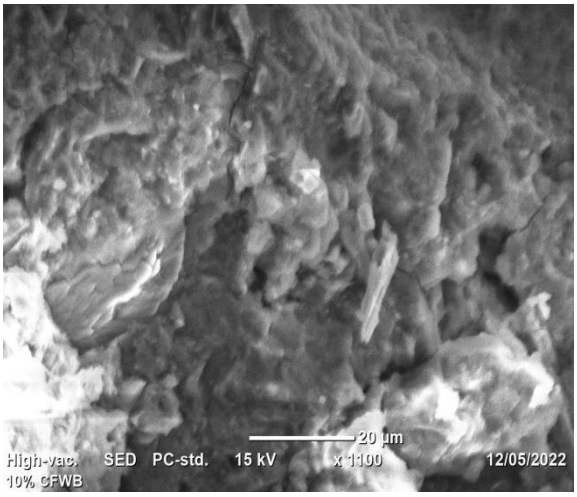

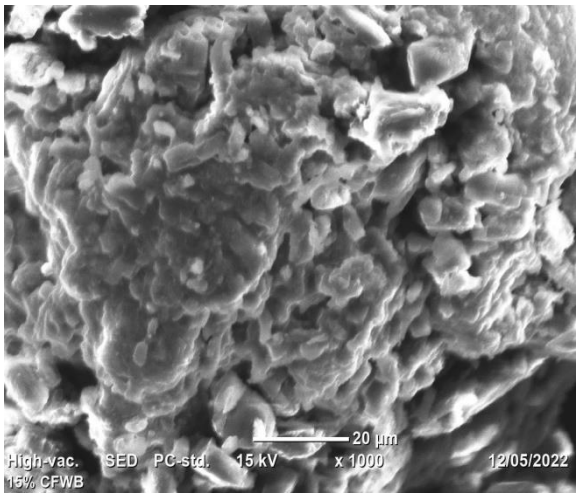

BET Result

Quantachrome NovaWin - Data Acquisition and Reduction
for NOVA instruments
©1994-2010, Quantachrome Instruments
version 11.0

Analysis			Report		
Operator:alex	Date:2022/05/19		Operator:alex	Date:5/19/2022	
Sample ID: TA 2		Filename:	C:\QCdata\Physisorb\TA 3.qps		
Sample Desc:		Comment:			
Sample weight: 0.05 g		Sample Volume: 0.012821 cc		Sample Density:3.9 g/cc	
Outgas Time: 8.0 hrs		OutgasTemp:	300.0 C		
Analysis gas: Nitrogen		Bath Temp:	77.3 K		
Press. Tolerance:0.100/0.100 (ads/des)		Equil time: 60/60 sec (ads/des)		Equil timeout: 240/240 sec (ads/des)	
Analysis Time: 81.1 min		End of run:	2022/05/19 13:29:15	Instrument:	Nova Station B
Cell ID: 2				F/W version:	0.00
Adsorbate	Nitrogen	Temperature	77.350K		
	Molec. Wt.: 28.013 g	Cross Section: 16.200 Å²		Liquid Density: 0.808 g/cc	

Relative Pressure P/Po	Volume @ STP cc/g	1 / [W((Po/P) - 1)]
5.37840e-02	17.5639	2.5894e+00
1.13995e-01	36.0486	2.8557e+00
1.74154e-01	54.3610	3.1038e+00
2.36243e-01	73.2099	3.3805e+00
2.97994e-01	91.7940	3.7000e+00

BET summary

Slope =	4.498
Intercept =	2.338e+00
Correlation coefficient, r =	0.999145
C constant=	2.924

Surface Area = 509.462 m²/g

Size Distribution Report by Intensity

v2.2

Sample Details

Sample Name: zeolite 1

SOP Name: mansettings.nano

General Notes:

File Name:	Example Results.dts	**Dispersant Name:**	Water
Record Number:	153	**Dispersant RI:**	1.330
Material RI:	1.59	**Viscosity (cP):**	0.8872
Material Absorbtion:	0.010	**Measurement Date and Time:**	Wednesday, May 4, 2022 5:5...

System

Temperature (°C):	25.0	**Duration Used (s):**	30
Count Rate (kcps):	233.0	**Measurement Position (mm):**	0.65
Cell Description:	Disposable sizing cuvette	**Attenuator:**	11

Results

			Size (d.nm):	% Intensity:	St Dev (d.n...
Z-Average (d.nm):	27.25	**Peak 1:**	73.22	100.0	5.375
PdI:	0.100	**Peak 2:**	0.000	0.0	0.000
Intercept:	2.20	**Peak 3:**	0.000	0.0	0.000

Result quality : **Refer to quality report**

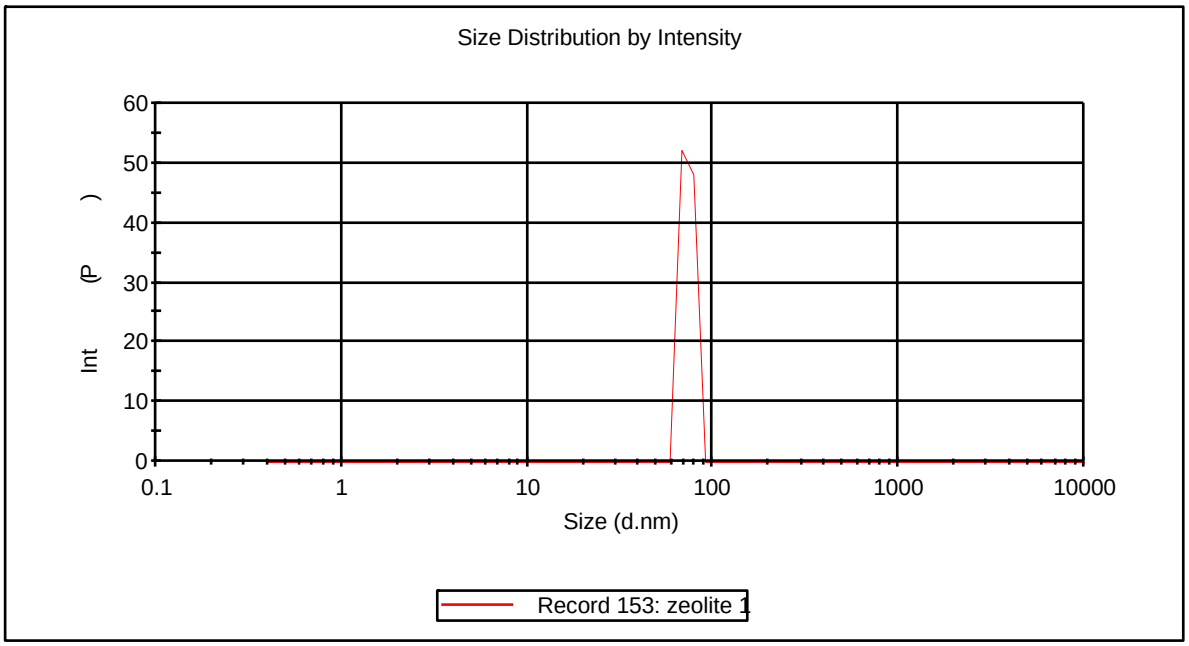

Raw XRD Graphs with JCPDS Card Number

CFW XRD

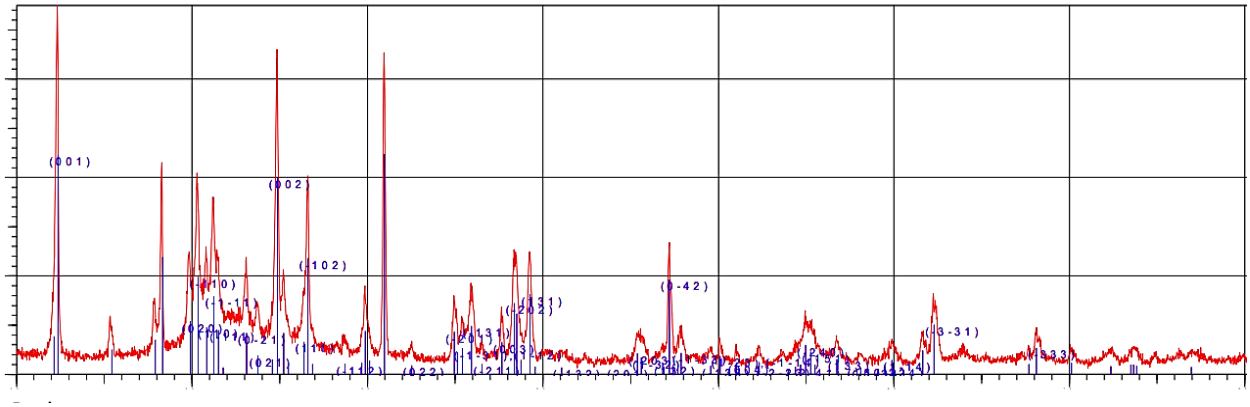

CFWA

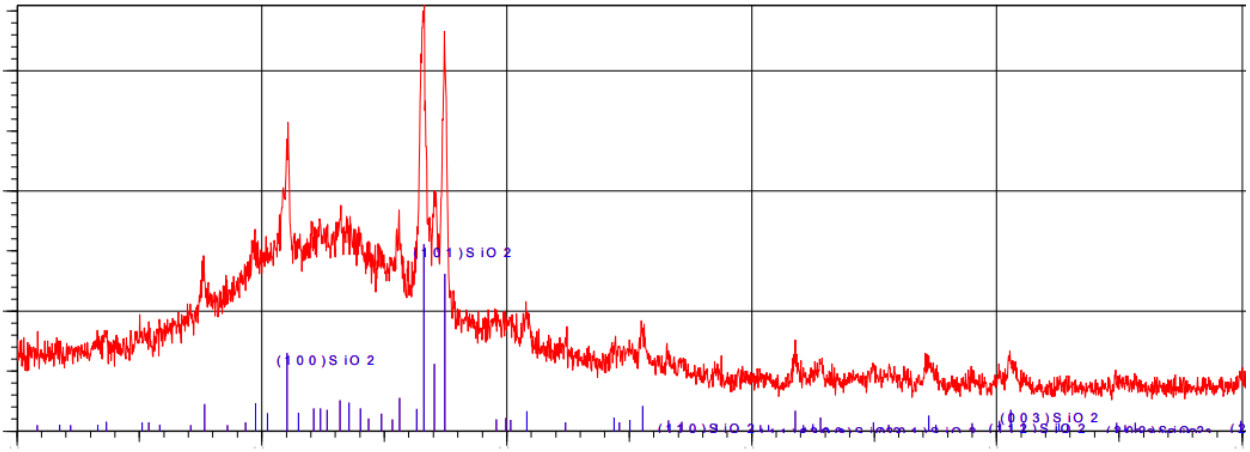

CFWB

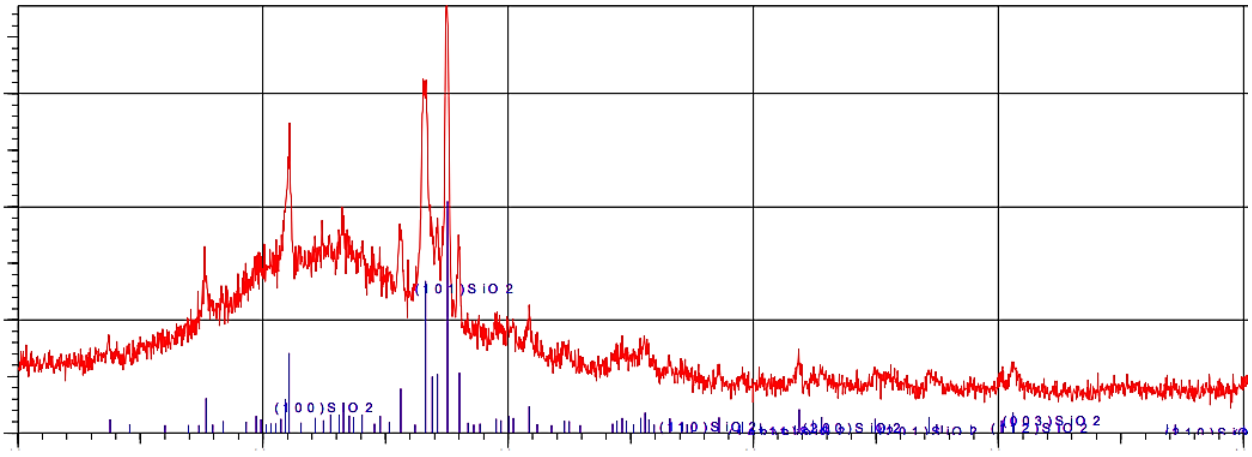

CFWC

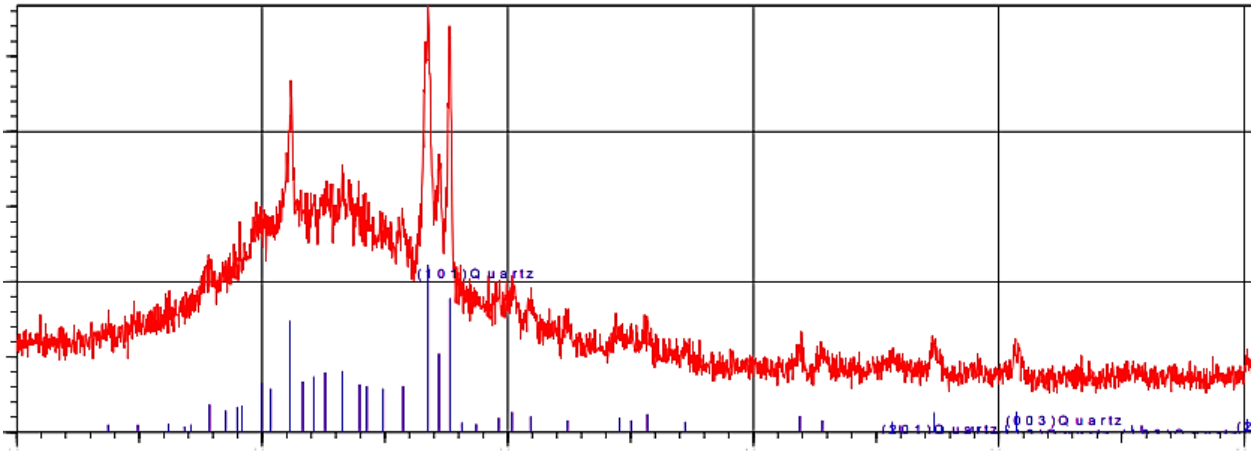

CFWD

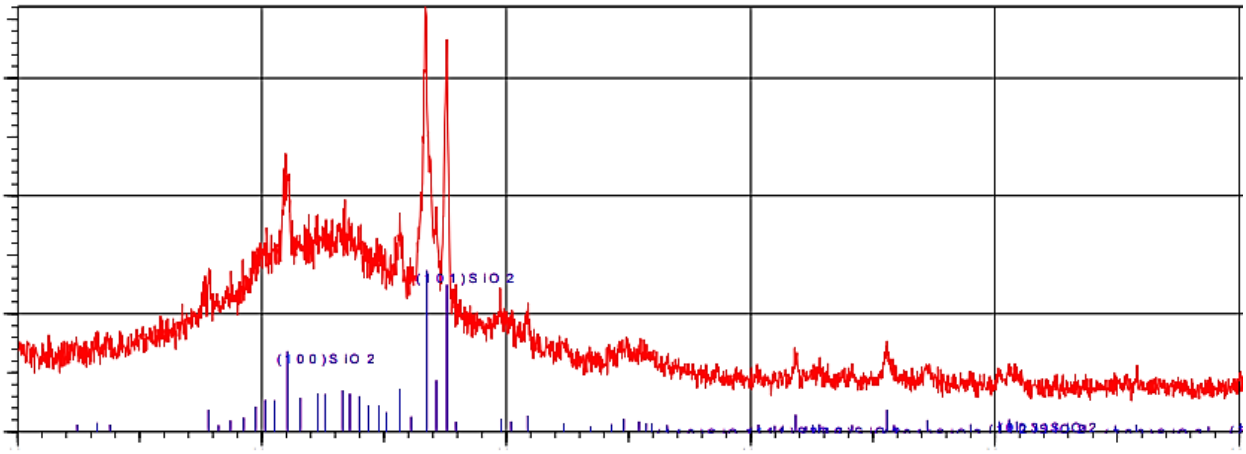

Zeolite Y